# Optical properties of DNA-hosted silver clusters

Markesevic, N.

# Optical properties of DNA-hosted silver clusters

**Nemanja Markešević**

# Optical properties of DNA-hosted silver clusters

PROEFSCHRIFT

ter verkrijging van
de graad van Doctor aan de Universiteit Leiden,
op gezag van Rector Magnificus prof. mr. C. J. J. M. Stolker,
volgens besluit van het College voor Promoties
te verdedigen op woensdag 16 december 2015
klokke 12:30 uur

door

**Nemanja Markešević**

geboren te Čačak, Servië
in 1985

| | | |
|---|---|---|
| Promotor: | Prof. dr. D. Bouwmeester | |
| Co-promotor: | Dr. D. Kraft | |
| Promotiecommissie: | Dr. S. Bidault | (Institut Langevin, Paris, France) |
| | Dr. P. Zijlstra | (TU Eindhoven) |
| | Prof. dr. T. J. Aartsma | |
| | Prof. dr. E. R. Eliel | |
| | Prof. dr. T. Schmidt | |

The research reported in this thesis was conducted at the 'Leids Instituut voor Onderzoek in de Natuurkunde' (LION). This work is a part of the research program, which is financially supported by the Netherlands Organization for Scientific Research (NWO).

Casimir PhD series Delft-Leiden 2015-27
ISBN 978-90-8593-233-8

*To the people I love*

# Contents

# CHAPTER 1

# Introduction

## 1.1 Metal clusters

Metal clusters have attracted a lot of attention mostly due to the fact that their size and shape determine their optical properties [1–5]. When the dimensions of the metal objects become comparable to the mean free path (MFP) of electrons in the metal, then the dielectric response function becomes wavelength-dependent. This typically happens at scales below 100 nm (the MFP for silver is 52 nm). However, if the dimension of the particle becomes comparable to the Fermi wavelength (for Ag: $\lambda_F$=0.55 nm), then the energy levels become discrete.

The small clusters are usually unstable and tend to aggregate which leads to the loss of their individual physical properties. Therefore, numerous capping techniques have been developed to stabilize the clusters. For example, the ligands used to protect the clusters from the environment are dendrimers [6], polymers [7], peptides [8], even single stranded RNA [9] and DNA [10].

## 1.2 DNA-hosted silver clusters

In this thesis we focus on DNA-hosted silver clusters (Ag:DNAs) (Figure 1.1 a, b). The main purpose is to investigate the optical properties of silver clusters, either at the level of individual emitters or as a collection of emitters positioned on DNA scaffolds.

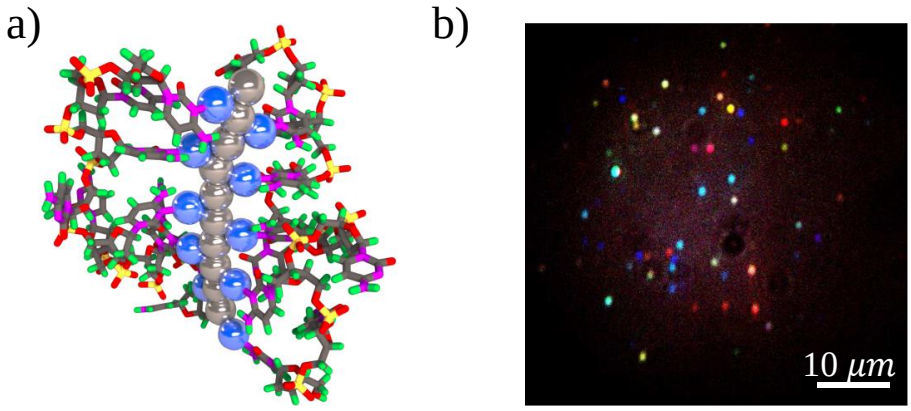


**Figure 1.1:** Single stranded DNA can stabilize fluorescent silver clusters. a) Neutral core of silver atoms is represented with gray spheres while positive ions are shown as blue spheres. Positive ions connect the neutral core and surrounding DNA bases [19]. b) False-color fluorescent image (Chapter 2) of the Ag:DNAs immobilized on the silica substrate [20].

While most of the cations interact with the negatively charged backbone of DNA, silver ions bind preferentially to the heterocyclic ring nitrogen on DNA bases [11, 12]. The base sequence determines the size and shape of the clusters which directly influences their optical properties [13]. Together with their small size, the tunability of the emission wavelength in the range from 400-900 nm, makes them suitable for various applications which drive the research in this field. These DNA-hosted metal clusters proved to be great sensors for single base mutations [14, 15] and mercury ions [16], and they also show a great potential for biological research [17, 18].

Thorough mass spectrometry studies of purified Ag:DNA material have discovered that the fluorescent clusters contain both positive ions and neutral atoms [19]. From the model proposed by Schultz and coworkers (Figure 1.1 a), it seems that the neutral core of silver atoms is surrounded by silver cations, which mediate between the core and the surrounding DNA bases [19]. In a more detailed study, it was further established that the number of ions and neutral atoms are not random, but rather 'magic' [21], shaping the size and the optical properties of the clusters.

For a better understanding of their optical tunability, one has to consider

the electronic structure of silver atoms. The energy necessary to excite the d-band transitions of silver is much higher than the energy necessary to excite the collective excitation mode of s-electrons. Furthermore, the optical transitions of the chains of silver atoms is length-dependent [22]. The model of the linear chain of atoms somewhat corresponds to the previously proposed nanorod model [19].

## 1.3 DNA scaffolds

The appealing possibilities of binding between complementary DNA strands paved the way to the construction of elaborate DNA scaffolds. In 2006, Paul Rothemund showed in his pioneering work [23] that short DNA strands with careful sequence design can fold long strands of M13 virus. A new field of DNA origami exploded and since then the creation of 2D [23] and 3D objects [24] with nanometer precision became simplified.

Generally speaking, DNA scaffolds stabilize organic dye molecules [25, 26], plasmonic particles [27], but also change a conformation on demand [28, 29] . Most recent results show that the DNA structures can be utilized for the drug delivery and to initiate an immune response [30, 31].

In our research, we use short DNA oligonucleotides which represent modular components in building quasi 3D objects [32–35]. Namely, the sequence of bases in the oligonucleotides is chosen such that one oligonucleotide is piecewise complementary to at least two other oligonucleotides.

For example, only 5 different types of nucleotides form a tile, which is a 'unit cell' of double-crossover (DX) tubes [33] as will be discussed in Chapter 4. The tiles are designed such that the complementary short sticky ends connect and form a larger 3D structure (Figure 1.2 a, b). On the other hand, 10 strands (Chapter 5) or 6 strands (Chapter 6) can be interwoven such that they form half crossover (HX) tubes [35, 36]. While DX tubes allow the direct synthesis of Ag:DNAs on the pre-defined positions (DNA loops) [33], the HX tubes give a possibility to attach subsequently purified Ag:DNAs [35] (Figure 1.2 c, d).

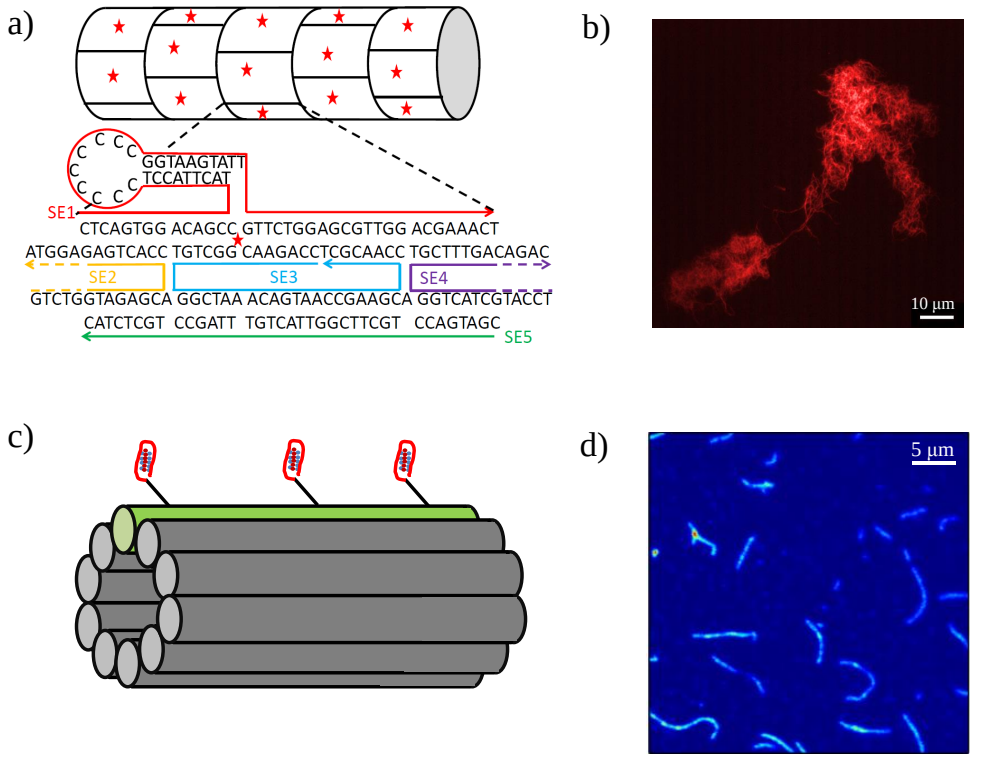


**Figure 1.2:** DNA tubes for organization of Ag:DNAs. a) Five different strands form a 'unit cell' of the DX tubes. Silver clusters are stabilized in the loop of strand SE1-9C [33]. b) Fluorescent image of the tangles of tubes immobilized in PVA (scale bar: 10 $\mu$m). c) Ten oligonucleotides form HX tube to which we attach purified Ag:DNAs [35]. d) Fluorescent image of the tubes immobilized in PVA (imaged area: 40X40 $\mu$m).

## 1.4 Experimental techniques

The synthesis procedure of Ag:DNAs consists of several steps: a water solution of DNA strands which can stabilize the cluster is mixed in a buffer (ammonium acetate/magnesium acetate) with silver nitrate ($AgNO_3$) and subsequently reduced by sodium borohydride ($NaBH_4$). Shortly after reduction, the solution changes color, but in order to reach a maximum fluorescence intensity, we kept our sample overnight at 4°C.

To form DNA tubes, we follow the procedure developed by O'Neill and

coworkers for DX tubes [33], and Yin and coworkers for HX tubes [34] with modifications suggested by Schiffels et al. and Copp et al. [35, 36] . A solution of carefully selected DNA strands was mixed in a buffer (ammonium acetate/magnesium acetate) and heated to 95°C. Then the system is slowly cooled down ($\sim$ 48 hours) in a thermos bottle to room temperature. In the case of DX tubes, where we synthesized the emitters directly on the tubes, the addition of $AgNO_3$ was followed by the addition of the reducing agent $NaBH_4$. On the other hand, the purified Ag:DNA emitters were added to the solution of HX tubes, and made connections through the docker-linker complementary bonds (Chapter 5).

The characterization of the emitters in solution was performed by UV-visible spectrophotometry (Cary 50 Bio) and fluorimetry (Cary Eclipse Varian). These two techniques enabled us to monitor the absorption and emission properties of the emitters in solution.

For single emitter spectroscopic cryogenic measurements we constructed the setup schematically presented in Figure 1.3. In this configuration it was not only possible to detect an ensemble of emitters immobilized in poly(vinyl alcohol) (PVA) by CCD camera as presented in Figure 1.1 b (in this case we used a lens to illuminate a larger area on the sample), but also to align a diffraction limited laser beam to individual emitters. The emission is then detected by a fiber-coupled spectrometer or a single-photon sensitive counting module (APD).

To perform polarization measurements we slightly modified the setup for spectroscopic measurements (Figure 1.4), introducing the computer controlled polarization rotator in the excitation path and the polarizer in the emission path. A wide field illumination lens enabled us to excite many emitters at the same time, improving the efficiency of data collection.

The setup schematically presented in Figure 1.5 was used for time-resolved measurements. A pulsed laser with a repetition rate of 20 MHz excited the emitters immobilized in PVA. For the data acquisition and data processing we used SymPho Time 200 PicoQuant software.

Microscopy was performed on commercially available setups: Fluorescence microscope (Zeiss Axiovert 40 CFL) with 100X oil- immersion objective and Nikon eclipse Ti-E microscope system with a Nikon 100x/1.45 NA Oil immersion DIC H objective.

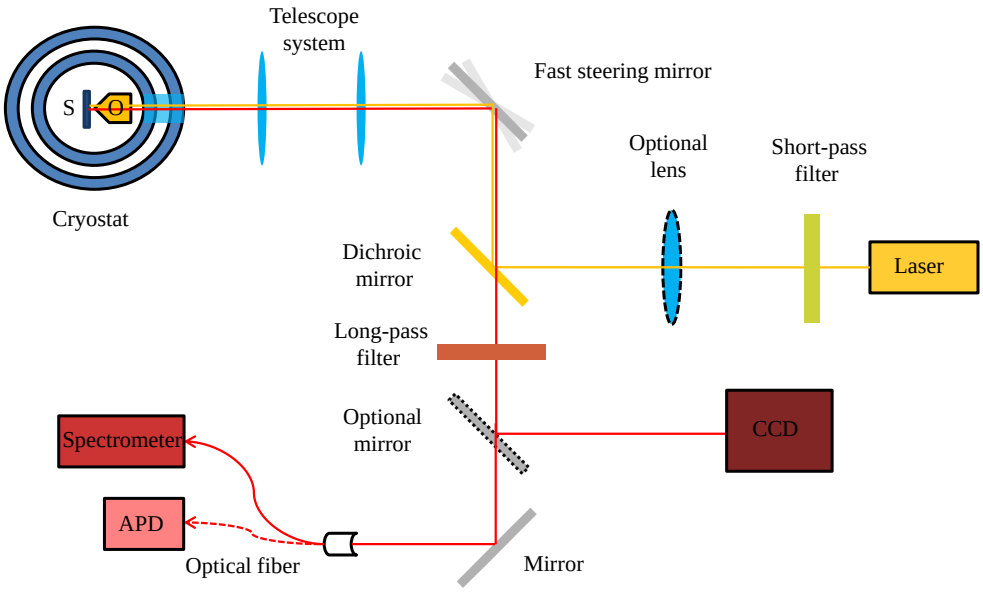


**Figure 1.3:** Setup for spectroscopic cryogenic measurements. Laser light from a tunable ring dye laser (Coherent 899) is filtered through the short-pass filter (edge at 600 nm). An optional lens is removed when we perform single-molecule type of measurements. Laser light is further reflected by the dichroic mirror and a fast steering mirror through the telescope system and objective (O). The illuminated sample (S) emits light which is directed with the same objective through the dichroic mirror and long-pass filter (edge at 600 nm). To detect the ensemble of emitters by a CCD camera, we use an optional mirror (an optional lens is also in the system). For single molecule measurements, light is directed by the mirror to the optical fiber and further to the single-photon counter (APD) or Spectrometer.

## 1.5 Thesis outline

In this thesis we are mainly focusing on the properties of the DNA-hosted silver clusters at the single emitter level. Previous research was mostly dedicated to the bulk solution properties at room temperature. We immobilize the emitters in PVA and perform cryogenic spectroscopic measurements on the single emitter level. Furthermore, we examine the formation of Ag:DNA on the DNA scaffolds such as DNA tubes and compare the properties of such emitters to the properties of free individual emitters. Time-resolved properties of individual emitters and densely packed Ag:DNAs have attracted our

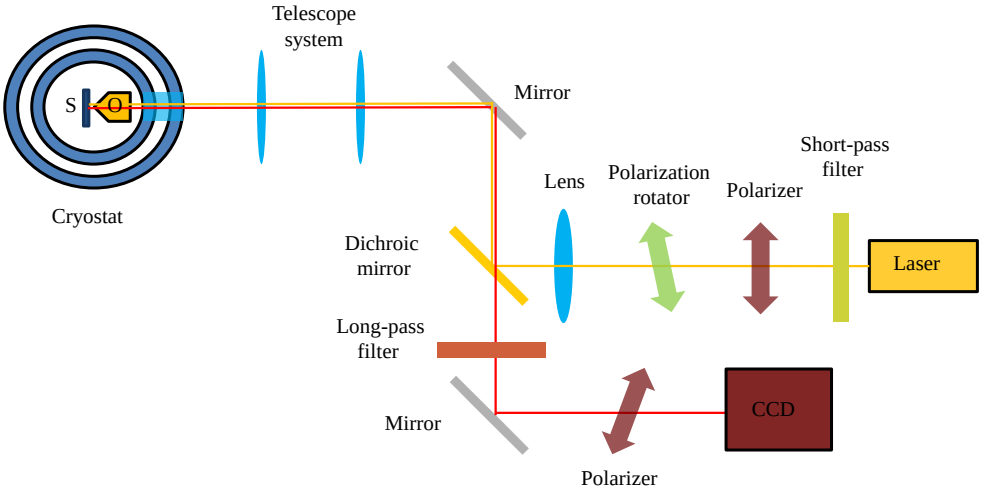


**Figure 1.4:** Setup for polarization cryogenic measurements. Laser light from a tunable ring dye laser (Coherent 899) is filtered through the short-pass filter (edge at 600 nm) and a polarizer. A polarization rotator is used to rotate the polarization angle of the excitation light. A lens inserted in the excitation beam enables the illumination of the larger field of view (diameter $\sim$ 100 $\mu$m ). Since the emitters are spatially well separated, we can extract the excitation and emission properties from each of them. Laser light is further reflected by the dichroic mirror and another mirror through the telescope system and objective (O). The illuminated sample (S) emits light which is directed with the same objective through the dichroic mirror and long-pass filter (edge at 600 nm). To detect the ensemble of emitters by the CCD camera, the light is reflected by the mirror and transmitted through the polarizer.

attention as well. Finally, we use the knowledge gained on the organization of the Ag:DNAs to guide the assembly of large colloidal particles (d= 1 $\mu$m) into flexible strings.

In Chapter 2, we present low temperature spectroscopic measurements of the Ag:DNAs. We show that by removing the ensemble broadening, we can probe the line widths and brightness of individual Ag:DNA emitters. The brightness of the emitters roughly increases five times from 295 to 1.7 K while the emission line width decreases two times, indicating the plasmonic properties of the Ag:DNAs.

Chapter 3 contains low temperature polarization measurements on the immobilized Ag:DNAs. From the polarization data, we conclude that the

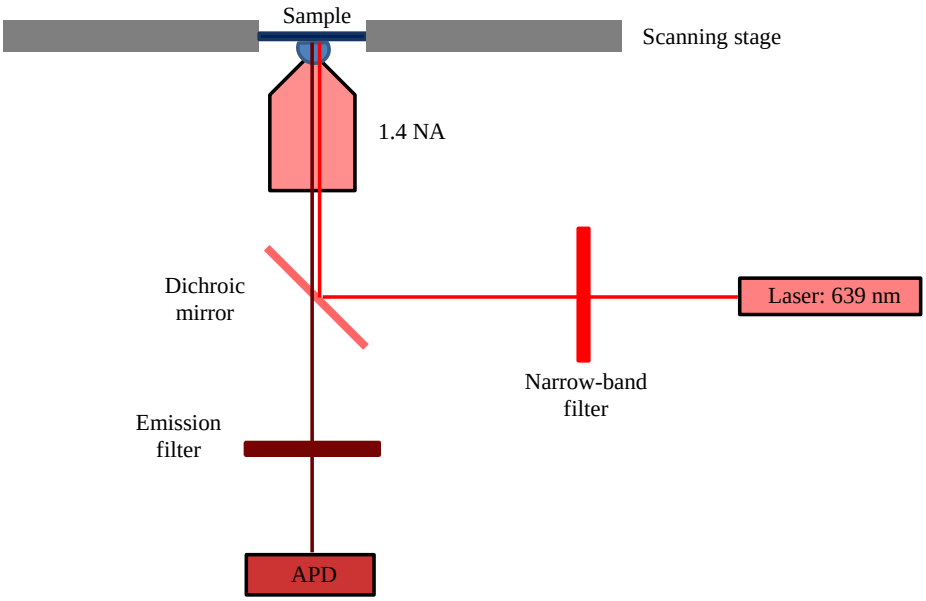


**Figure 1.5:** Setup for time-resolved measurements. A pulsed laser light ($\lambda$= 639 nm) is filtered through the narrow-band filter and reflected by the dichroic mirror through the oil-immersion objective onto the sample mounted on the scanning stage. The emitted light is collected by the objective and transmitted through the dichroic mirror and emission filter to a single-photon counter (APD).

emission is strongly polarized, whereas the excitation does not strongly depend on the polarization of the excitation light. This brings us to the conclusion that the clusters are rod-shaped and that the DNA is involved in the excitation/emission process.

In Chapter 4 we focus on the synthesis of Ag:DNAs on the DNA tubes. We discover that the emitters formed on the tubes show different temperature stability with respect to their free counterparts. The temperature increase leads to the deterioration of free emitters, whereas the emitters formed on much larger structures, tiles and tube, show the increase in fluorescence as a consequence of formation of new fluorescent emitters. This is supported by the increase of absorption.

Lifetime measurements on the individual emitters and emitters organized on the DNA tubes with high densities are presented in Chapter 5. Single emitters show single exponential decay after the excitation with short laser

light pulses, while the emitters immobilized on the DNA tubes show double exponential decay path. This can be explained by the interaction between the emitters.

In Chapter 6, we describe how to use the properties of DNA tubes with sticky ends (similar to those used in Chapter 5) to glue together colloidal particles into stable strings. Generally, the superparamagnetic particles align in magnetic field, but the thermal fluctuations break strings after the magnetic field is switched off. Here we show that the DNA nanotubes can be used as a nano-contact glue between the DNA functionalized colloids.

# CHAPTER 2

## Spectral Properties of Individual DNA-Hosted Silver Nanoclusters at Low Temperatures

In this Chapter the first single emitter fluorescence spectra of DNA-stabilized silver clusters (Ag:DNAs) at ambient and cryogenic temperatures are presented. While Ag:DNAs have received much attention recently due to their sequence-tunable emission wavelengths, the nature of the optical transitions (molecule-like or collective, cluster-like) is an open question. By removing the ensemble broadening present in previous spectroscopic studies, we probe the line widths $\Gamma$ and brightness of individual Ag:DNA emitters. A roughly 5-fold increase in brightness from 295 to 1.7 K is accompanied by a factor of 2 decrease in $\Gamma$. The symmetric emission line shape, its sensitivity to embedding medium, and the independence of emission wavelength on excitation energy together indicate that the measured $\Gamma$ represents the homogeneous line width, while the large, $\sim$ 100 meV values of $\Gamma$ suggest rapid dephasing of a collective excited state of the silver cluster.

This Chapter is based on: S. S. R. Oemrawsingh, N. Markešević, E. G. Gwinn, E. R. Eliel, D. Bouwmeester, *Spectral properties of individual DNA-hosted silver nanoclusters at low temperatures*, J. Phys. Chem. C **116**, 25568 (2012).

## 2.1 Introduction

Nanoclusters of noble metals bridge the gap between the atomic and nanoparticle (plasmonic) regimes. They typically consist of a few to tens of atoms, corresponding sub-nanometer sizes comparable to the Fermi wavelength ($\sim$ 0.5 nm in Ag and Au). In this quantum size regime, nanoclusters possess interesting chemical and physical properties [37]. The strong fluorescence exhibited by silver nanoclusters [38, 39], and the fact that their absorbance and fluorescence spectra depend strongly on cluster size and shape [40, 41], is a striking example. The potential to size-tailor these properties for use in solution or solid state has motivated extensive efforts to develop strategies for chemical stabilization of quantum-sized noble metal clusters. In recent years, a wide range of ligands has been employed to stabilize clusters of both gold and silver, including dendrimers, various functionalized amino acids and thiols, and biological matrices [6, 10, 42–46]. Because most of the atoms in nanoclusters are at its surface, the ligands controlling the cluster size can potentially alter the electronic states that dominate optical transitions to involve both ligand and cluster orbitals, thereby changing the optical properties of the ligated cluster. Understanding and exploiting the effects of the ligand environment on the optical properties of metal nanoclusters, particularly the poorly understood but empirically important effects of ligand choice on fluorescence, is the focus of current research [47, 48].

DNA-stabilized silver nanoclusters (Ag:DNAs), the subject of this Chapter, are drawing increasing interest due to their sequence tunable fluorescence wavelengths, as well as the high quantum yields and good photostability shown by some specific Ag:DNAs [10, 13, 49–54]. Recently demonstrated applications include advanced biological imaging [17], molecular logical schemes [55], and sensors for single base mutations [14], miRNAs [56], and metal ions [16]. Of particular interest is the wide spectral range spanned by fluorescent Ag:DNAs that form on various host strands [10, 51, 52, 57], covering the visible through the infrared. This large color space offers the potential to encode positional information as wavelength, by anchoring Ag:DNAs to DNA scaffolds [33] or incorporating them into living cells [17], In such applications, the line width of individual Ag:DNAs will limit the number of spectrally distinct color channels.

Advances in techniques for isolating specific Ag:DNA comlexes have

recently enabled identification of the numbers of silver atoms in several $Ag_n$:DNAs, with $n$ from 10 to 24 and emission wavelengths from 500 to 800 nm [53]. For the same 10-24 atom size, the dominant optical transitions of ligand-free clusters are collective in nature (plasmon-like) [58]. However, previous reports on Ag:DNA have considered them to be molecular in character. The distinction becomes important when considering line widths. The single-electron excitations of isolated molecules are usually spectrally narrow, but the collective excitations of multiple, delocalized electrons are subject to broadening by intrinsic dephasing processes [59–62]. These are well-understood for larger metal clusters but have been little explored in the quantum size regime [59, 61].

In this work, we report on the first spectroscopic measurements of Ag:DNA on the single-emitter level at ambient and low temperatures, and determine their fluorescent line width. To our knowledge, this has not previously been determined for ligand-stabilized noble metal clusters in the quantum size regime. In the limit of low temperatures, where vibronic degrees of freedom are mostly frozen out, the remaining spectral line shape and width of a single Ag:DNA will provide important information on whether the optical transitions have a cluster-like, collective, or molecule-like character.

To develop Ag:DNAs that are excitable within the 575-595 nm spectral range of the dye laser used for these studies, we carried out preliminary solution fluorescence studies of Ag:DNAs synthesized on some dozens of different DNA strands. We selected the strands used in this study, 5′-CCG-CCA-CCC-CGC-GGT-3′ (DNA1) and 5′-CCG-CCC-CCC-TGC-GGT-3′ (DNA2), on the basis of their relatively bright emission from bulk solution under excitation within that wavelength range. DNA1 differs from DNA2 by a two-base mutation that produces distinct spectral properties.

## 2.2 Experimental methods

Synthesis of the fluorescent Ag:DNAs is identical for both oligomers. The DNA strands (Integrated DNA Technologies) are hydrated in ammonium acetate buffer (99.999%, Sigma Aldrich), and subsequently, $AgNO_3$ (99.9999%, Sigma Aldrich) is added to the solution. After $\sim$ 15 min, a freshly prepared solution of the reducing agent $NaBH_4$ (99%, Sigma Aldrich) is added. Final concentrations were 50 $\mu$M DNA, 350$\mu$M AgNO3, 100 $\mu$M NaBH4, and 20

mM ammonium acetate. All solutions were prepared with nuclease-free water (Integrated DNA Technologies). The Ag:DNA samples are used without further purification.

The sample solutions are spectrally characterized in the visible regime (400-800 nm) with a Cary Eclipse fluorimeter (Varian), at a DNA concentration of 25$\mu$M. This is achieved by diluting either with nuclease-free water or with the medium, poly(vinyl alcohol) or glycerol, in which we suspend the Ag:DNAs for low-temperature studies.

To achieve the high photon fluxes needed for single emitter studies of Ag:DNAs, we used a sub-GHz-line width ring dye laser (Coherent 899) with Rhodamine 590 Tetrafluoroborate dye (Exciton). The excitation light is filtered with a short-pass filter (edge at 600 nm), to remove weak emission from the laser that is redder than the main excitation peak, which would otherwise generate a large spectral background. The excitation and emission paths are separated by a dichroic mirror (edge at 600 nm). The emission path contains an additional long-pass filter (edge at 600 nm), to exclude residual excitation light. This setup provides a usable excitation range of 575-595 nm. Fluorescence spectra were recorded with a thermoelectrically cooled fiber-coupled spectrometer (Ocean Optics QE65000) that has a spectral resolution of $\sim 1.5$ nm. The integration time was set at 60 s. Use of a cooled CCD camera (Ikon-M 934-BRDD, Andor Technology) enabled us to take images of single emitters, using a custom cryogenic objective assembly in the helium sample space of our cryostat, with a total magnification of 120X. Finally, we measured intensity fluctuations from single Ag:DNA emitters by using a fiber-coupled single-photon counting module (SPCM-AQR-14-FC, Perkin-Elmer).

For low-temperature ensemble measurements, the sample is diluted to a 25 $\mu$M DNA concentration, by adding a 50% (by volume) solution of glycerol. The glycerol ensures that a high quality optical glass forms at low temperatures, by preventing the formation of small, light-scattering ice crystals. We found that the glycerol reduced the emission brightness by a factor of 3 or more and thus significantly reduced the signal-to-noise ratio, making it a poor host medium for single-emitter measurements. Therefore, most single-emitter measurements were made on Ag:DNAs that were spin-cast onto a fused silica substrate from a dilute solution of poly(vinyl alcohol) (PVA). The PVA forms a robust film for cryogenic measurements. To prepare samples for single-emitter studies, the Ag:DNA solution is diluted to a concentration

of 20 nM in a 5 mg/ mL solution of PVA (98%, 16 kD, Acros Organics). The Ag:DNA and PVA solution is then spin-coated for 90 s at 4000 rpm onto a fused silica substrate. Ensemble measurements on Ag:DNA in PVA showed no decrease in fluorescence brightness, consistent with previous measurements [51]. The single-emitter line shapes, widths, and wavelengths did not change significantly when embedded in either PVA or glycerol.

For the low-temperature measurements, the sample is placed in a custom-built helium-bath cryostat. The temperature of the liquid helium is then lowered below the helium lambda point to 1.7 K, by pumping on the bath. This is crucial for the measurements, as it suppresses the formation of bubbles associated with the boiling of the liquid helium, which would otherwise scatter the light. Due to changes in alignment that result from thermal contraction during cooling, it was not possible to reliably track a particular emitter during cool-down. The result is that spectra at room temperature and at low temperature are taken for different individual emitters.

## 2.3 Results

After synthesis of the Ag:DNAs, we first characterize the fluorescence by recording the excitation and emission spectra in solution, at room temperature. In Figure 2.1, the fluorimetry results are shown, where the horizontal and vertical axes indicate the excitation and emission wavelengths, respectively, and the coloring represents the intensity detected in the emission path. The figure shows that the Ag:DNA2 sample has two fluorescent peaks, while the Ag:DNA1 sample has three, all at different spectral locations. As such, Figure 2.1 visualizes that the nucleotide sequence indeed influences the spectral distribution of the Ag:DNA emitters that form on different strands, as has been reported previously [13]. Each peak represents a different fluorescent species, which is typically defined by the size of the silver cluster and the folding of the Ag:DNA molecule as a whole [50, 51].

In our study, we concentrated on the Ag:DNA1 emitters that excite near 565 nm and fluoresce near 620 nm, and the Ag:DNA2 emitters that excite near 605 nm and fluoresce near 685 nm, because these emitters lie close enough to the 575-595 nm laser range to be excited. Prior studies of Ag:DNAs with known composition identified a trend to longer emission wavelengths for larger numbers of silver atoms [53]. Based on this trend, we infer that the

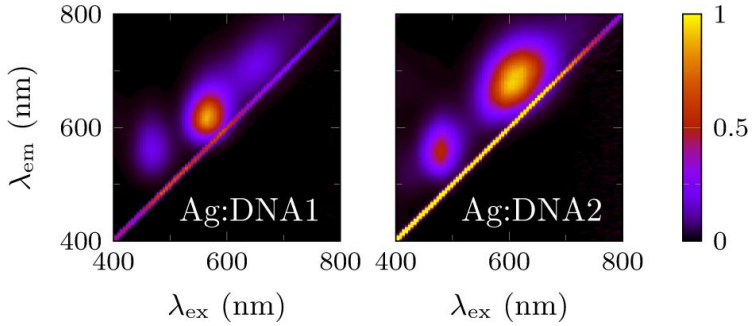


**Figure 2.1:** Fluorimetry results of Ag:DNA1 and Ag:DNA2 ensembles in solution at room temperature. Excitation and emission wavelengths are plotted along the horizontal and vertical axes, while the color indicates the detected intensity. The diagonal is caused by scattered excitation light.

Ag:DNA1 and Ag:DNA2 emitters contain 14-16 silver atoms. The prior finding that there is a systematic relation between color and silver atom number suggests that the actual cluster size scales with the total Ag content; however, the specific arrangement (geometry and degree of coordination) are not known.

At room temperature in solution, the emission lines are typically broadened by effects such as collision of the emitters with solvent molecules, fluctuating polar interactions with the solvent, and thermal excitation of vibronic states. It has been suggested that isomer interconversions of $\sim 10$ atom silver clusters may also be a source of line broadening at room temperature [63].

In solution, an ensemble of identical emitters will be influenced by the constantly changing environment, which randomizes the phase of the excited state on the dephasing time scale, $T_2$. If $T_2$ is much smaller than the excited state lifetime $T_1$, the line width $\Gamma = (1/2\pi T_1 + 1/\pi T_2)$ will be much broader than that set by the lifetime limit $T_1$. For Ag:DNAs, $T_1$ is in the nanosecond range [52], corresponding to line widths in the $\mu$eV range, in the absence of dephasing.

When cooling down the ensemble, the aqueous solution freezes and becomes glassy. The emitters are immobilized in this inhomogeneous environment, in which local, microscopic variations in the medium shift the electronic energy levels of one emitter relative to another. So while the single-emitter line width could be reduced by an increase in the $T_2$ time at low tem-

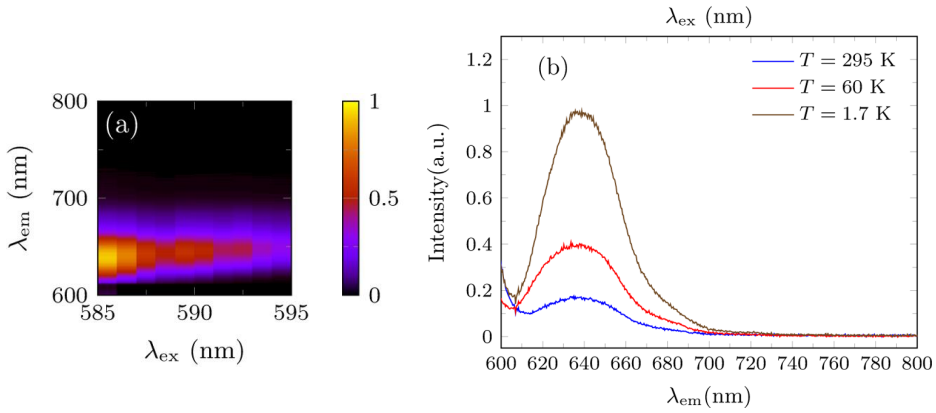


**Figure 2.2:** a) Emission intensity of an Ag:DNA1 ensemble at 1.7 K as a function of the excitation and emission wavelengths. Results for Ag:DNA2 were similar. b) Ensemble emission spectrum of Ag:DNA1 at different temperatures, excited at 585 nm. The width and position of the emission peak are only very weakly dependent on the temperature, indicating that thermal broadening effects are negligible in the ensemble. Nevertheless, the efficiency of the radiative path is seen to increase by a factor of 5.

peratures, the spectrum of a collection of emitters which experience different environments is inhomogeneously broadened.

The results of such ensemble measurements are shown in Figure 2.2 for Ag:DNA1. Results for Ag:DNA2 were similar. The excitation and emission spectra are plotted in Figure 2.2 a, where the emission intensity (color) is shown as a function of excitation wavelength (horizontal axis) and emission wavelength (vertical axis) at 1.7 K. Figure 2.2 b shows the emission spectra for three different temperatures of the same ensemble at a fixed excitation wavelength of 585 nm.

Figure 2.2 a shows that, when tuning the excitation wavelength at 1.7 K, the emission peak of the ensemble tends to shift in the same direction by the same amount. This is a signature of inhomogeneous (ensemble) broadening. Namely, as the excitation wavelength is detuned, the corresponding subensembles become more efficient at absorbing the laser light and will thus become brighter, and therefore, the ensemble will predominantly emit at a wavelength that is shifted accordingly.

The full width at half-maximum (fwhm) at 295 K in a glycerol solution is

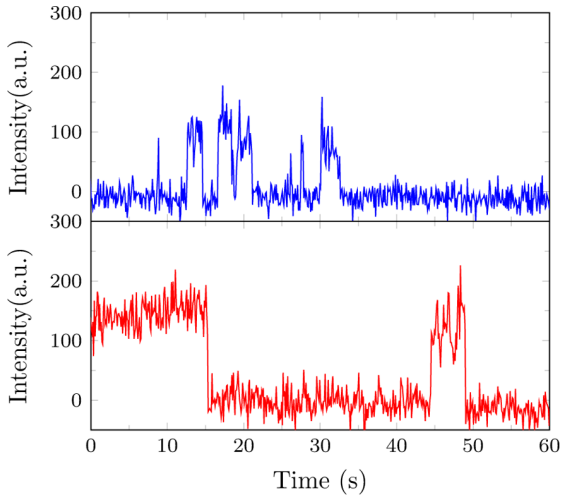


**Figure 2.3:** Emission intensity as a function of time, of two different Ag:DNA1 emitters embedded in PVA at room temperature, exposed to air. The fact that there are only two states, on and off, implies that we are indeed looking at single Ag:DNA emitters.

50 nm, and at 1.7 K, the fwhm is 41 nm, as seen in Figure 2.2 b. The 600 nm long-pass emission filter affects the measured line shape at the short-wavelength side. Integrating the area under the curves in Figure 2.2 b shows that the ensemble emission brightens by a factor of 2.3 from 300 to 59 K, and by a factor of 2.2 from 59 to 4 K.

The experiment was repeated for different concentrations of glycerol in the host medium, with no significant spectral differences. No additional broadening was observed as a function of excitation intensity, but at higher powers, the emitters did bleach in a very short time.

The aforementioned inhomogeneous broadening can be circumvented by studying individual emitters. For data at the single-emitter level, we preferred a host medium containing PVA rather than glycerol, as explained before. Thus, we spincoated Ag:DNA emitters in PVA onto the substrate, using low Ag:DNA concentrations to ensure average emitter separations well above the diffraction limit, enabling us to study them individually.

At first, we verify at room temperature that our sample has a suitable spatial distribution of emitters. While still at room temperature, with the sample exposed to air, blinking on the second time scale is observed, and

bleaching in about five minutes. We proceed to flush the sample space with He gas, which reduced both blinking and bleaching. We conclude that, on the second time scale, blinking and bleaching are caused by the presence of components in air, most likely oxygen. Typical blinking at room temperature in air can be seen in Figure 2.3, where the sudden jump from an on to off state, and vice versa, indicates that we are indeed only observing a single Ag:DNA emitter, instead of a small group of emitters lying within an area of the size of the diffraction limit.

Due to their limited brightness at room temperature, single molecule spectra were quite noisy, as can be seen in Figure 2.4 a. There, the spectrum of an individual Ag:DNA1 emitter is shown with an emission peak at 646 nm and a fwhm of 51 nm (0.15 eV). This is comparable to the fwhm of the ensemble at room temperature shown in Figure 2.2 b. The single-emitter spectra will be discussed further below.

After cooling down to 1.7 K, we again excite a wide area of the sample and record images, for different excitation wavelengths. The images reveal that the individual emitters become brighter at low temperature, that the peak excitation wavelength varies from emitter to emitter, and that the excitation spectrum is broad at the $\sim 10$ nm scale. This is visualized in Figure 2.5. The false-color image shown there is constructed from three different images, collected at 575, 585, and 595 nm and encoded as red, green, and blue, respectively. These three images are then superimposed, resulting in Figure 2.5. The varying colors show that different individual emitters have different excitation wavelengths. Emitters with mixed colors absorb at two or three of the mentioned excitation wavelengths, as can be found in the schematic on the left of Figure 2.5, and roughly indicates the large width of the excitation line for that emitter. Because the peak emission wavelengths lie outside the laser tuning range, it was not possible to determine excitation line widths, but in all cases, they appear to be well above 10 nm.

From such an image, we pick several emitters, and for each of those, we use a fast-steering mirror to direct the focused laser spot to excite only that single emitter, and record its emission spectrum. Such a single-emitter emission spectrum is shown in Figure 2.4 c, and can be compared to a typical emission spectrum at room temperature in Figure 2.4 a, and a spectrum at 223 K shown in Figure 2.4 b. There, it can be seen that on a single emitter level, and an integration time of 60 s, the spectral width of the emission at

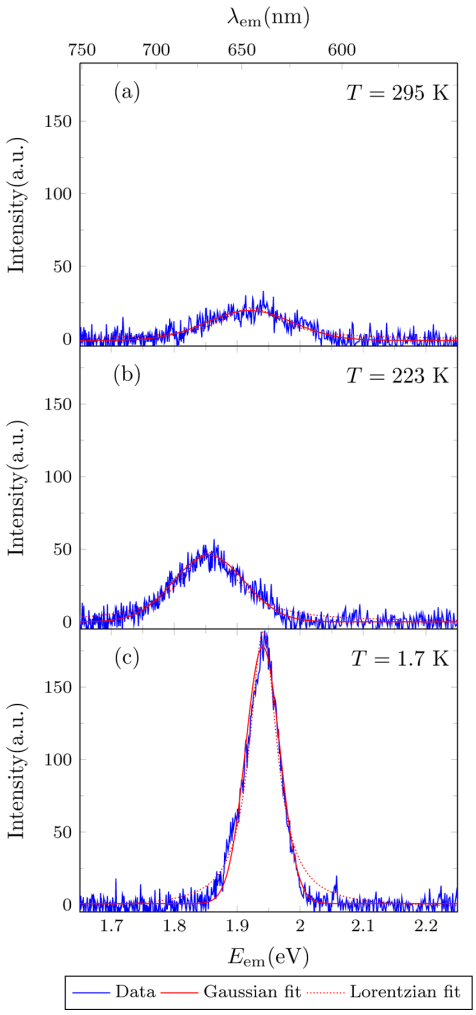


**Figure 2.4:** Emission spectra plotted versus photon energy of three different Ag:DNA1 emitters, with both Gaussian and Lorentzian fits. a) At room temperature, the single emitters are generally very dim, with an average fwhm of 50 nm or 0.15 eV. b) At 223 K, the brightness goes up. The spectrum shown here is of a different, individual emitter than the one from (a). As such, the position of the central peak is not related to temperature, but rather due to the difference in the individual emitters and their electronic environment, as discussed in the caption of Figure 2.7 and surrounding text. c) The spectrum of yet another individual Ag:DNA1 emitter, now at 1.7 K. As compared to the spectrum in (a), the brightness has increased by a factor of 5 and the line width has decreased to 23 nm or 0.070 eV for the specific emitter shown in (c). Averaging over 17 emitters, we find a fwhm of 26 nm or 0.079 eV at 1.7 K. The line shape is closer to Gaussian than Lorentzian, which is most apparent in the wings.

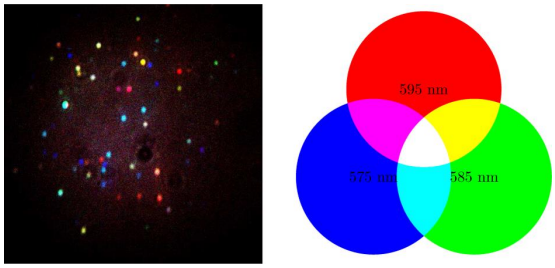


**Figure 2.5:** False-color image of the excitation dependence of emission from Ag:DNA1 emitters embedded in PVA. Results for Ag:DNA2 were similar. This left image consists of three superimposed CCD images: Excitation at 575 nm in blue, at 585 nm in green, and 595 nm in red, as schematically shown on the right. As such, the image illustrates (i) the spatial distribution, (ii) the variation of peak excitation wavelengths, as different emitters are indicated with different colors, and (iii) the $\sim$20 nm width of the absorption lines, as many emitters are mixed in color. Note that one or two emitters appear to be magenta-colored, i.e., they are bright at both 575 and 595 nm, but dim at 585 nm. This is due to the fact that they blinked during recording, and were mostly dark when recording the image at 585 nm. The size of the CCD image is 50 $\mu$m.

1.7 K has decreased by roughly a factor of 2, from 51 nm (0.15 eV) at room temperature to 26 nm (0.079 eV) at 1.7 K. Figure 2.4, where the spectra are plotted versus photon energy, clearly shows that a Gaussian profile fits better than a Lorentzian profile.

As discussed before, during cool-down we do not track the location of any given emitter continuously as a function of temperature. From the collection of individual emitters, we find that the average brightness at 1.7 K is, on average, a factor of 5.1 $\pm$ 0.9 higher than of an individual emitter at room temperature. This is consistent with the increase in brightness we found in the ensemble spectra, as seen in Figure 2.2. Additionally, this result is reminiscent of earlier work on 77-300 K ensemble emission spectroscopy of histidine-protected $Au_{10}$ clusters [64], where the decrease in brightness with increasing temperature was attributed to an increase in the non-radiative energy loss rate, due to thermally activated trapping of electrons in surface states. The same mechanism may account for the dimming of emission with increasing temperature that we observe. Note, however, that the line widths we obtain here are much smaller than found in the ensemble studies of $Au_{10}$, in which

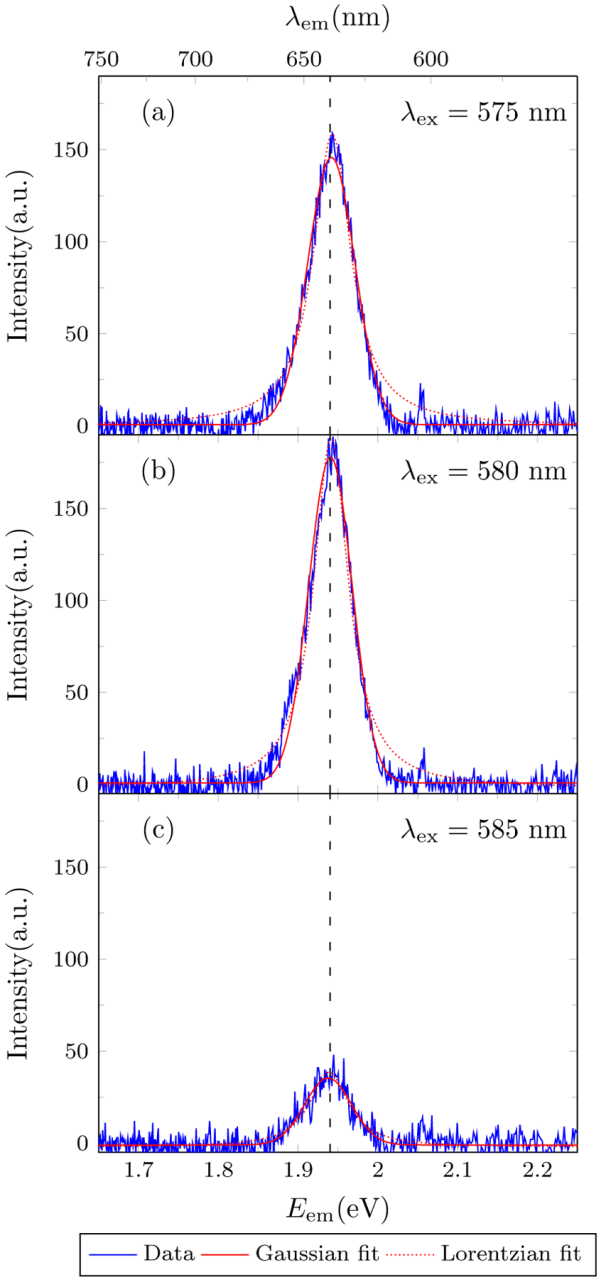


**Figure 2.6:** Emission spectra as a function of photon energy of the same Ag:DNA1 emitter at 1.7 K, for the excitation wavelengths (a) 575 nm, (b) 580 nm, and (c) 585 nm. The emission peak stays at 1.94 eV, or 639.1 nm, as indicated by the dashed line. The spectrum in (c) appears less bright, due to the fact that the emitter bleached during data acquisition.

the contribution of the inhomogeneous broadening to the line width was unknown.

As Figure 2.6 illustrates, (i) the single emitter has a broad excitation line and thus fluoresces for excitation for all three wavelengths, and (ii) the single emitter spectral shape does not depend on the excitation wavelength. As long as the individual emitter can be excited, its emission spectrum is a Gaussian shape with the same width, centered at the same spectral location. The specific emitter shown in Figure 2.6 is more efficiently excited at 580 nm than at 575 nm, and thus, the emission peak is stronger in Figure 2.6 b. Note, however, that the peak in Figure 2.6 c is much weaker due to the fact that the emitter bleached during data acquisition.

Across the population of Ag:DNA1 emitters in the field of view, the peak emission wavelength varies by tens of nm at 1.7 K (see Figure 2.7). The most 'blue' emitters that we found were centered around 620 nm, and the most 'red' emitters were centered at 670 nm. When averaging over multiple emitters, we find that the emission peak lies at 636 $\pm$ 17 nm (1.95 $\pm$ 0.05 eV). The variation in peak wavelength among individual emitters could be caused by local, nanoscale variations in the PVA embedding medium, such as local strain fields that deform Ag:DNA conformations and shift peak wavelengths. Another possible cause is that the different peak wavelengths correspond to slightly different structural isomers, e.g., with differences in binding sites on the DNA.

In contrast to the spread in emission peak locations, the single emitter line width varies relatively little across the population. At 1.7 K, we find a line width of 26 $\pm$ 4 nm (averaged over 17 emitters), corresponding to a line width of 79 meV. Thus, this large line width appears to be a property intrinsic to the Ag:DNA1 itself. Comparison to data on Ag:DNA2, which shows a substantially larger line width of 45 nm (124 meV), indicates that the line width is sensitive to the specific structure of the emitter.

Note that, for room-temperature data, the single-molecule spectra in Figure 2.4 a, with spin-coated PVA as the embedding medium, cannot be compared to the ensemble spectra in Figure 2.2 (bottom), with a glycerol solution as the embedding medium. Therefore, we repeated the single-molecule experiment in glycerol. At 1.7 K, the single emitter brightness was reduced by a factor of at least 3 relative to PVA, but the distribution of peak emission wavelengths, and the line widths, were similar. This indicates that the quantum

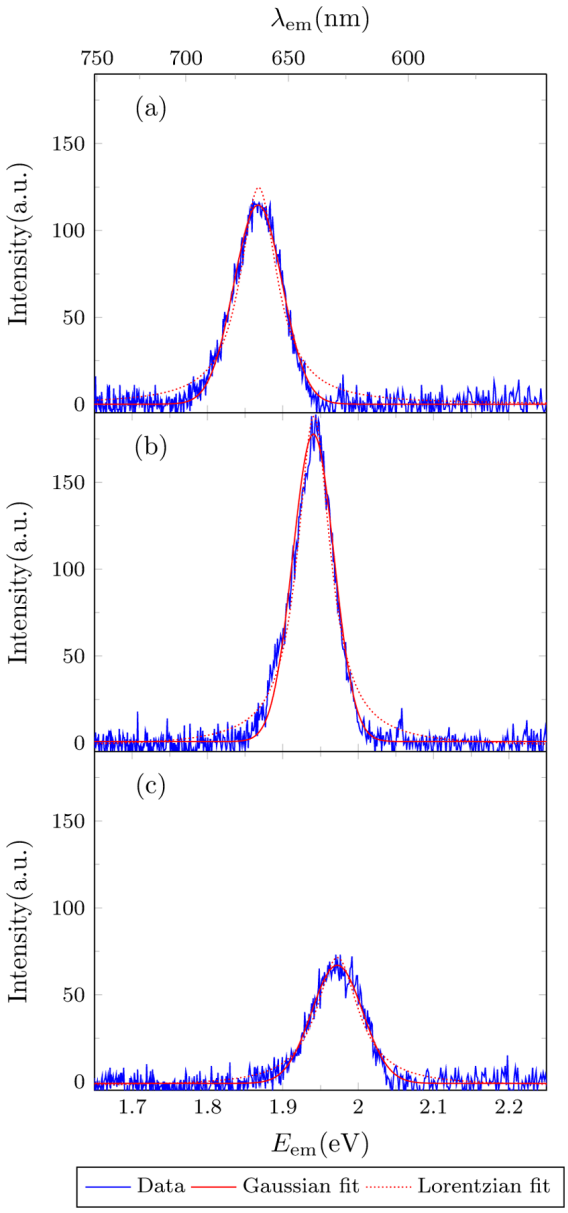


**Figure 2.7:** Emission spectra as a function of photon energy of three Ag:DNA1 emitters at 1.7 K excited at 585 nm, illustrating how the peak wavelength differs among different individual emitters. (a) and (c) lie toward shorter and longer wavelengths, respectively, when compared to an emitter closer to the mean (b). However, they all have a Gaussian profile with similar line widths. The spectra in (a) and (c) appear less bright than that in (b), most likely due to the fact that the peak of their absorption line is located farther from the laser excitation wavelength.

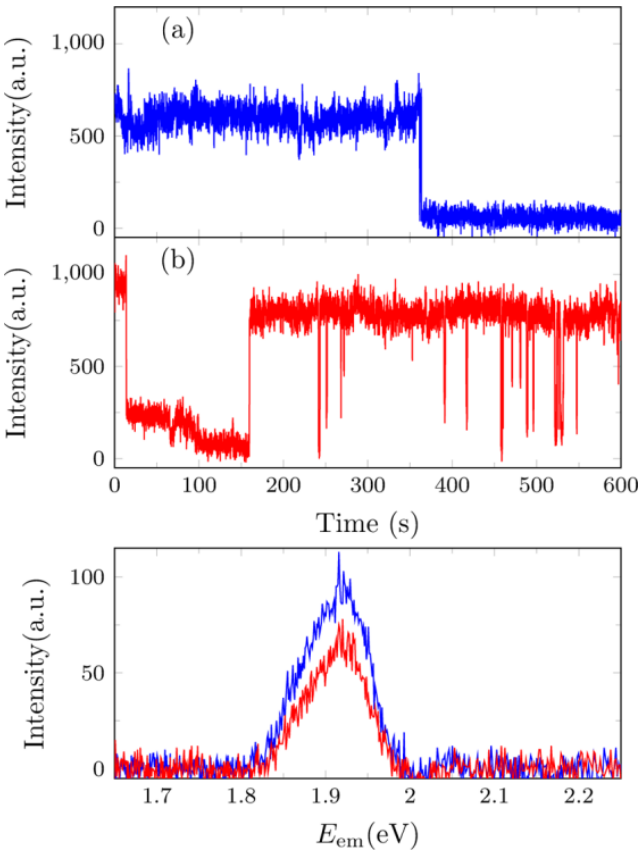


**Figure 2.8:** (a, b) Emission intensity as a function of time, of two Ag:DNA1 emitters embedded in PVA, at 1.7 K. a) Typical emitter, showing a single transition after 360 s, from the 'on' to the 'off' state. b) An atypical emitter, showing multiple on-off transitions, with many too short to be temporally resolved. c) Emission spectra of the aforementioned emitters. Spectrally, they are nearly identical, thus the slow blinking dynamics is apparently unrelated to the line width.

yield, and therefore the efficiency of the possible decay paths, can depend greatly on the chosen environment. In this case, it seems that, when comparing glycerol to PVA as a host medium, non-radiative decay is preferred over radiative decay.

Finally, we investigate the emission intensity as a function of time at low temperature, in order to study the dynamics on the second to minute time scale. In Figure 2.8 a, b we show the behavior of two single Ag:DNA1 emitters at 1.7 K embedded in PVA. Figure 2.8 a shows a single transition after 6 min, constituting bleaching. The fact that bleaching occurs in one step indicates that we were indeed observing one emitter. The stability of this emitter was representative of Ag:DNA1 at low temperature. The second emitter, Figure 2.8 b, was unusual in that it displayed blinking with short and long off-times. Considering that these emitters were spectrally quite similar, as shown in Figure 2.8 c, we attribute the differences in their blinking dynamics to the distinct, local microscopic environments. Regardless, the stability of the emitters at low temperature, as seen in Figure 2.8 a has improved when compared to the stability at room temperature, as shown in Figure 2.3.

## 2.4 Discussion

The main result of this work is that, on the single-emitter level, at low temperature, the Ag:DNA1 emission spectrum has a line width of 26 nm (79 meV) and shows a Gaussian profile. The factor of 5 difference in brightness at 1.7 K relative to room temperature can be explained by activation at higher temperatures of non-radiative decay, such as trapping. The behavior of Ag:DNA2 is very similar, with an even larger single-emitter line width of 45 nm. The question that remains is which mechanism causes this relatively broad spectral line at low temperatures.

Since the Ag:DNA solutions we study here are not chemically purified, we first comment on the fact that a given DNA strand can host different Ag:DNA species, with different spectral properties [9, 13, 65]. Of course, such Ag:DNA population heterogeneity affects the bulk solution measurements (Figure 2.1): different Ag:DNA complexes produce different emission peaks. However, population heterogeneity makes no contribution to the spectral properties of a single emitter, unless the individual emitter undergoes dynamic changes in bonding during the time required to collect the single emit-

ter spectrum. Such changes in bonding within a silver cluster are highly unlikely below 2 K [63]. Because calculations indicate that typical silver-base binding energies are $\sim$100 meV [65], it is also implausible that silver-base bonds would be breaking and reforming at the low temperatures we employ ($k_B T$ = 0.17 meV at $T$ = 2 K).

We next consider the possibility that dynamic interactions of an individual emitter with low- nergy fluctuations in its local environment are the source of the large line width. In particular, for fluorescent molecules embedded in amorphous media, the coupling of electronic transitions to fluctuations of the medium can produce temporal wandering of optical transition energies [66]. This spectral diffusion persists at low temperatures due to the presence of low-energy localized modes in polymer and glassy embedding media.

Due to the fact that the averaging times required to measure emission spectra of single emitters are typically longer than time scales for spectral diffusion, emission lines are broadened. Therefore, unless other broadening mechanisms dominate the line width, we would expect to see evidence for spectral diffusion in single emitter spectra of Ag:DNAs. The properties of the single Ag:DNA spectra lead us to conclude that spectral diffusion is unlikely to account for the broad emission lines at low temperature. Namely, if the absorbance line were wandering over time, a change in the excitation wavelength would shift the emission peak, because the emitter would excite most efficiently during times when the absorbance peak wandered closest to the excitation wavelength. Instead, we find that the emission peak is independent of excitation wavelength (Figure 2.6). Moreover, spectral fluctuations that arise from conformational changes are implausible as a major source of broadening, because emitters embedded in glycerol exhibit the same line widths as those embedded in PVA. Glycerol forms a hard glass, and is known to immobilize emitters in more compact conformations, as has been observed with light-harvesting complexes [67]. In contrast, PVA consists of long polymer chains with many degrees of freedom. It seems unlikely that these two very different media would result in the same line width, if spectral diffusion were the broadening mechanism.

Another potential, nonintrinsic source for the broad emission lines of Ag:DNAs is the excitation of phonon modes of the embedding medium or of the DNA, via the emitters dipole moment. In general, electron-phonon

coupling results in emission of a low-energy phonon of the immediate surroundings of the emitter, simultaneous with the electronic transition. The width of the resulting emission feature, the phonon sideband, is governed by the phonon density of states in the emitters environment and the energy dependence of the electronphonon coupling. For polymer embedding media at low temperatures, diverse fluorescent molecules all exhibit phonon sidebands with widths of $\sim$10 meV [68–70] and line shapes that are asymmetrically broadened toward high energies. The $\sim$100 meV, Gaussian emission lines of single Ag:DNA emitters are qualitatively different, in line width and line shape.

Because the typical broadening mechanisms that arise from environmental couplings of fluorescent molecules do not appear to fit the behavior of Ag:DNAs, we consider whether the vibronic levels of the cluster itself might result in the observed line shape. Vibrational mode energies for silver clusters of tens of atoms are on the order of 100 $cm^{-1}$ [71]. At low temperatures, transitions from the excited state to different vibronic levels of the ground electronic manifold would then give rise to a vibrational progression of narrow emission lines spaced by $\sim$10 meV ($\sim$ 3.5 nm, at 650 nm emission wavelength), resulting in an asymmetric comb-like shape. While the superposition of phonon sidebands from multiple vibronic transitions might result in a smooth rather than multi-peaked emission spectrum, we would still expect an asymmetric line shape at low temperatures, due to the absence of anti-Stokes processes. However, we observe a featureless, symmetric Gaussian line shape (see Figures 2.4 and 2.7).

From the above considerations, it appears that the optical transitions do not have a typical molecular character. While previous work on Ag:DNAs has assumed that the clusters are too small to support collective, plasmon-like excitations [10], we nevertheless turn to such a description in search of an explanation for the line width and shape. Comparison to results for small, bare silver clusters indeed suggests that the Ag:DNAs have collective, multi-electron excitations. Recent theoretical work has established the collective nature of the dominant optical excitation of Ag clusters composed of just $\sim$ 10 atoms [58], which display incipient plasmons at energies quite close to the value predicted by Mie theory, once the cluster shape is taken into account. Studies of smaller clusters of Na found a collective character in the low-energy excitations of $Na_2$, with just two free electrons [72]. For such a

phased collective excitation of multiple electrons, any process that kicks the phase of the collective excitation results in dephasing [73].

Because most quantum calculations for small clusters introduce the line width as a phenomenological constant, presently there is little information on what to expect for lifetimes in quantum-sized clusters. In much larger clusters, the decay of plasmons into single particle excitations (Landau damping) produces rapid energy relaxation together with dephasing, resulting in short excited-state lifetimes [60] that are incompatible with $T_1 \sim$ 1-5 ns, typical of Ag:DNAs [52]. However, in the quantum size regime, Landau damping can be strongly suppressed [60]. The few calculations that have treated dephasing at the fundamental level find complex dependencies of surface plasmon line widths on the size of spherical clusters [60], and dephasing line widths of $\sim$100 meV from surface plasmon coupling to zero-point shape fluctuations in $Na_8$ [59]. This latter mechanism leads to the expectation for strong dependencies of line widths on cluster shape. It also leads to line shapes with Gaussian tails, consistent with our results.

Our results, and comparison to previous work, indicate that dephasing in Ag:DNAs is quite sensitive to the specific cluster structure. In particular, the single-emitter line widths for Ag:DNA2 emitters are nearly twice as broad as for Ag:DNA1, even though their rather similar emission wavelengths ($\sim$ 620 nm, vs $\sim$ 680 nm) suggest similar overall structures. For ligand-free silver clusters frozen in noble gas matrices, ensemble measurements on size-selected clusters also indicate such structural sensitivity of the line width. Namely, fluorescence spectroscopy performed on small silver clusters (n = 2, 3) in gas matrices at room temperature [38, 74] suggest line widths around 80-160 meV, while ensembles of $Ag_9$ clusters frozen in Ar matrices showed very narrow emission lines ($\sim$2 meV) [41]. However, other measurements on absorption of $Ag_{5-11}$ clusters embedded in an Ar matrix at low temperatures [75] also yielded line widths on the order of 125 meV, and spectral data on matrix-stabilized $Ag_4$ revealed a line width of 0.1 eV [40], which is comparable to our results. These empirical results indicate that, even in the relatively simple regime of unligated silver clusters, line widths appear to be strongly dependent on the details of the cluster structure. If we assume that the $Ag_4$ results [40] are not artificially broadened by the ensemble, this could indicate that, while the Ag:DNA emitters we studied contain a larger total number of silver atoms, they may have a similarly low degree of Ag

coordination.

These considerations lead us to believe that the smooth, Gaussian line shape is intrinsic to the Ag:DNA itself, and that dephasing of a collective, multiple electron excitation is the most likely broadening mechanism.

## 2.5 Conclusion

In summary, we have performed a low-temperature spectroscopic study on single fluorescent Ag:DNA emitters. We find that when a single emitter is cooled from 295 to 1.7 K, the brightness goes up by a factor of 5, while the line width decreases by a factor of 2. These results indicate that cooling increases the efficiency of the radiative decay channels, while reducing the number of non-radiative mechanisms such as electron-phonon scattering. The single emitter line width of 26 nm (0.079 eV) at low temperature for an individual emitter, which is more than half of the ensemble spectral width, corresponds to a dephasing time of 17 fs, which we suggest arises from dephasing of collective excitations. Considering the line width of 26 nm (0.079 eV) and the $\sim$ 300 nm ($\sim$ 1 eV) spectral range of Ag:DNA peak emissions identified to date, this corresponds to the availability of roughly 10 independent color channels to future labeling applications.

# CHAPTER 3

## Polarization resolved measurements of individual DNA-stabilized silver clusters

Polarization resolved excitation and emission measurements on individual 10-15 atom silver clusters formed on DNA are presented. The emission is highly linearly polarized, typically around 90% for all emitters, whereas the polarization dependence of the excitation strongly varies from emitter to emitter. These observations support the hypothesis that the luminescence arises from collective electron oscillations along rod-shaped silver clusters, whereas the excitation process does not necessarily have a strong preferential polarization direction and thus may involve energy and/or charge transfer between the cluster and DNA. In addition to stabilizing the clusters, the DNA also appears to strongly influence the available paths for excitation.

This Chapter is based on: N. Markešević, S. S. R. Oemrawsingh, D. Schultz, E. G. Gwinn, D. Bouwmeester, *Polarization resolved measurements of individual DNA-stabilized silver clusters*, Adv. Optical Mater. **2**, 765 (2014).

## 3.1 Introduction

Advances in DNA nanotechnology and separation science have recently enabled the isolation of DNA-stabilized clusters of silver at the size scale of 10 to 24 silver atoms [53, 76]. Because these small clusters can be fluorescent [10], with high quantum yields, and because the specific DNA sequence strongly influences the optical properties of the stabilized clusters, these Ag:DNAs are beginning to be intensively studied for applications in sensing [16] and biolabeling [17]. Such silver "nanoclusters", with just tens of metal atoms, are in a different size regime from metal nanoparticles of several to tens of nanometers dimensions that are the focus of current nanoplasmonics research [1, 2, 77]. Thus, beyond their current uses as biolabels and sensors, metal nanoclusters that are stabilized by such a versatile ligand as DNA, which itself can assemble into elaborate nanoscale shapes [23], have the potential to realize metal-organic hybrid materials at truly nanoscale dimensions, enabling functionality at enormously high spatial densities [33, 78]. Given their nanometer size scale, such cluster-based materials may also combine desirable properties usually associated with the molecular regime, such as high fluorescence quantum yields and large Stokes shifts, with emergent near-field interactions arising from the polarizability of free electron systems, as currently exploited in Surface-enhanced Raman Spectroscopy (SERS) [79], and plasmonic coupling schemes with metal nanoparticles [78].

Despite the numerous Ag:DNA [13, 17, 20, 51, 52, 65, 80] studies, little is known about the mechanism by which fluorescent excitation and emission occur. It was previously established in the literature on small metal clusters that the excitation energies are considerably up-shifted from the particle-in-box energies, due to Coulomb interactions that lead to collective, phased oscillation of the clusters valence electrons [72, 81]. Recent experimental works [19, 21] indicate that fluorescent Ag:DNA contains a neutral silver core that is surrounded by base-bound silver ions. This arrangement is analogous to the known structure of gold clusters that are stabilized by small organic ligand molecules [4, 82, 83], which possess both transitions associated with the gold core, and transitions involving charge transfer between the gold core and the surrounding ligands plus their directly attached gold atoms [82, 83]. For Ag:DNAs, the specific mode of cluster-DNA binding is unknown, but given the existence of a neutral silver core one might expect both core-centered tran-

sitions and charge transfer transitions between the core and base-attached silver ions.

In the case of such silver core-ligand transitions, small variations in the specific conformation of the DNA might be expected to affect directions of transition dipole moments. Thus it is of great interest to study individual Ag:DNAs under conditions that minimize environmental fluctuations, using techniques that can probe such orientational effects.

In this Chapter, we present single-cluster optical studies of Ag:DNAs that investigate both their response as a function of the polarization of the excitation light and the polarization of the light they emit. Single particle polarization studies have previously been used to investigate individual fluorescent molecules, providing insight into the orientation of the emitters in the surrounding medium [84, 85] as well as photophysical events of single molecules, such as rotational jumps of a single dipole, transitions into a dark state (reversible and irreversible photobleaching) and spectral jumps [86]. Another example of the strength of polarization resolved measurements is the study of $Au_{25}$ nanoclusters stabilized by bovine serum albumin (BSA) [5]. Such experiments have also been carried out on much larger, individual metal nanoparticles, revealing the strong dependence of polarization response on shape [3].

We will use conventional far-field polarization imaging in which the detected dipole is projected onto the imaging plane. A polarization rotator controls the polarization of the excitation light, and the emission is collected after passing through a polarizer. This technique determines the sensitivity of the emission to the polarization of the excitation light together with the polarization of the emission. A tilt of an individual Ag:DNA out of the imaging plane will only reduce the detection intensities without affecting the polarization modulation depths [87].

Here we focus on two distinct Ag:DNA emitters. Emitter A is a silver cluster stabilized by a native DNA hairpin strand with 6 bases in the loop and 4 base pairs in the stem. Emitter B is a silver cluster stabilized by 28 base long DNA strand. These emitters produce relatively stable and bright fluorescence following excitation within the spectral range of a ring dye laser (see section 3.4 for details).

## 3.2 Results and discussion

The focus of this work will mainly pertain to linear polarization properties. We will show that the emission of Ag:DNAs is nearly completely linearly polarized, whereas the polarization of the absorbed light largely varies from emitter to emitter. While the linearly polarized emission of the Ag:DNAs is consistent with collective electronic oscillations along the longitudinal axis of a rod, the emitter-dependent excitation polarization behavior implies the importance of the DNA environment of the Ag cluster in the absorption process.

For a given set of excitation and detection polarizations, we obtain a number of bright spots on the CCD camera (Figure 3.1 a). Most spots are circularly symmetric and diffraction limited. Furthermore the maxima of the emission from different spots have comparable intensities but occur at different polarization settings. These features indicate that we are observing an ensemble of individual optical emitters. A small number of spots, approximately 5%, have very different properties; in particular they are significantly brighter, show hardly any polarization dependence, and have sometimes an asymmetric shape. These emission properties are typical for small clumps of multiple emitters and of certain fluorescent impurities, and therefore we exclude them from our study of individual emitters.

To determine the intensity of each individual emitter, we first select a rectangular area, typically 30 by 30 pixels, approximately 10 times as large as diffraction limited spot, containing an emitter (Figure 3.1 a). Taking the pixel with the maximum number of counts as the center of the Gaussian, it can be plotted as a function of radius (Figure 3.1 b), and fitted according to:

$$f = a + b \cdot exp(-x^2/\sigma^2), \tag{3.1}$$

where $a$ is a constant offset representing background fluorescence, $b$ describes the height of the Gaussian, and $\sigma$ is the width which is set by the point spread function of the optical system.

The detected intensity $I$ of an emitter (which is in general a function of the angle between the excitation and detection polarization and of the orientation of the Ag:DNA) is then proportional to the volume of the Gaussian term in Eq. 3.1. Since the spots are diffraction limited $\sigma$ should be mainly determined by the optical imaging system, not by the properties of the emitter.

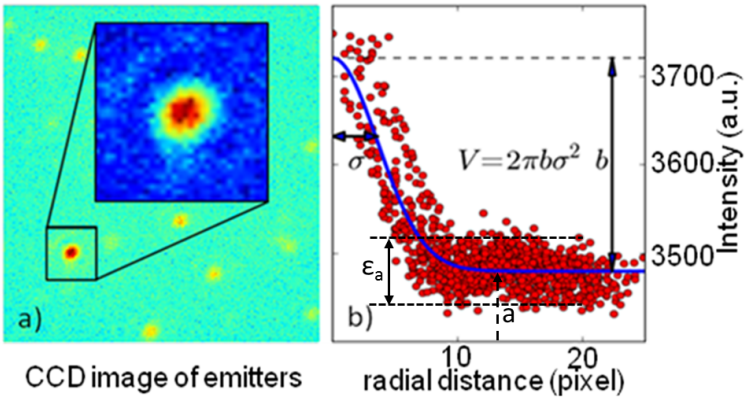


**Figure 3.1:** DNA:Ag emitters observed by a cooled CCD camera. The intensity per emitter is determined by selecting a rectangular area around the emitter (a), and fitting a cylindrical Gaussian function with a constant offset to the pixel intensity as a function of distance from the intensity maximum, which is the position of the emitter (b). From the fitted parameters, we calculate the emitter intensity. $\varepsilon_a$ represents the noise floor of the measurements.

Indeed, this fitting parameter turns out to have approximately the same value for emitters when measured near the optimal polarization settings. Therefore the integral of the exponent in Eq. 3.1 can be approximated by a constant, and the measured intensity $I$, becomes proportional to $b$. In order to determine the error bars on a given data point we perform an error propagation using the full covariance matrix based on the fitting parameters $b$ and $\sigma$. Applying the same procedure to each image, for each set of excitation and emission polarization angles (361 images in total), allows us to produce a contour plot, where the emitter intensity (color scale) is given as a function of the excitation, $\theta_{ex}$, and emission, $\theta_{em}$ , polarization angles (Figure 3.2).

In order to extract polarization modulation characteristics of the emission process, we consider the intensity of the emitter as a function of excitation (emission) polarization angle, for a fixed emission (excitation) angle. The vertical and horizontal slices of the contour graph in Figure 3.2 b, c show examples. For each slice, we fit the modulation depth, $M$, and a scaling factor, $N$, using the following relation:

$$I(\theta) = N(1 + M\cos(2(\theta - \phi))), \tag{3.2}$$

Here, $\theta$ is the fixed emission (or excitation) polarization angle and $\Phi$ is the (random) orientation angle that the Ag:DNA makes with the polarization axes. Thus we extract a modulation depth, $M$, for each fixed polarization angle, $\theta$. Applying the same procedure to cross-sections $10^\circ$ apart, we find the modulation depth of the emitter, $< M_{em} >$, and the orientation angle, $< \Phi_{em} >$ as the error-weighted averages over all angles for which there was sufficient signal.

We note that the typical offset, $a$, as extracted from fitting graphs like the one presented in Figure 3.1 b is an order of magnitude larger than $b$, indicating a significant background emission. The noise level of this background emission is indicated as $\varepsilon_a$ in Figure 3.1 b. For polarization settings at which a specific emitter is near its minimal emission, $b$ becomes comparable to, or smaller than $\varepsilon_a$, and the fit becomes unreliable. Those data points are indicated as blue points in graphs d)-g) and are omitted in determining $< M >$ and $< \Phi >$.

To place the results shown in Figure 3.2 within a broader context, we discuss results of prior polarization measurements on individual dye molecules and metal nanoparticles. For individual fluorescent dye molecules, polarization measurements are limited to highly photostable dyes that permit collection of many photons before bleaching. [86] The dependence of the emission intensity, $I$, from a single molecule on the excitation polarization angle, $\theta_{ex}$, probes the orientation of the molecule's absorption dipole moment, $\mu_{ex}$. The dependence on the angle of emission polarizer, $\theta_{em}$, probes the orientation of the molecule's emission dipole moment, $\mu_{em}$.

Single molecule polarization studies on various dye molecules have found the same functional dependence on both angles, $\theta_{ex}$ or $\theta_{em}$, given by Eq. 3.2. In principle, the molecular orientation, described by $\Phi$, can differ for excitation and emission if the molecule undergoes orientational reorganization within the fluorescence lifetime. As long as emission is from the same electronic manifold as that of the initial excited state, such effects are typically small: the largest quantified shift in single molecule orientation was $\sim 5\%$, for Cy5. Regardless, for single molecular fluorophores the modulation depth $M$ is unity for excitation and for emission, corresponding to ideal dipole behavior in both cases [86, 88].

In contrast, the polarization modulation depth for metal nanoparticles, much larger in size than the few atom silver clusters addressed in this

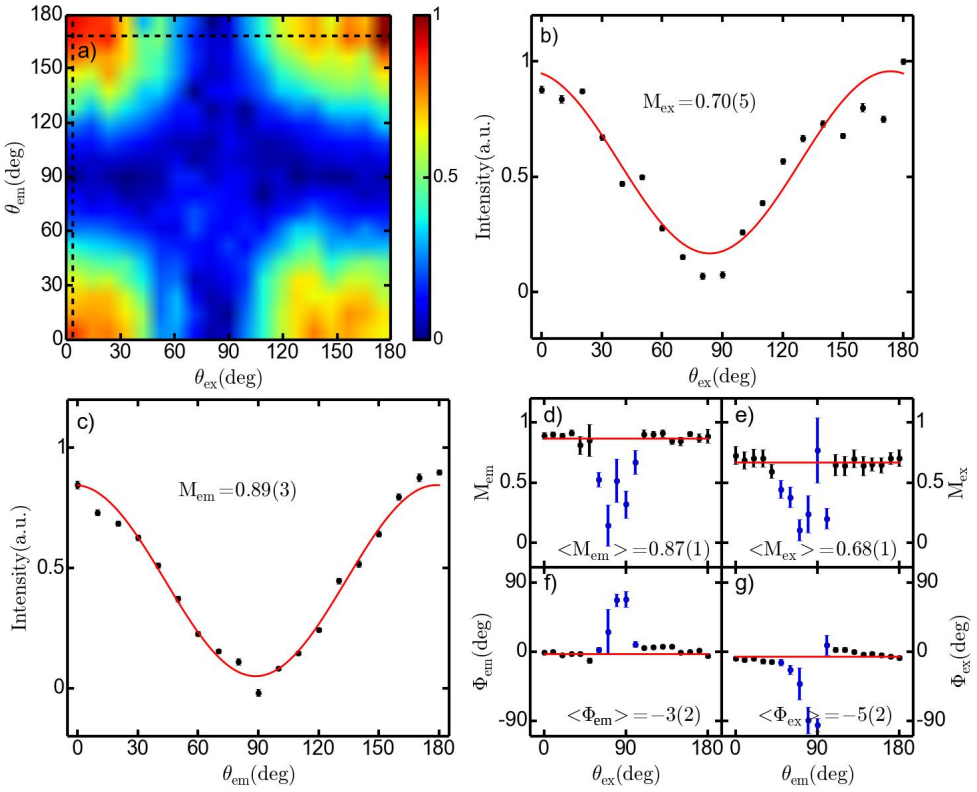


**Figure 3.2:** Polarization measurement of a single emitter. a) Intensity (color scale) of the emitter is presented as a function of excitation, $\theta_{ex}$, and emission polarization angles, $\theta_{em}$. Each of the cross-sections at constant excitation or emission polarization angle (vertical and horizontal) is fitted with the expected dependence for an ellipsoidal cluster (in the text) from which we obtain modulation depth, $M$, and phase, $\Phi$. b) Cross-section for $\theta_{em} = 170°$ gives $M_{ex} = 0.70(5)$. c) Cross-section for $\theta_{ex}$=0° gives $M_{em} = 0.89(3)$. d) Averaged emission modulation depth and e) averaged phase of the emitter are extracted from an error weighted linear fit (red line) of the data points from the cross-section fits. f) Averaged excitation modulation depth and g) averaged phase are found similarly as for d) and e). Cross-sections for which the intensity of the emitter is smaller than, or equally to the noise floor $\varepsilon_a$, (see Figure 1b) are indicated as blue regions in (a). As explained in the text, data points extracted from those cross-sections (blue data points in 2d-g) are not reliable and are therefore excluded in determining the average modulation depth $< M >$.

work, varies widely with a strong dependence on the specific nanoparticle shape [3]. Since the fluorescence quantum yields of metal nanoparticles are very small ($\sim$ 0.001% or less) [2, 89], most polarization measurements have focused on determining the single nanoparticle extinction as a function of the polarization, $\theta_{ex}$, of the excitation light, using techniques such as photothermal imaging [90], light scattering microscopy [91], and extinction microscopy [92]. The intensity dependence on $\theta_{ex}$ has the same overall sinusoidal form as for individual molecules ( Eq. 3.2). The modulation depth $M$ vanishes for perfectly spherical particles, because any polarization angle gives the same excitation rate of the collective, plasmonic mode of the free electrons. For real nanoparticles with slight deviation from perfectly spherical shapes, $M$ is found to be $<\sim 0.1$ [3].

In the case of rod-shaped or ellipsoidal metal nanoparticles, the polarization response is quite different from that of spherical particles [3]. The anisotropic shape results in more than one collective excitation: a low-energy longitudinal mode and a higher energy transverse mode [83]. The development of sensitive photothermal imaging techniques has enabled direct measurement of the dependence of the absorbance of gold nanorods on excitation polarization, for rods with dimensions of $\sim$ 25 nm x 75 nm, corresponding to $\sim 10^6$ Au atoms [89]. For these nanorods, single particle measurements at the energy of the longitudinal mode find modulation indexes $M$ very close to 1 for rods with aspect ratios (length to diameter) of $\sim 3$, while measurements at the energy of the transverse mode find $M << 1$. Thus, at energies near the longitudinal mode, the polarization dependence of the absorbance again has the ideal dipolar form.

Based on these prior studies, we would expect that if silver nanoclusters behaved like single dye molecules, the fluorescence intensity would exhibit $M = 1$ for both excitation and emission. If instead they behaved as nearly spherical nanoparticles, the fluorescence intensity should exhibit $M << 1$, as a function of both $\theta_{ex}$ and $\theta_{em}$. On the other hand, for rod-shaped nanoparticles near the longitudinal resonance, the fluorescence intensity should exhibit $M = 1$ as a function of both $\theta_{ex}$ and $\theta_{em}$. Figure 3.2 shows that for an Ag:DNA emitter of type B, we obtained $< M_{ex} >= 0.70(5)$ and $< M_{em} >= 0.89(3)$. Other individual emitters of both types B and A that were photostable enough to enable a collection of the full two-dimensional polarization scan also showed similar characteristics. However, because the

two-dimensional raster scan of $\theta_{ex}$ and $\theta_{em}$ in Figure 3.2 a requires long exposure times, approximately 1 hour, most emitters photobleach before the full contour map can be collected. The full contour plot has some redundancy of information for determining the excitation and emission modulation. We removed this redundancy, thereby decreasing the measurement time and enabling the study of a larger population of emitters, in the following way. To determine the excitation modulation depth, for each individual emitter we collect all emission while varying the excitation polarization angle. To determine the emission modulation depth, we excite emitters using right circularly polarized light, while varying the emission polarization angle. In order to check that the emission modulation $< M_{em} >$ is independent of the excitation polarization, we performed additional measurements using linear and circularly polarized excitation light and confirmed that there is no significant modulation dependence on the excitation polarization.

For individual emitters we extracted the excitation and emission modulation depths. Figures 3.3 a, b show the results for type A emitters. From the obtained statistics and the scattered values of excitation modulation depth, we can conclude that the excitation properties vary significantly amongst emitters. This variation can be rationalized by considering that the DNA may adopt a range of conformations relative to the clusters. Even at low temperatures, small changes in conformation of the polymer-like DNA strand around an individual cluster may occur over the timescale of the experimental measurement. To the extent that the DNA affects the excitation of the cluster, for example by energy or charge transfer processes, such conformational variation could produce fluctuations in the excitation moment orientation, resulting in a lowered excitation modulation depth on the time-average. Variation in the details of the average DNA conformation from emitter to emitter could then account for the wide spread in excitation modulation depths evident in both Figure 3.3 a (type A emitters) and Figure 3.3 c (type B emitters). This picture can give a plausible explanation for an excitation modulation depth significantly different from the value of 1.0 expected for an ideal dipole.

Comparing our polarization resolved data with the results from reference [5] on BSA-stabilized $Au_{25}$ nanoclusters, we come to the conclusion that the systems are quite different. For the stabilized $Au_{25}$ clusters, absorbance spectra spread broadly across the UV-visible and the excitation polarization anisotropy depends on excitation wavelength. For the DNA-stabilized sil-

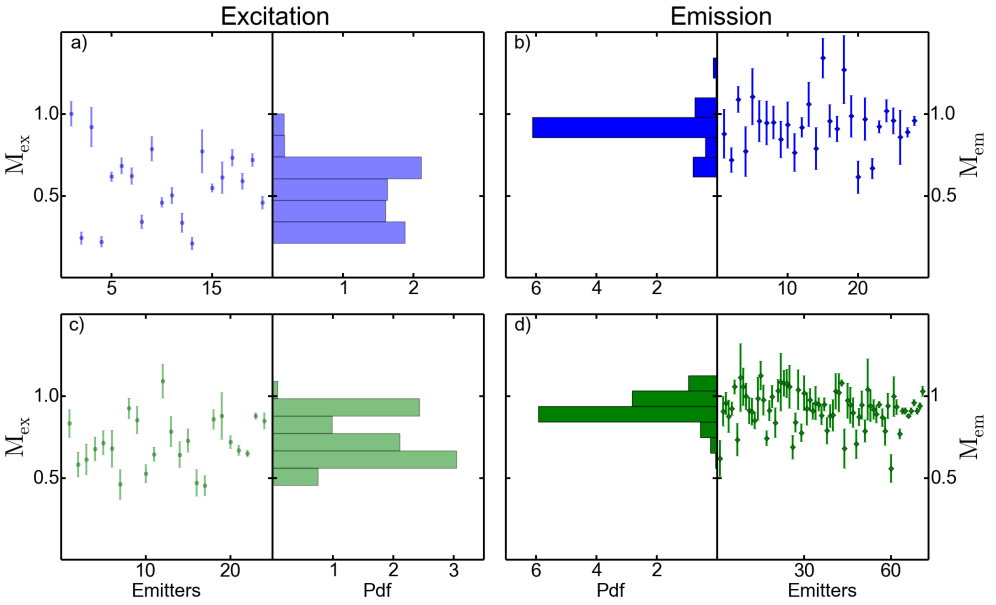


**Figure 3.3:** Modulation depth of Ag:DNAs of type A (blue) and B (green). Histograms of excitation modulation depth values for 20 emitters of type A (a) and 24 emitters of type B (c) show scattered values. On the other hand, the emission modulation depths for 28 emitters of type A (b) and 71 emitters of type B (d) clearly show peaks centered around 0.92 and 0.88 for types A and B, respectively. The value of the probability density function (Pdf) is normalized, such that the integral over the range is equal to one.

ver clusters, pure solutions exhibit a single, narrow peak in the absorbance at an energy that depends on cluster size [53]. Corresponding to this qualitative spectral difference from BSA-$Au_{25}$, our single emitter polarization measurements on Ag:DNA found no dependence on the excitation wavelength (within the tunable range of our laser, 575-595 nm). These marked differences in behavior may arise from the smaller $s - d$ splitting in gold, which produces more complex optical properties in Au relative to Ag clusters due to mixing of d and s orbital transitions in the former [22].

In striking contrast to the excitation modulation depth, Figures 3.3 b and 3.3 d show that emission modulation depth values are close to unity, the ideal dipole limit, for both types A and B emitters. Apparently the additional degrees of freedom that result in widely spread, and overall lower, excita-

tion modulation depths have much less effect on emission polarization. It seems that the emission path is much better defined, consistent with a longitudinal collective electronic mode along the cluster, as suggested in previous work [89].

Single emitter studies of the MEH-PPV heptamer also showed highly polarized emission but not excitation, similar to the Ag:DNA, but with more broadly distributed excitation modulation depths [93, 94]. For this molecular chain the polarization properties were explained by considering that excitation can take place anywhere along the generally bent chain, but the emission is only coming from a small, approximately straight, section where the optically generated electron-hole pairs will be trapped and recombine.

In the case of the Ag:DNA we expect that both the absorption and emission are localized within a relatively small region that holds the few atom silver cluster since the silver is essential for both the absorption and emission. Together with the typical shift of $\sim 60$nm between the excitation and emission wavelengths, this suggests that the excitation involves energy and/or charge transfer to the Ag cations and/or host DNA that support the central silver cluster. The excitation is therefore only partially linearly polarized along the axis of the cluster. The small metallic cluster is likely to act as an antenna that enhances the incoming optical field, thereby enhancing the absorption probability in its direct vicinity. The excitation will rapidly decay due to the numerous degrees of freedom in the complex system to an electronic excitation within the central silver atoms. Modeling the emitter as a several-atoms long silver rod with conducting electrons gives reasonable agreement with the observed emission wavelength [22].

## 3.3 Conclusion

We have measured the polarization-dependent excitation and emission properties of single Ag:DNA emitters. Measurements on many individuals of two different types of emitters at 1.7 K reveal a large emission modulation depth, indicating that these small clusters have properties similar to noble metal nanorods, typically containing millions of atoms. For comparison, the typical emission modulation depths of $\sim 0.9$ that we find for fluorescent silver clusters would correspond to a length to diameter aspect ratio of $> 1.6 : 1$ in the limit of much larger silver nanoparticle rods [95]. On the other hand, the

disperse values for excitation modulation depth indicate that the excitation pathways differ from those for emission. Thus we ascribe the luminescence mechanism to the collective electron oscillations, while the excitation may involve energy and/or charge transfer between the cluster and DNA. The improved characterization of the optical properties of the individual Ag:DNA emitters provides qualitative insight in the optical processes and valuable input for the quantum mechanical modeling of these complex structures.

Furthermore, it also provides information on how to construct more elaborate patterns containing many interacting emitters with aligned dipole moments. The above findings are likely to apply to all DNA-encapsulated noble metal clusters. The DNA molecule is likely not only a stabilizing agent, but may also actively participate in the excitation process. Our polarization microscopy studies reveal behavior of DNA-stabilized silver nanoclusters that differs in distinctive ways from the characteristic behaviors of both the molecular and metal nanoparticle regimes. Thus, novel photophysics is emerging from metal clusters with $\sim$ 1nm size scales, held within a DNA environment.

## 3.4 Experimental methods

Synthesis of fluorescent Ag:DNA clusters: Samples were prepared by mixing oligonucleotide (IDT, standard desalting) with ammonium acetate (99.999%, Sigma Aldrich) and $AgNO_3$ (99.9999%, Sigma Aldrich). After 20 minutes of incubation, a reducing agent $NaBH_4$ (99%, Sigma Aldrich) was added to the solution, producing fluorescent emitters. The emitter A is stabilized by a native DNA hairpin (5-CCG-CCA-CCC-CGC-GGT-3), containing 5 Cytosines (C) and 1 Adenine (A) in the loop and four base pairs in the stem. It was used without further purification. Final concentrations are: (50 $\mu$M) DNA, (350 $\mu$M) $AgNO_3$, (100 $\mu$M) $NaBH_4$, and (20 mM) ammonium acetate.

The second emitter, B, is stabilized by a 28 base long DNA strand (5-CAC-CGC-TTT-TGC-CTT-TTG-GGG-ACG-GAT-A-3). Final concentrations are: (5 $\mu$M) DNA, (50 $\mu$M) $AgNO_3$, (25 $\mu$M) $NaBH_4$, and (10 mM) ammonium acetate. Emitter B was HPLC purified using a Waters 2695 Separations Module with autoinjector and a Waters 2487 Dual Wavelength absorbance detector (10 $\mu$L volume), set to monitor the visible peak of each silver cluster. Separations used linear gradients from 15% to 35% of B (35 mM TEAA/MeOH) with A (35 mM TEAA/$H_2O$) on a 50 mm 4.6 mm Kinetex C18 core shell col-

umn with 2.6 $\mu$m particle size and 100 Å pore size (Phenomenex). Following HPLC purification, samples were dialyzed overnight into (50 mM) ammonium acetate using 10 kDa MWCO MINI dialysis units (Thermo Scientific).

The composition of emitters B, 15 silver atoms on the DNA strand, was identified previously by mass spectrometry of the pure material [19]. Based on the established correlation between the silver content and the excitation/emission properties, the number of silver atoms in emitter A is similar.

Characterization method: Samples were diluted in 5 mg/ml poly(vinyl alcohol) (PVA) and spin-cast onto a fused silica substrate. In order to suppress blinking and increase signal to noise ratio, all the measurements were performed at 1.7 K. The samples were mounted in a custom-built helium-bath cryostat and were excited at a wavelength of 585 nm by the ring dye laser (Coherent 899) with Rhodamine 590 Tetrafluoroborate dye (Exciton). The excitation light was filtered with a short-pass filter (edge at 600 nm), while the emission path contained a band-pass filter centered at 647 nm, with a width of 57 nm. A dichroic mirror (edge at 600 nm) was used to separate the excitation and emission paths. A polarization rotator controlled polarization of the excitation, whereas the emission was collected after passing through a polarizer. In order to preserve excitation and emission polarization in our experiment, we used a 0.8 NA objective inside the cryostat for both the excitation and the collection of the emission light. Fluorescence of the emitters was detected with a cooled CCD camera (Ikon-M 934-BR-DD, Andor Technology).

# CHAPTER 4

## Optical properties of the DNA-hosted silver clusters (Ag:DNAs) on DNA tiles and tubes

In this Chapter we investigate the influence of temperature on fluorescent silver clusters stabilized by single-stranded DNA, both free in solution and as a part of larger self-assembled structures such as DNA tiles and tubes. The emitters we investigate exhibit two fluorescent species, 'green' and 'red', which behave differently during the heating process. Namely, the 'green' species typically shows a fluorescence intensity increase during the heating process in the case of free emitters, emitters on the DNA tubes, and emitters on DNA tiles. However, in the case of the 'red' fluorescence species, the free emitters show a significant decrease of the fluorescence signal, whereas the signal increases for the emitters on the tubes and tiles. By sets of measurements at different temperatures, we explore the origin of these differences which might be associated to the intrinsically different structures and stability of the 'green' and 'red' fluorescent species. One important aspect appears to be that the silver atoms/ions attached to the DNA structure are mobile and can rearrange into the optically active clusters. This mobility seems restricted to distances smaller than the tile dimensions; thus, going from tiles to tubes would not have a significant impact on the fluorescent properties.

This Chapter is based on a manuscript in preparation for publication: N. Markešević et al.

## 4.1 Introduction

The DNA molecule is an important building block in nanotechnology [23, 24]. Self-assembly of DNA strands enables creation of elaborate DNA scaffolds which are not accessible with top-down techniques. These scaffolds are used for precise positioning of organic molecules [25, 26, 96], quantum dots [26], and plasmonic particles [26, 96, 97], and also for creation of chiral structures [28, 78].

Here we examine the optical properties of a very special kind of emitters, DNA-stabilized silver clusters (Ag:DNAs) [10, 13], both free in solution and on DNA scaffolds such as tiles and tubes. Ag:DNAs can be synthesized directly onto DNA scaffolds following the already published procedure [33]. DNA encapsulated silver clusters have attracted a lot of attention due to their small sizes (10-20 atoms) [19], high fluorescent quantum yields [80], low cytotoxicity [17], and spectral sensitivity to certain heavy metals [16] and even to single base mutations in DNA [98]. Ag:DNAs represent an intermediate size regime between organic dyes and large metal clusters [3]. The sequence of the encapsulating DNA strand determines the optical properties of the silver cluster [13, 52]. From cryogenic microscopy and spectroscopy, it has been concluded that the fluorescence spectra of individual Ag:DNA emitters are very broad, even at 1.7 K ($\sim$ 27 nm) [20] and that their shape is rod-like [19, 99], leading to linearly polarized emission [99]. In general, the chemical yield of fluorescent cluster formation is low, but the samples can be purified [53, 76]. The properties of Ag:DNAs have been discussed in more detail in the recent review articles [100, 101] and in Chapters 2 and 3.

In this chapter we focus on temperature-induced changes in the optical properties of Ag:DNAs. Synthesized on much larger DNA structures such as DNA tubes (where the distance between emitters is smaller than 10 nm) [33] and tiles, their properties, including chemical stability and emission, differ from the properties of their free counterparts. There are several possible reasons for this difference. Emission quenching could take place as a result of a high density of emitters on the tubes. Or, emission enhancement could be caused by coherent collective effects. Also, extended DNA structures might lead to changes due to different strain conditions, different electronic conditions, and/or different mobility of Ag atoms. Furthermore, such larger DNA structures can be a reservoir for Ag ions that are mobile, especially at higher

temperatures.

To investigate the possible causes of DNA scaffold-induced changes on Ag:DNA, we perform temperature-controlled measurements on solutions of free emitters, emitters synthesized on the tubes, and emitters synthesized on tiles which cannot form tubes. Above the melting temperature of the tubes, the emitters are sufficiently far apart in solution such that their potential near-field interactions cannot occur. Our approach is to monitor the change of the emission intensity of the emitters during the heating process.

## 4.2 Synthesis of Ag:DNAs, DNA tiles and tubes

The optical emitter used in this chapter is the 9C emitter so-called because the encapsulating DNA strand contains 9 cytosines in a single-stranded loop that is closed with a double-stranded stem (see Table 4.1, top row, and Figure 4.1a). To synthesize free 9C emitters, that is, 9C emitters are not attached to a larger DNA scaffold, we dilute native strands 9C-hairpin, in an ammonium acetate/magnesium acetate buffer (8 mM/2 mM). Then we add $AgNO_3$, and after 30 minutes we reduce the silver ions with $NaBH_4$. The final concentrations are 20 $\mu$M DNA, 140 $\mu$M $AgNO_3$, 40 $\mu$M $NaBH_4$ and 2 mM/0.5 mM ammonium acetate/magnesium acetate buffer .

For the synthesis of DNA tube scaffolds, we followed the procedure by O´Neill et al. [33]. Five DNA strands from Table 4.1, SE1-9C, SE2, SE3, SE4 and SE5 (final concentrations 2 $\mu$M) were mixed together in ammonium acetate/magnesium acetate buffer (40 mM/10mM), heated to 95°C and then cooled to room temperature over two days. These five strands are programmed to form tiles, 'unit cells' of the tubes. Each tile has four sticky ends, chosen such that the 'diagonal' sticky ends are complementary (Table 4.1). There are typically seven tiles in the circumference of the tube. Upon formation of tubes, we synthesize silver clusters by adding $AgNO_3$ and $NaBH_4$ (2.8 $\mu$L of 192 $\mu$M $AgNO_3$ and 2.8 $\mu$L of 1 mM $NaBH_4$ in 50 $\mu$L of DNA tubes). The schematic representation of the tiles and the tube formation is given in Figure 4.1b. To form tubes, it is necessary to neutralize the negatively-charged backbone of the DNA with $Mg^{2+}$ ions. For comparison of the emitters on the tubes to the free emitters, we synthesized the free 9C emitters in a similar buffer.

Because the sticky ends on the tiles are only 5-base long, and because the

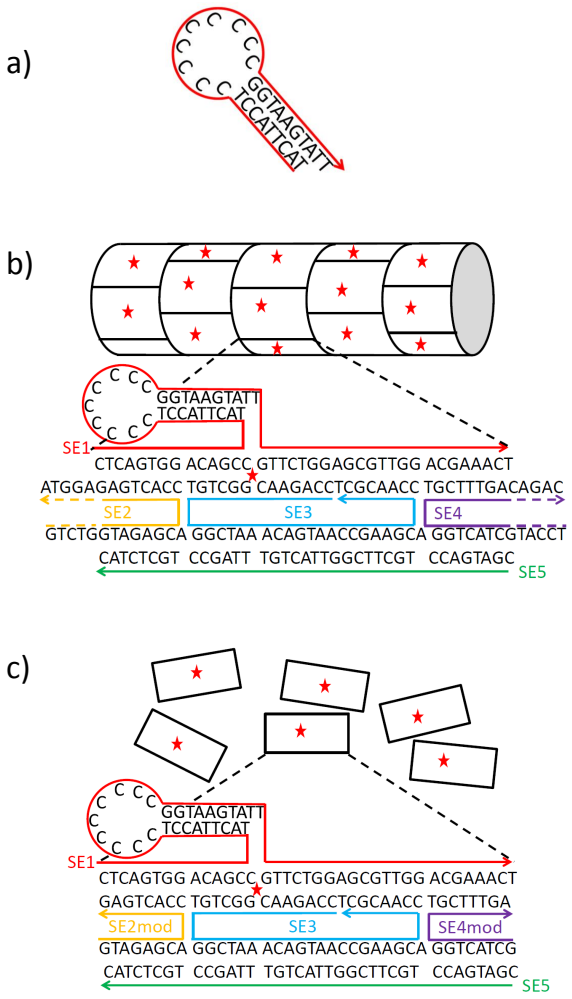


**Figure 4.1:** Schematic representation of the 9C hairpin (a), DNA tubes (b), DNA tiles (c). a) 9C hairpin consists of 9 cytosines in the loop and 9 base-pair-long stem. b) As demonstrated by O´Neill et al [33], five strands SE1-9C, SE2, SE3, SE4, SE5 can be mixed together such that the tiles with 5-base-long protrusions, sticky ends, are formed (dashed lines of strands 2 and 4). The neighboring tiles are connected, since the sticky ends 'on the diagonal' of the tiles are complementary. 9C hairpin is formed on each of the tiles and protrudes outside the tube. c) Five strands SE1-9C, SE2mod, SE3, SE4mod and SE5 are mixed together forming the tiles without sticky ends. In this case, the absence of the sticky ends prevents the tube formation.

| Name | DNA sequence (5′-3′) |
|---|---|
| 9C-hairpin | TAC-TTA-CCT-CCC-CCC-CCC-AGG-TAA-GTA-TT |
| SE1-9C | CTC-AGT-GGA-CAG-CCT-ACT-TAC-CT-CCC-CCC-CCC-A-GGT-AAG-TAT-TGT-TCTGGA-GCG-TTG-GAC-GAA-ACT |
| SE2 | GTC-TGG-TAG-AGC-ACC-ACT-GAG-AGG-TA |
| SE3 | CCA-GAA-CGG-CTG-TGG-CTA-AAC-AGT-AAC-CGA-AGC-ACC-AAC-GCT |
| SE4 | CAG-ACA-GTT-TCG-TGG-TCA-TCG-TAC-CT |
| SE5 | CGA-TGA-CCT-GCT-TCG-GTT-ACT-GTT-TAG-CCT-GCT-CTA-C |
| SE2mod | GTA-GAG-CAC-CAC-TGA-G |
| SE4mod | AGT-TTC-GTG-GTC-ATC-G |

**Table 4.1:** DNA strands used for synthesis of the free 9C emitters (9C-hairpin), the 9C emitters on the DNA tubes (SE1-9C, SE2, SE3, SE4, SE5), the 9C emitters on the DNA tiles (SE1-9C, SE2mod, SE3, SE4mod, SE5).

tubes are not ligated (there is a discontinuity in the sugar-phosphate backbone), their melting temperature is $\sim$40°C degrees [32]. Upon heating above the melting temperatures, the tubes are falling apart, making the tiles with the emitters free in solution. The melting temperature of the tiles is significantly higher due to the numerous Watson-Crick pairs between the strands within the tile itself.

## 4.3 Temperature-dependent fluorescence and absorption spectroscopy

The emission of 9C emitters formed on tubes can be visualized when the tubes are diluted in poly(vinyl alcohol) (PVA) and spin-cast on the glass substrate. For detection we used fluorescence microscope (Zeiss Axiovert 40 CFL) with a 100X oil- immersion objective. Excitation light from a halogen lamp was transmitted through a band pass filter (center: 530 nm, width: 30 nm). A dichroic mirror with edge at 560 nm reflected excitation light and transmitted emission light. Emission light was further directed directed through a second band pass filter (center: 600 nm, width: 75 nm). Figure 4.2 displays the red fluorescence signal (false color) from 9C emitters positioned

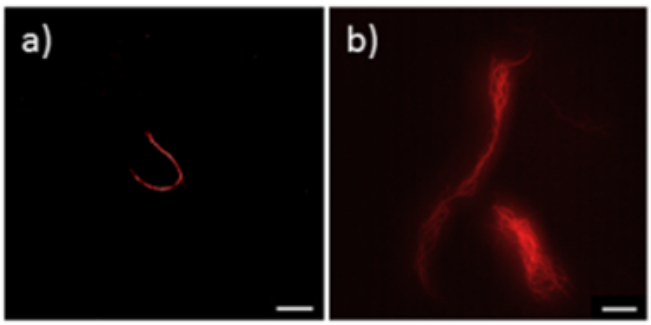


**Figure 4.2:** Fluorescent images of the tubes immobilized in PVA. a) Single tube(s), and b) tube tangles. Silver ions can mediate the non-Watson-Crick base pairing and cause the tube tangling [33]. In the case of the tiles without sticky ends, the structures could not be detected, but only a faint glow (not presented). Scale bar: 10 $\mu$m.

on DNA tubes.

To examine the optical properties of the clusters, we performed fluorescence and absorption measurements using a Cary 50 Bio UV-visible spectrophotometer and Cary Eclipse fluorimeter (Varian). For fluorescence measurements, we held the excitation wavelengths at 460 nm and 560 nm, around the excitation maxima of the 'green' and 'red' fluorescent species of 9C emitters, respectively. The 'green' fluorescent species, which consists of 11 silver atoms encapsulated by DNA, has a quantum yield that is 11 times lower than the 13-silver-atom 'red' fluorescent species [51]. This is the main reason of the large difference in the intensities of the two species. Also, from the electrophoretic mobility of the free emitters in solution and diffusivity measurements, it has been concluded that 'green' and 'red' species have distinct conformations [102]. Namely, the 'red' species most likely retains the form of the hairpin structure, whereas the 'green' species is more compact and reshapes the hairpin structure. Emission spectra were fitted with Gaussian curves, and the peak values were used to extract the emission intensity (Figure 4.3). The temperature of the examined solution of emitters was controlled by a Peltier element from 25°C to 55°C. Emission measurements were performed in several steps. The temperature of the solution was held con-

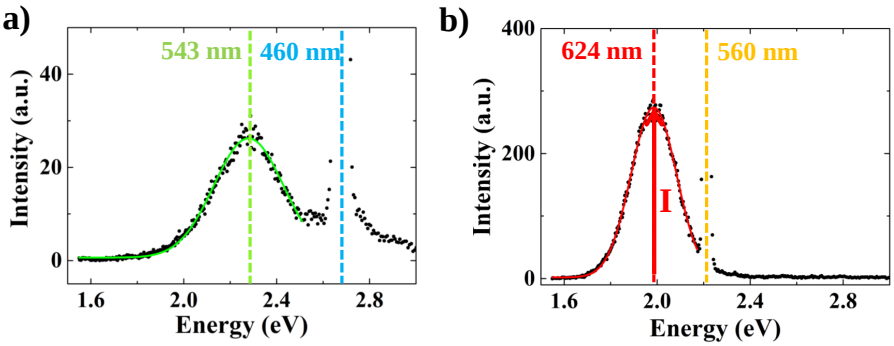


**Figure 4.3:** Emission intensity of 9C emitters on tubes. a) 'Green' emitters excited at 460 nm (blue vertical line is in the center of the excitation peak), show fluorescence spectra (black squares) which can be fitted with Gaussian peak (green solid line) centered at 543 nm. b) 'Red' emitters excited at 560 nm (yellow vertical line is in the center of the excitation peak), show fluorescence spectra (black squares) which can be fitted with Gaussian peak (red solid line) centered at 624 nm. The peak value of the Gaussian function is taken as a measure for the intensity of the emitter, $I$, presented by the red arrow. The emission intensity of the 'green' emitters is significantly lower (approximately a factor 10) than in the case of 'red' emitters, mostly due to the difference in the quantum yields.

stant and the intensity was monitored every 5 minutes. After a cycle of 12 points, the temperature was decreased to 25°C (a reference point), and then a new cycle was started after the temperature had been increased by 5°C with respect to the temperature in the previous cycle. The measurements at 25°C enabled us to distinguish permanent changes that took place in the ensemble of emitters from temporary changes due to increased temperature of the solution.

## 4.4 Characterization of the free 9C Ag:DNA emitters

We first characterize the optical properties of free 9C emitters synthesized in ammonium acetate/magnesium acetate. In Figure 4.4, the emission properties of two ensembles are presented; the lower data set represents the emission intensity of the 'green' fluorescent species excited at 460 nm, whereas the upper data set represents the emission intensity of the 'red' fluorescent species excited at 560 nm.

The emission intensity of 'red' emitters decreases with temperature, while emission intensity of the 'green' species first increases and then decreases. There are at least two reasons for the decrease in emission intensity of the 'red' species. First, the stability of fluorescent Ag:DNA at higher temperatures may be perturbed leading to formation of the non-fluorescent systems or green fluorescent Ag:DNA. Second, a temperature increase also increases vibrational occupation which leads to an enhancement of non-radiative decay processes. It can be notices that the emission intensity of the emitters kept at the constant temperature decreases as the time progresses. To separate the two effects, after each cycle at the constant temperature we cool down the system back to 25°C (red circles). The intensity difference between two neighboring red points (intensity values at 25°C) separated by the constant temperature cycle indicates the destruction of active 'red' emitters during the cycle caused by heating. On the other hand, the difference between the emission intensity at 25°C and the first point in the following cycle provides the information both of the phonons introduced in the system and the reversible changes of the clusters. It is also shown that the emission intensity of the 'red' species decreases slowly when the emitters are kept at 30°C and 35°C and faster at the temperatures above 40°C. The intensity ratio between the highest intensity value at 25°C and the value at the end of the cycle is 1.6.

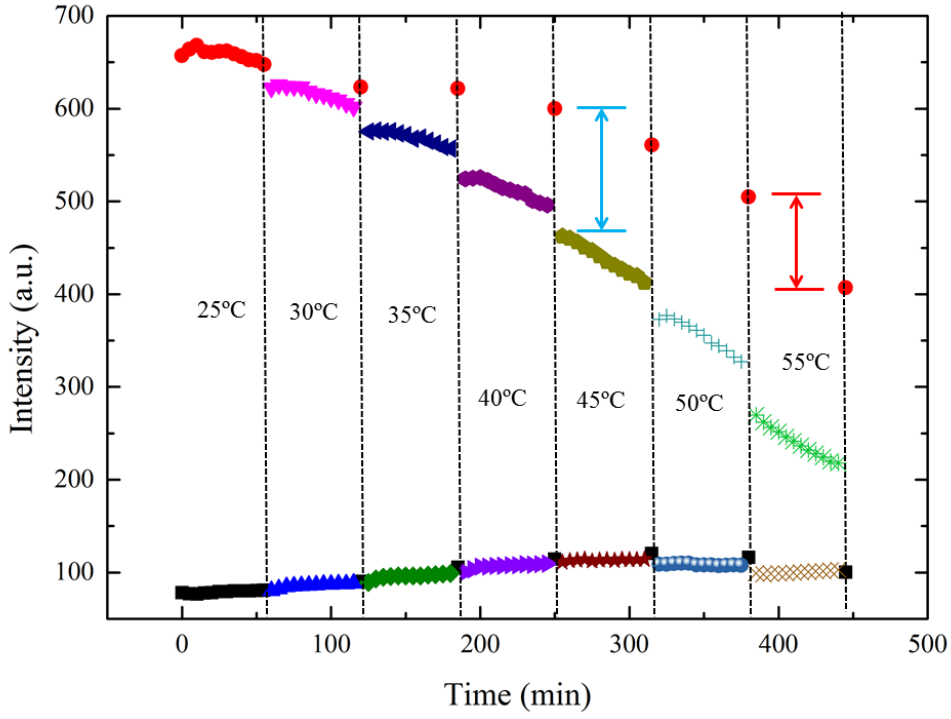


**Figure 4.4:** Emission intensity of free 9C emitters. The emission intensity of the 'green' ensemble excited at 460 nm (data set at the bottom) increases slightly when the temperature of the solution is increased from 25°C (black squares) to 55°C. The emission intensity of the 'red' ensemble excited at 560 nm (data set at the top) decreases as the temperature is increased from 25°C to 55°C. After each one-hour cycle at the constant temperature, the temperature is returned to 25 °C (black squares for 460 nm excitation and red circles for 560 nm excitation ). The difference between the intensity values at 25°C and the first data point in the following cycle (blue arrow) indicates that the new phononic degrees of freedom provide non-radiative decay channels. The intensity difference between two neighboring data points taken at 25°C separated by the cycle at the constant temperature (red arrow) represents the heat-induced degradation of emitters.

Based on Figure 4.4, the emission intensity of the 'green' fluorescent species is slightly increasing as the temperature increases to 45°C and then slowly decreases at higher temperatures. After each cycle at a constant temperature, the temperature of the system was brought back to 25°C (black squares). It appears that the 'green' species is less susceptible to vibrational degrees of freedom, as the intensity differences between the points at 25°C and the points at the end and beginning of the new cycle are similar. The emission intensity of the green species at the end of the process increases 1.3 times with respect to the initial value.

It has been shown previously that the 'green' and 'red' species are connected with the chemical reaction in which the disappearance of the 'red' emitters directly relates to the appearance of the 'green' emitters [102]. Thus, it is likely that in the heating process, 'red' emitters are (at least partially) transformed into 'green' emitters. Since the 'red' emitters contain 13 silver atoms and green emitters 11 silver atoms, it seems reasonable that two end point Ag atoms (ions) get detached.

## 4.5 Fluorescent properties of Ag:DNAs on DNA tubes

We now present optical measurements on the tubes (Figure 4.5). The emission intensity of the 'green' fluorescent species increases 1.9 times in the heating process with respect to its initial value. The intensity initially decreases at the temperatures lower than 40°C, but starts increasing at the higher temperatures. In the case of the 'red' species the difference between the free PC emitters and the 9C emitters on tubes is more dramatic than for the 'green' species. Whereas the free emitters steadily decreased in intensity as function of temperature, the emitters on the tubes significantly increase in intensity, especially at the temperatures above 40°C, which corresponds to the temperatures at which the tubes break [32]. As mentioned in section 4.2, the synthesis of the tube is a two-day process starting at 95°C, therefore after tubes have been broken into the tiles, they will not significantly reassemble into tubes on the time scales and temperatures of the current experiments. At the end of a process, we obtained an overall intensity increase of $\sim 1.5$ times with respect to value before heating. The emission intensity of the emitters increases in the heating process up to 50°C, but starts slowly decreasing at the temperatures above. In this case 9C hairpins are part of a much larger structure, a tube, so

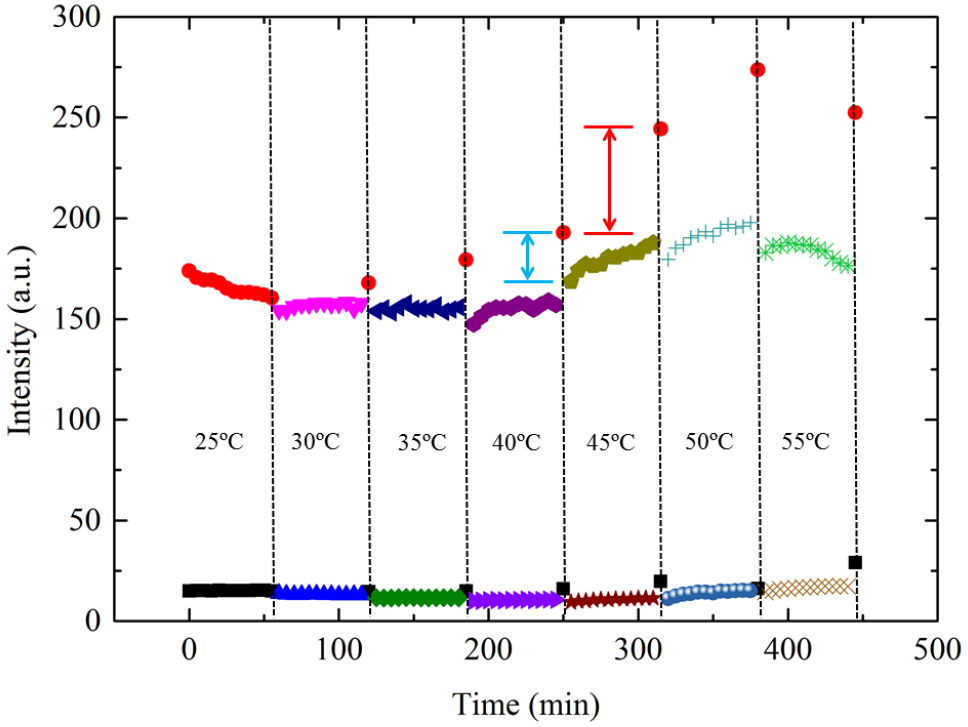


**Figure 4.5:** The emission intensity of 9C emitters formed on the tubes as a function of temperature. The emission intensity of the ensemble excited at 460 nm (data set at the bottom) slightly decreases at temperatures below 45°C, whereas it increases at temperatures above 45°C. The ensemble excited at 560 nm (data set at the top) shows increase ot the emission at the temperatures below 40°C. For the temperatures above 40°C, the intensity increase is more significant. However, at 55°C the intensity decrease is obvious, due to the degradation of the emission species. Black squares ('green' species) and red circles ('red' species)after each cycle represent the intensity values at 25 °C, which is taken as a reference value. The intensity increase (red arrow) between two neighboring red points (intensity values at 25°C) separated by the constant temperature cycle shows that the new are being formed at the temperatures up to 50°C, whereas at 55°C the emitters are being destroyed . On the other hand, the difference between the emission intensity at 25°C and the first point in the following cycle gives the information about the phonons introduced in the system and the reversible changes of the clusters (blue arrow).

their structural stability is significantly improved with respect to the case of free emitters where the temperature can induce reconfiguration of the clusters into non-fluorescent species. However, at the temperatures above 50°C, they start degrading slowly. This suggests that breaking of the tubes into tiles plays an important role.

## 4.6 Fluorescent properties of Ag:DNAs on DNA tiles

In the previous section we demonstrated that the temperatures at which the tubes break into tiles under the influence of temperature increase has a significant effect on the emission of Ag:DNA emitters.

To investigate the phenomena further, we synthesized emitters on modified tiles. The procedure is similar to the previous case, except that we now use two modified strands, SE2mod and SE4mod (Table 5.1). The modified strands are created by removing 10 bases from the original strands (SE2 and SE4), 5 bases from $5^{'}$ end and 5 bases from $3^{'}$ end. In this case the tiles can be formed but not the tubes, since the removed sticky ends are crucial for connecting the neighboring tiles. The heating and measurement procedures are repeated and the results are presented in the Figure 4.6.

The emission intensity of the 'green' fluorescent species is very low and the absolute value of the intensity change with the temperature increase is also very small. We observe that the intensity increases in the heating process such that the emission intensity at the end of the process is 1.9 times higher than at the beginning. The 'red' species also shows an emission increase after each temperature cycle. The final intensity is 1.6 times higher than the initial intensity. The fluorescent 9C emitters show a very similar behavior as the emitters on the tubes. This additional set of measurements indicates that the breaking of the tubes is not the dominant effect in the change of optical properties. Rather, it seems that the temperature increase influences modifications of the emitters on the tiles, such that the emitters form more efficiently on the tiles. This is not connected to the distance between the emitters, since each tile only hosts at most one 9C emitter, but to the state of the clusters encapsulated by the DNA. The emission intensity increases with heating, indicating that DNA-cluster systems undergo a structural change which leads to the intensity increase. Since each tile can be seen as a net that can have several Ag atoms weakly bound to its structure, those atoms might migrate and support

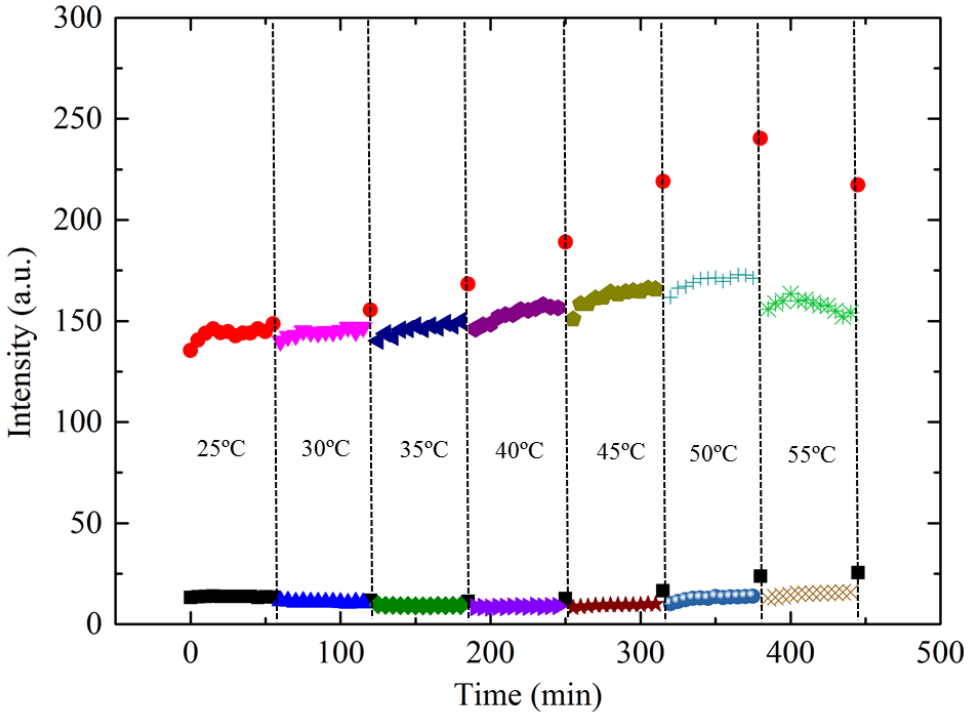


**Figure 4.6:** The emission intensity of 9C emitters on the tiles without sticky ends as a function of temperature. The emission intensity of the ensemble excited at 460 nm (data set at the bottom) slightly decrese at the temperatures lower than 40°C, whereas it increases at the higher temperatures. The emission intensity of the ensemble excited at 560 nm slowly increases with the heating process up to 50°C, and then the intensity decreases as a consequence of the degradation of emitters. Black squares (bottom data set) and red circles (top data set) represent the emission intensity value at 25°C after each heating cycle.

the formation of the 'green' and 'red' optically active clusters.

## 4.7 Absorption properties of Ag:DNAs

Clearly, multiple physical and chemical processes have to be taken into consideration as possible explanations for the observed effects. In order to gain additional insight we also performed absorption measurements before and after heating periods of the sample. Absorption measurements were per-

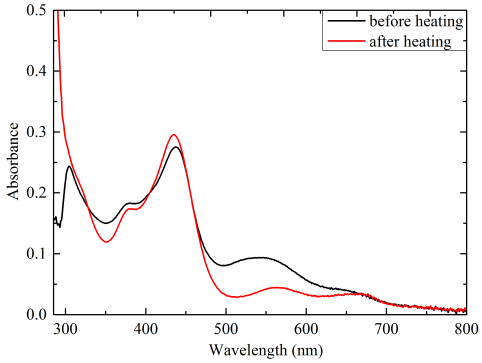


**Figure 4.7:** Absorption measurements of free 9C emitters. We measured the absorbance of the emitters at 25°C as a function of wavelength before heating (black solid line) and after heating to 55°C (red solid line). After heating, the absorbance remains almost similar around 460 nm, whereas the absorption peak around 560 nm reduces, which is in good agreement with the fluorescence spectra ( Figure 4.4).

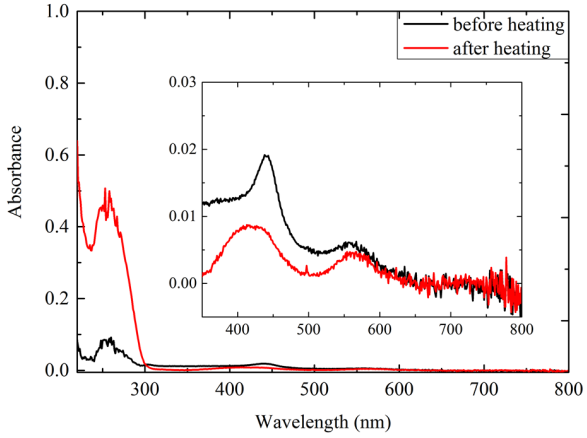


**Figure 4.8:** The absorption of 9C emitters formed on the tubes. Before heating (black solid line) the absorption peak around 260 nm, which corresponds to the absorption of DNA is 5 time lower than after heating (red solid line). Also, the change in the absorption in the visible range (inset) suggests the structural change of the fluorescent species.

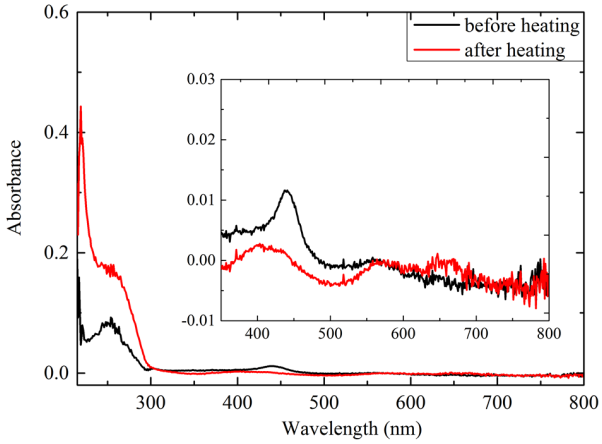


**Figure 4.9:** Absorption of 9C emitters formed on the tiles without sticky ends. The absorption peak around 260 nm increases approximately 2 times after the heating process. Also, in the visible spectral range, the absorption spectra change indicates the change of the emitters.

formed at 25°C.

From the absorption spectra for the free 9C emitters presented in Figure 4.7, we realize that after heating the most significant changes occur around 560 nm approximately the absorption peak of the 'red' 9C emitters (a decrease of $\sim$ 2 times) and below 320 nm. The absorption below 320 nm is typically associated to DNA itself and in this chapter we focus on the emission around the Ag cluster wavelength of 460 nm for 'green' and 560 nm for 'red' species. The change in absorption around 560 nm roughly corresponds to the decrease of the emission spectra of $\sim$ 1.6 times from Figure 4.4 . The small discrepancy is caused by the fact that the absorption spectra contain also the contribution of other non-emissive species which make the analysis more difficult, whereas the emission spectra give a clear Gaussian distribution.

Figure 4.8 presents absorption measurements of the emitters on tubes before and after tube heating to the temperature of 55°C . Since the concentration of the emitters is very low ($\sim$10 times lower than in the case of free 9C emitters), the absorption values are very low in the visible range. That is why we consider the absorption results relevant only as a proof that the absorption

spectra qualitatively change below 300 nm and in the visible range (see the inset of Figure 4.8 ). This data set is difficult to analyze due to the low signals compared to an overall background level. Especially before heating, there seems to exist almost a uniform absorption level (from 300 nm to 500 nm). This lifts the 'before heating' curve (black solid line) compared to the 'after heating' curve (red solid line) where this overall background level is significantly reduced. Perhaps before heating there are various sizes of Ag:DNA clusters that are not emissive, but do contribute to absorption over a broad wavelength range. Only after heating, optically active emitters become more prominent and the background absorption reduces. Of course, there is another effect that is clearly visible and that is the huge increase in absorption below 300 nm. As mentioned above, this absorption is typically due to DNA itself. It seems that after heating this absorption is strongly enhanced due to the 'integration' of Ag atoms into the DNA. Additional studies have to be carried out to investigate this mechanism and in this chapter the goal was to focus on the typical 9C Ag emission of the 'green' and 'red' fluorescent species.

In Figure 4.9 we show that the absorption properties of the emitters on the tiles before and after heating show similar character as in the case of the emitters formed on the tubes.

## 4.8 Conclusion

The combined fluorescence and absorption measurements on free 9C emitters, 9C emitters on the DNA tubes and DNA tiles indicate that the lower emission intensity of the emitters on the tubes before breaking is not a consequence of the emission quenching due to a high density of emitters. This was supported by performing the experiments on the 9C emitters formed on the modified tiles, which cannot form tubes. Instead, the fact that the emitters formed on the modified tiles behave similarly, indicates that the intensity increase is not related to the mutual distance between the emitters. A naive picture would be that the tiles represent the 'nets' which can catch silver atoms and ions. At elevated temperatures those atoms would be more mobile and could migrate to the hairpin loops to form the fluorescent clusters. The heating process is in this case an annealing process in which the new emitters are formed through the changes of the silver-DNA structure. An additional new

effect has been identified, namely strong enhancement of the typical DNA absorption (below320 nm) after heating suggesting an important role for Ag atoms also in this process.

# CHAPTER 5

## Lifetime measurements of the DNA-hosted (Ag:DNAs) silver clusters

In this Chapter, time-resolved optical measurements on individual and collections of Ag:DNAs immobilized in poly(vinyl alcohol) (PVA) are presented. Two cases of Ag:DNA collections are considered. The first case is simply a high density of individual Ag:DNAs that might form small aggregates. The second case makes use of a DNA nanotube scaffold onto which Ag:DNA emitters can be attached with a sub 10 nm spacing. We investigate the effect of the density of emitters on the optical lifetime of the emitters. Single emitters show single exponential decay when excited with a pulsed laser. The lifetime value slightly changes for longer exposure periods. A collection of emitters excited at the same time shows a double exponential decay. The longer lifetime corresponds to the value of single emitters and the shorter lifetimes are attributed to the interaction between nearby emitters. The interaction provides addition energy decay channels leading to a shorter optical lifetime. Emitters organized on the DNA tubes also show a double exponential decay, with the longer lifetimes corresponding to the values of single emitters and shorter lifetimes again indicating the interaction between the emitters. Comparing the case of the random collection of individual emitters and the case of the ordered array of emitters on a tube, we find that the weight of the shorter lifetime component significantly increases for the ordered array.

## 5.1 Introduction

The advances in DNA nanotechnology have completely changed the perspective of the possibilities in the manipulation and organization of matter at the nanometer scale [23, 24]. The organization of organic dyes [25, 26] and plasmonic particles [26, 78, 96, 97] as well as the dynamic change of the DNA structures [28, 97] are only some of the achievements in the field. DNA scaffolds also enabled the formation of 'hybrid' systems stabilizing plasmonic particles and organic dyes [96, 97] in special geometric configurations. This kind of constructs helps in understanding the behavior of organic dyes in plasmonic cavities, with further applications in chemistry and physics.

The formation of elaborate DNA structures relies on the complementarity of the DNA base binding (Watson-Crick pairing). The rest of the process focuses on a careful salt concentration adjusting which provides the stability of the construct. Furthermore, these constructs may have sticky ends, single strands of DNA, which typically protrude from the structure in order to perform various functions, such as connecting to other DNA constructs or stabilization of the particles, again based on the principle of complementarity.

In this Chapter, we are particularly interested in structurally and spectrally pure Ag:DNAs [53, 76], formed separately from the DNA tubes, unlike the approach in the previous chapter. Namely, the Ag:DNAs are spectrally impure and more than 90 % of the DNA strands stabilize non-fluorescent products. Working with spectrally pure emitters facilitates the process of the examination of the interactions between the emitters. Therefore, in this research we use the emitters purified with high performance liquid chromatography (HPLC). Furthermore, the emitters are designed to have sticky ends (linkers) which will enable them to connect to DNA scaffolds with complementary sticky ends (dockers).

To form the scaffolds with dockers, the procedure published by Yin et al. [34] was slightly modified appending the U6 strand with the docker, which will protrude outside the DNA construct. Finally, the purified emitters and the tubes are brought together and the attachment took place leading to the decoration of the DNA tubes with Ag:DNAs.

The fluorescence behavior of organic dyes strongly depends on their environment. For example, a fluoresncent lifetime values of FAM and Cy3 are

3.53 ns and 1.3 ns, respectively, but in the vicinity of a gold nanoparticle (d=1.5nm), the values change significantly [103]. Also, Busson and coworkers demonstrated the decay rate enhancements of 2 orders of magnitude for ATTO 647N coupled to the bright mode of plasmonic cavity [104].

The interaction between Ag:DNAs has already been discussed previously, where we used spectrally matched donors and acceptors to detect Förster energy transfer [80]. A different way to show the interaction of the emitters positioned in close proximity of one another is to measure their fluorescence lifetime, similarly to the cases where the organic dyes are positioned in the vicinity of metal particles [103, 104]. Shortening of the fluorescence lifetime can be caused by a collective emission of resonantly interactions or quenching of emission due to energy transfer to non-radiative Ag clusters. Our main aim is to examine the interactions of the DNA-hosted silver clusters precisely positioned on the DNA scaffolds.

Single DNA emitters show single exponential decay as discussed by Hooley et al. [105]. This value changes slightly during the exposure period. The lifetimes of the single emitters should be, in principle, significantly different from the lifetimes obtained from interacting emitters. In general, if a mixture of the individual emitters and collection of interacting emitters is produced, we would expect to see (at least) two lifetime components, one which corresponds to the lifetime of single emitters, and another shorter, as a consequence of the interaction between the emitters.

## 5.2 Synthesis procedure

The samples are provided by the group of professor Elisabeth Gwinn at University of California, Santa Barbara and the detailed synthesis procedure is given in reference [35]. The oligonucleotide sequences used in this study are presented in the Table 5.1 Single stranded DNA has two roles: to enable a formation of the stable cluster and to have an appended linker sequence. The later role will enable an efficient attachment to the DNA scaffolds via complementary single stranded 'docker' sequences. Final concentrations for synthesizing Ag:DNAs were 15.0 $\mu$M DNA, 188 $\mu$M $AgNO_3$, and 93.8 $\mu$M $NaBH_4$ .The fluorescent emitters were HPLC purified as explained in references [19, 35].

The 10-helix DNA nanotubes are chosen as scaffolds for Ag:DNAs (see

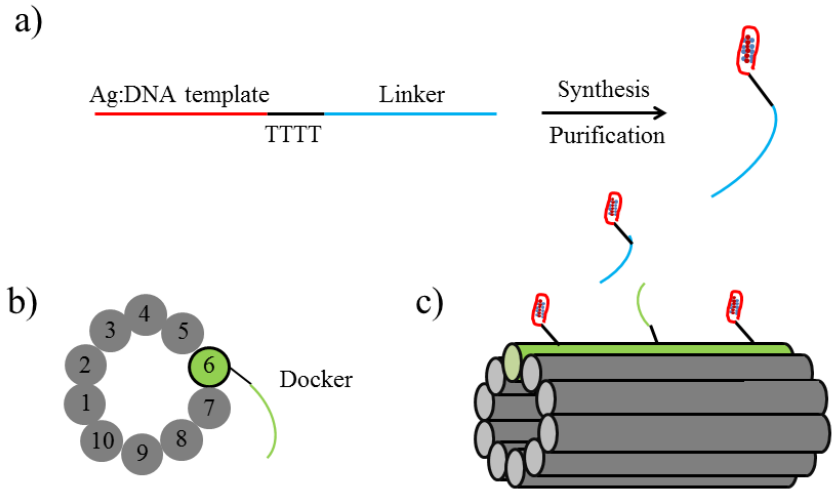


**Figure 5.1:** Schematic representation of the attachment of Ag:DNAs to the 10-helix DNA nanotubes [35]. a) A red-labeled part of the strand stabilizes silver cluster, which is separated by four thymines (TTTT) from the linker part which does not participate and does not influence the formation of the cluster. b) A cross-section of the DNA tube with a modified U6 strand which is appended by the docker strand. c) A schematic representation of the Ag:DNA attachment to the DNA tube. A single-stranded linker (blue) of the strand which carries silver cluster and a single-stranded docker (green) which is a part of the DNA tubes are complementary strands and thus enables the attachment.

| | Name | DNA sequence (5′-3′) |
|---|---|---|
| 1 | U1 | GGC-GAT-TAG-GAC-GCT-AAG-CCA-CCT-TTA-GAT-CCT-GTA-TCT-GGT |
| 2 | U2 | GGA-TCT-AAA-GGA-CCA-GAT-ACA-CCA-CTC-TTC-CTG-ACA-TCT-TGT |
| 3 | U3 | GGA-AGA-GTG-GAC-AAG-ATG-TCA-CCG-TGA-GAA-CCT-GCA-ATG-CGT |
| 4 | U4 | GGT-TCT-CAC-GGA-CGC-ATT-GCA-CCG-CAC-GAC-CTG-TTC-GAC-AGT |
| 5 | U5 | GGT-CGT-GCG-GAC-TGT-CGA-ACA-CCA-ACG-ATG-CCT-GAT-AGA-AGT |
| 6 | U6 | GGC-ATC-GTT-GGA-CTT-CTA-TCA-ATG-CAC-CTC-CAG-CTT-TGA-ATG |
| 7 | U7 | GGA-GGT-GCA-TCA-TTC-AAA-GCT-AAC-GGT-AAC-TAT-GAC-TTG-GGA |
| 8 | U8 | TAG-TTA-CCG-TTT-CCC-AAG-TCA-AAC-ACT-AGA-CAC-ATG-CTC-CTA |
| 9 | U9 | GTC-TAG-TGT-TTA-GGA-GCA-TGT-CGA-GAC-TAC-ACC-CTT-GCC-ACC |
| 10 | T10 | GTG-TAG-TCT-CGG-GTG-GCA-AGG-CCT-AAT-CGC-CTG-GCT-TAG-CGT |
| 11 | U6-docker | GGC-ATC-GTT-GGA-CTT-CTA-TCA-ATG-CAC-CTC-CAG-CTT-TGA-ATG-TTT-TAT-TTA-TAC-AAC-GGA |
| 12 | Ag15-DNA host | CAC-CGC-TTT-TGC-CTT-TTG-GGG-ACG-GAT-ATT-TTT-CCG-TTG-TAT-AAA-T |

**Table 5.1:** DNA sequences [35]. DNA oligomers used for the construction of 10-helix DNA tubes (1-10), tubes with dockers (1-11) and Ag:DNA host strands (12). Ag:DNA host strands consist of templates which stabilizes silver cluster, TTTT spacers and a linker which will enable binding to the DNA tubes.

Figure 5.1) because their architecture allows a formation of single-stranded DNA docker extrusions at separations of 7.1 nm along, but also due to the fact that their length of $\sim 10$ $\mu$m allows visualization by fluorescence microscopy. Using a similar approach as previously published for gold nanoparticles [36],

one of the ten 42-base long oligomers that form tubes (3'-end of U6 in our case) was appended to the docker sequence which is complementary to the linkers. The oligomers were mixed in 0.2 mL PCR tubes, each oligomer at a final concentration of 1.4 $\mu$M, in 40 mM ammonium acetate and 12 mM magnesium acetate to a final volume of 50 $\mu$L. After the annealing process using a Mastercycler personal (Eppendorf), the tubes were stored at 4°. For nanotubes with 50 % docker coverage, U6 and U6-docker site oligomers were mixed at 1:1 ratio to a total final concentration of 1.4 $\mu$M.

In order to attach Ag:DNAs to the annealed nanotubes, the Ag:DNAs were added at 5 time greater concentration than the concentration of docker sites appended to nanotubes. Buffer concentration was maintained (40 mM ammonium acetate and 12 mM magnesium acetate) to preserve the stability of the nanotubes.

## 5.3 Experimental section

Figure 5.2 is a schematic overview of the experimental setup. A pulsed laser (639 nm) driven at 20 MHz repetition rate was controlled by PDL 800-B (PicoQuant) in order to excite the fluorescent emitters. Linearly polarized laser light was transmitted through a narrow band filter (LD01-640/8-25, Semrock) and coupled into a single-mode optical fiber (OZ Optics). After reflection from a dichroic mirror (ZT640 RDC, Chroma) the beam was sent through an infinity-corrected high numerical aperture (NA) oil immersion objective (1.4 NA, 100X oil, Zeiss). The sample immobilized on a glass substrate was mounted on a scanning stage which was controlled by nanopositioning piezo elements (P517.3CD, Physik Instrumente). The same objective was used to collect emitted light which was further transmitted through the dichroic mirror and filtered through an emission filter (ET655LP, Chroma) to reject the reflected and scattered light. In order to remove the out-of-focus signal, the emission light was then focused onto a 75 $\mu$m pinhole and finally on the single-photon counting module (SPCM-AQR-14, Perkin Elmer). A photon counting PC-board (TimeHaro 200, PicoQuant) in the time-tagged time-resolved mode was used for data acquisition. For the controle of hardware and data acquisition as well as data processing, we used software SymPhoTime (PicoQuant).

Emitters immobilized in PVA are first detected in a raster scan. After

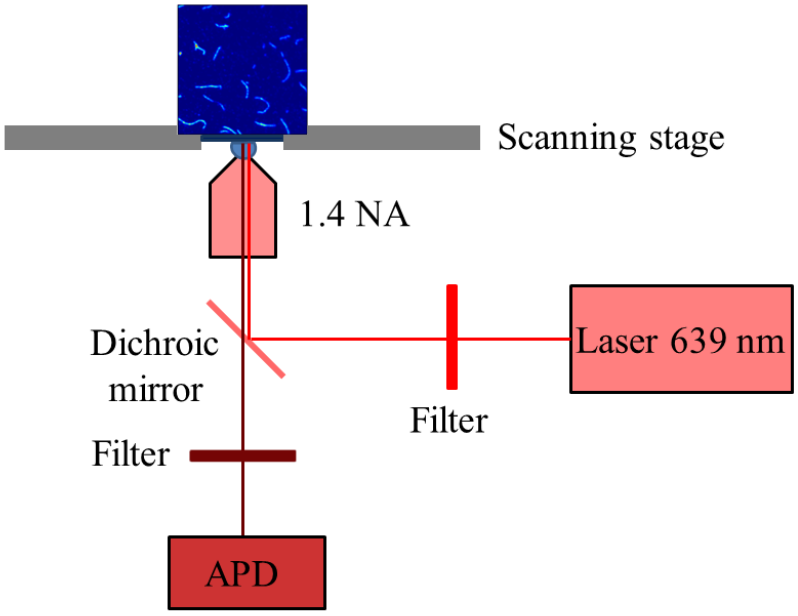


**Figure 5.2:** Experimental setup. Emitters immobilized in PVA on the glass slide are mounted on the scanning stage in the focus of an oil-immersion objective (1.4 NA). The laser light (excitation wavelength: 639 nm, repetition rate: 20 MHz) is transmitted through the narrow-band filter and reflected from the dichroic through the objective. The emission light is collected by the same objective, transmitted through the dichroic mirror and the emission filter, and focused on the single-photon counting module (APD).

acquiring an image, it is further possible to examine the points of interest by focusing laser light (0.5 $\mu$W) and collecting photons for 60 s. From the photon statistics we can extract information about blinking and lifetime of the emitter(s). The time-traces typically show one or several blinking steps depending on the number of emitters in the focus. To estimate lifetimes, we fit a single exponential decay function or a double exponential depending on the obtained experimental results. The functions are given in the Equations 5.1 and 5.2:

$$f = A_0 + A_1 \cdot exp(-t/\tau), \tag{5.1}$$

where $A_0$ represents a 'local' background, $A_1$ is an amplitude and $\tau$ corresponding lifetime.

$$f = A_0 + A_1 \cdot exp(-t/\tau_1) + A_2 \cdot exp(-t/\tau_2), \tag{5.2}$$

where $A_0$ represents a 'local' background, $A_1$ and $A_2$ are the amplitudes and $\tau_1$ and $\tau_2$ are longer and shorter lifetimes, respectively.

To determine the background, we use a linear fit (constant function) in the time segment before the pulse. We perform a tail-fitting routine neglecting all photons which come in the time domain of the instrument response function (IRF). To justify this, it is important to mention that the lifetimes of the Ag:DNAs are of the order of few nanoseconds, which is significantly longer than the laser pulse width of 80 ps.

## 5.4 Results for single emitters

Firstly, we present measurements performed on singe Ag:DNA emitters immobilized in PVA. The fluorescence image of the emitters immobilized in PVA is presented in Figure 5.3 a. By focusing light on an arbitrary chosen bright spot, we select single emitters according to the recorded time trace. Namely, the time traces that show one step blinking/bleaching are considered to belong to single emitters. In Figure 5.3 b, we present one such time trace, where it can clearly be seen that the emitter switches on and off during the excitation process. To estimate lifetimes, we split the time trace into 20 equal intervals and determine the lifetimes on each of the interval. In Figure 5.3 c, we present the average fluorescence lifetime on the interval from 24 to 27 s (red segment in Figure 5.3 b). In Figure 5.3 c the black solid line represents the instrument response functions (IRF), the red curve represents the fluorescence decay curve, and the blue line is a single exponential decay fit.

In Figure 5.4, we present the average lifetime of the emitter. The lifetime changes slightly during the process and the average value is $3.6 \pm 0.1$ ns. However between 39 and 42 s, we cannot estimate lifetime, because the emitter is in the off-state. In this case, the lifetime value increases during the excitation process, which is not a general trend for other emitters. We have performed similar measurements on other emitters and the average lifetime value spans between 3.2 and 3.6 ns.

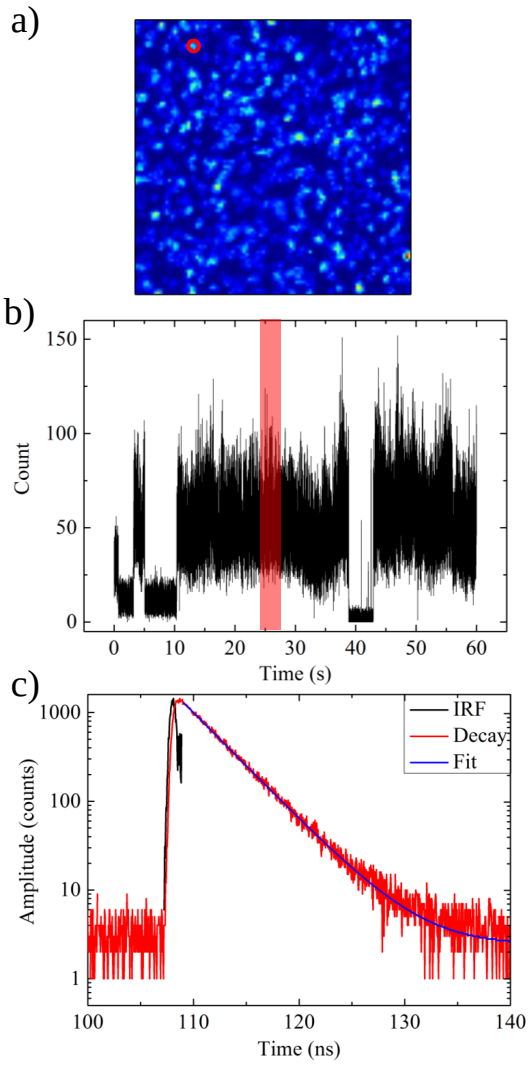


[h!]

**Figure 5.3:** Fluorescence properties of single emitters. a) Fluorescence image of emitters immobilized in PVA (imaged area: 20X20 $\mu$m). The excitation spot is marked with a red circle. b) Time-trace shows an on-off state of a single emitter. We want to estimate the average lifetime of the emitter along the time trace. c) The average fluorescence lifetime of the single emitter in the interval between 24 and 27 s (red segment in b)) is 3.6 ns. The red curve represents the decay curve, the blue line represents the fit (single exponential), and the black line represents an instrument response function (IRF).

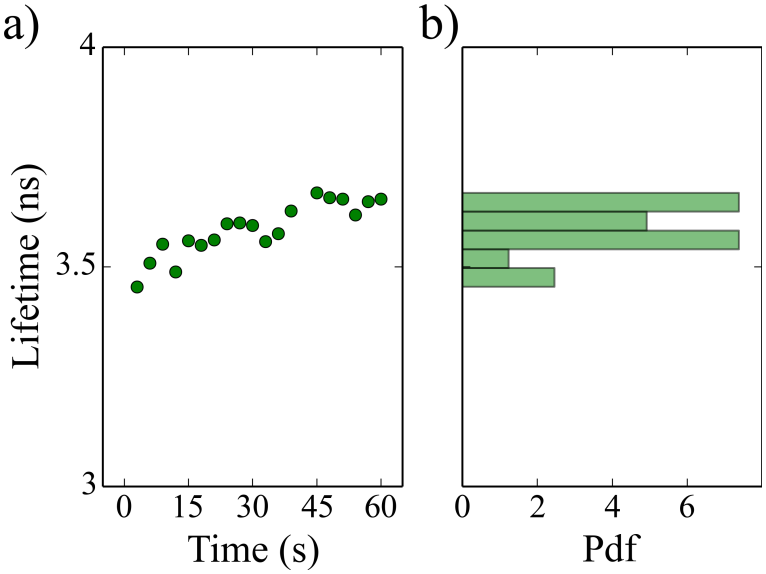


**Figure 5.4:** Lifetime of single emitter. a) The lifetime of a single emitter averaged every 3 s. The value increases slightly, but this can be attributed only to this emitter and does not represent a general rule. Since the emitter is in the off state the lifetime cannot be estimated in the range from 39 to 42 seconds. b) A histogram represents probability density function (PDF) of lifetime values. The average lifetime value for this emitter is 3.6 ns.

## 5.5 Results for multiple emitters

To examine the behavior of multiple emitters excited at the same time, we spincast the emitters dissolved in PVA with 100 times higher concentration than in the case of single emitters. A typical fluorescence image is presented in Figure 5.5 a. In Figure 5.5 b, we present the typical time-trace of the emitters excited by the pulse laser. The emitters show blinking behavior, switching on and off. For example, after 20 seconds, several of them bleached, but some recovered again. Similarly to the case of single emitters, we split the time trace into 20 intervals and estimate the average lifetimes. In this case, a single exponential decay curve does not fit to the data, but a double exponential provide a reasonable fit. In Figure 5.5 c we present the decay of the photons from the interval 45-48 s (Figure 5.5 b). This is expected, because the emitters have different orientations in space and they will have different

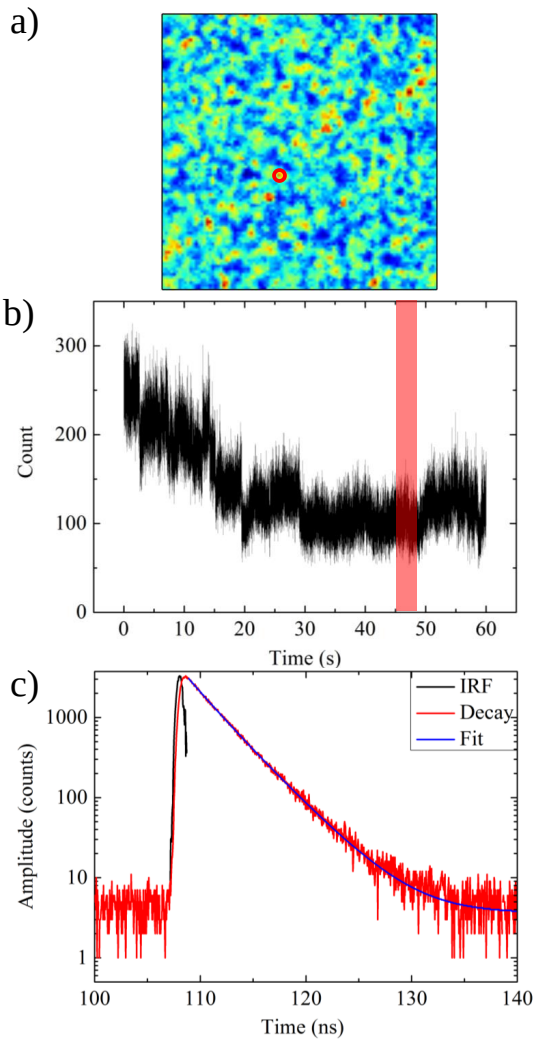


**Figure 5.5:** Fluorescent properties of multiple emitters. a) Fluorescence image of emitters immobilized in PVA (imaged area: 20X20 $\mu$m). The excitation spot is marked with red circle. b) Sixty-second-long time-trace shows several blinking/bleaching steps of the collection of emitters. For example, after 20 s, some of the emitters switch on again. c) To estimate the average lifetime in the interval 45-48 s (a red segment in b)) it is necessary to use double-exponential curve with lifetimes (lifetime values are 3.4 ns and 2.2 ns and the amplitude of the longer lifetime is 1.8 times larger). The red curve represents the decay, the blue curve is the double exponential function, and the black curve is the IRF.

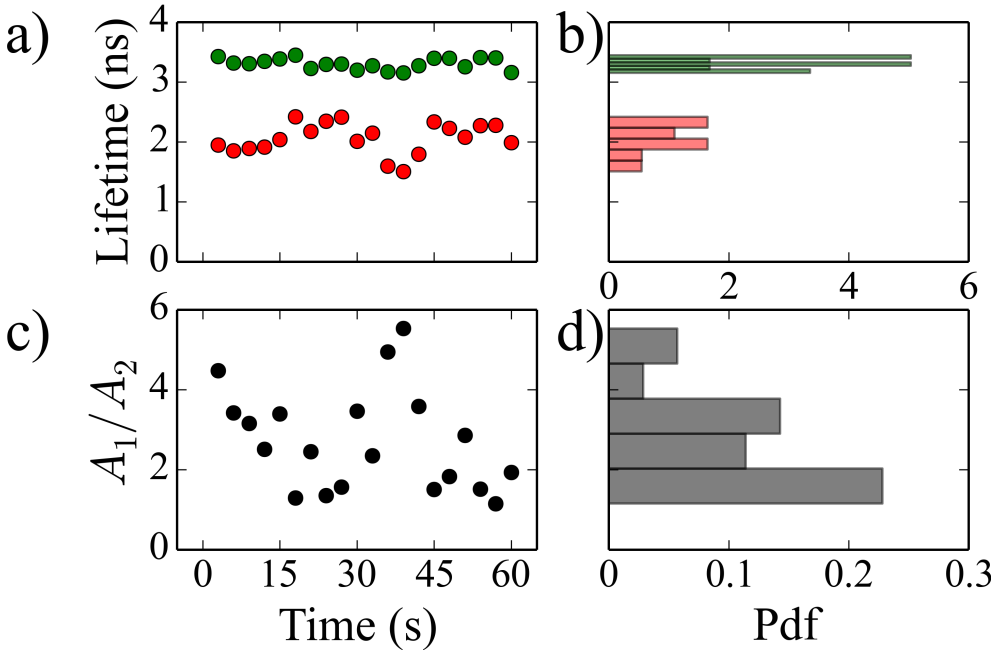


**Figure 5.6:** Lifetime of multiple emitters. a) The lifetime of the emitters averaged every 3 s show that the lifetimes curves can be approximated with double exponential curves. b) Probability density function (PDF) of the longer and shorter lifetime components is presented in the histogram. The longer lifetime values are centered around 3.3 $\pm$ 0.1 ns, whereas the average shorter lifetime is 2.1 $\pm$ 0.3 ns. c) A contribution of the longer and shorter lifetime components is given by the ratio of the amplitudes $A_1$ and $A_2$. d) A histogram of the amplitude ratio shows that most of the time, a shorter lifetime component has a significant contribution.

contributions. However it is possible to approximate the multi-exponential decays with double exponential.

To get better insight into the lifetime statistics along the time-trace in Figure 5.6 a we present both longer lifetimes (green circles) and shorter lifetimes (red circles). The longer lifetimes values are centered around 3.3 $\pm$ 0.1 ns, whereas the values of shorter lifetimes have an average value of 2.1 $\pm$ 0.3 ns, as presented in Figure 5.6 b. If we ascribe the shorter lifetime value to the interaction between the emitters, it seems that the shorter lifetime component is more sensitive to fluctuations than the longer, which is ascribed to the non-interacting emitters. This can be concluded from comparison of the dis-

tribution widths in Figure 5.6 b. To estimate the relative contributions of the longer and shorter lifetime components, we find the ratio between the amplitudes of the longer ($A_1$) and shorter lifetime ($A_2$) components (Figure 5.6 c). We make the following observations. First, it seems that the shorter lifetime component has a significant contribution to the exponential decay. As we can observe from the histogram in Figure 5.6 d, most of the time, the contribution is larger than 25 %. Second, despite the fact that the number of active emitters over time is decreasing as presented in Figure 5.5 b, the contribution of the shorter component does not decrease. It seems that the contribution of the shorter lifetime component is somewhat random, and does not depend on the number of active emitters.

## 5.6 Results for emitters on DNA tubes

In this section we investigate emitters organized on predetermined sites on the tubes which have 50 % or 100 % U6 strands appended with dockers which can stabilize the silver clusters. First we start with emitters on the 50 % labeled tubes. Their average mutual distance should be larger than 7.1 nm. From the fluorescence image presented in Figure 5.7 a, it seems that the emitters are distributed inhomogeneously on the tubes, which is in good correspondence with results presented in reference [35] . U6 strands with dockers are randomly interwoven in the tubes and also Ag:DNAs attach randomly, which is a reason for their non-uniform distribution. The time trace presented in the Figure 5.7 b shows that at the beginning of the process there are several emitters which blink and bleach during the acquisition process. After 25 s, most of them bleached. It is difficult to estimate the number of emitters within a diffraction limited spot due to the fact that the emitters are randomly orientated in space. The excitation efficiency and the emission intensity of each of them will be different, leading to the diverse step sizes. This is one of the reasons why the steps may have different sizes. Also, it is possible that two or more emitters switch on and off at the same time. As before, we tend to determine the average lifetimes of the emitters on the tubes. In Figure 5.7 c we present the average lifetimes estimated form the photons which arrived in the interval between 3 and 6 seconds (red segment in Figure 5.7 b). In this interval, the longer lifetime has a value of 3.6 ns and shorter lifetime 1.8 ns.

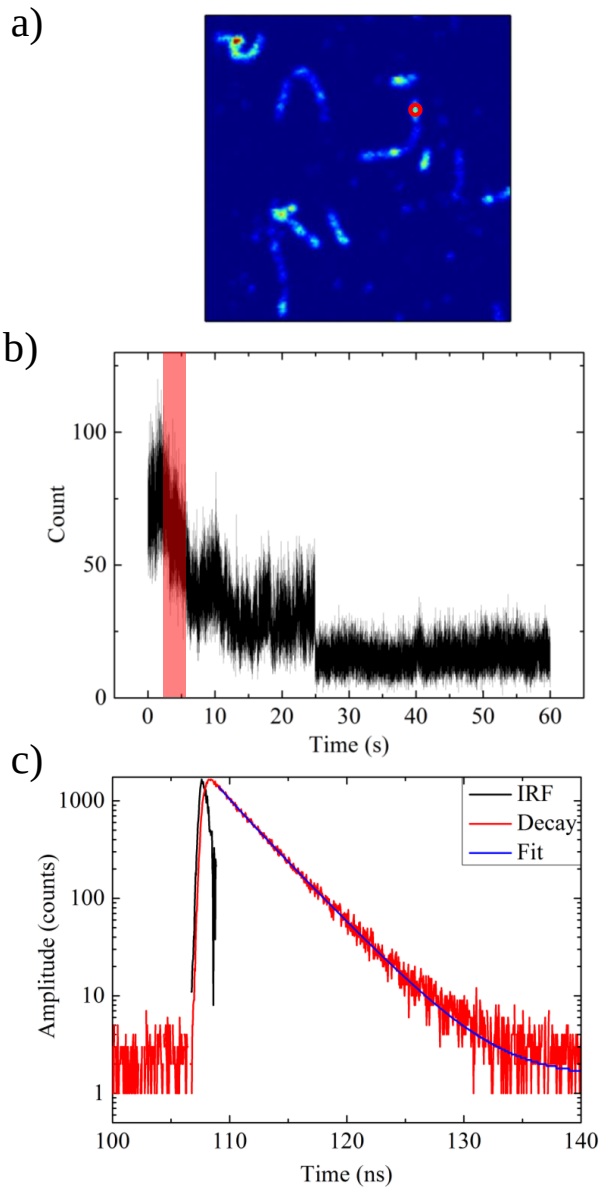


**Figure 5.7:** Fluorescent properties of the emitters on 50 % labeled tubes. a) Fluorescence image of the emitters stabilized on DNA tubes immobilized in PVA (imaged area: 20X20 $\mu$m). b) Time-trace of the emitters shows multiple steps indicating numerous emitters in the excitation spot (red circle in a)). c) To estimate the average lifetime of the emitters in the interval from 3 to 6 s, it is necessary to fit the double exponential curve (3.6 ns and 1.8 ns, the contribution of the longer component is 7.5 times larger).

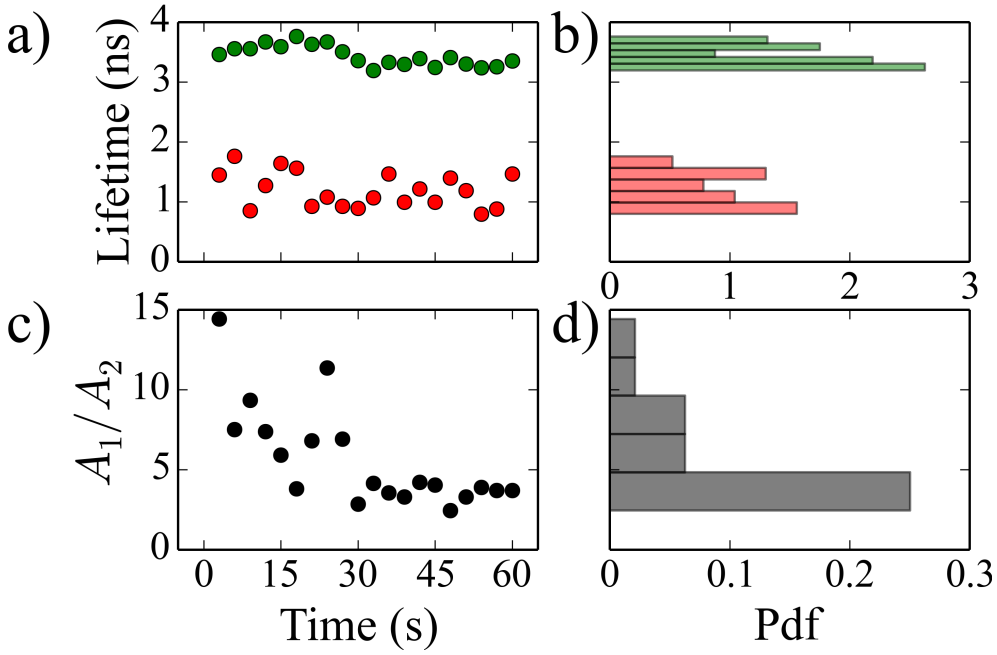


**Figure 5.8:** Lifetime of the emitters on 50 % labeled DNA tubes in PVA. a) The lifetime of the emitters averaged every 3 s shows that the lifetime curves can be approximated with double exponential curves. b) A histogram represents the probability density function (PDF) of the lifetime values. The average value of the longer lifetime component is 3.4 $\pm$ 0.1 ns, whereas the shorter components is around 1.2 $\pm$ 0.3 ns. c) The ratio of the amplitudes $A_1$ and $A_2$ represents the contribution of the longer and shorter lifetime components. d) A histogram of the amplitude ratio differs from the case of multiple emitters, showing that the shorter lifetime component most of the time has more than 20 % contribution in the decay.

To investigate further this process, we follow the change of the lifetimes by dividing the interval of 60 s into 20 equal intervals and estimate the average lifetime on each of those. The results shown in Figure 5.8 a show that on the entire interval the decay curves can be approximated with the double exponential curves. The average value of the longer lifetime is 3.4 $\pm$ 0.1 ns, and 1.2 $\pm$ 0.3 ns for the shorter lifetime. Histograms in Figure 5.8 b shows the probability density distribution (PDF) of the lifetimes. The contribution of the shorter and longer components are presented in 5.8 c through the amplitude ratio. From Figure 5.8 a and Figure 5.8 c, it seems that the blinking

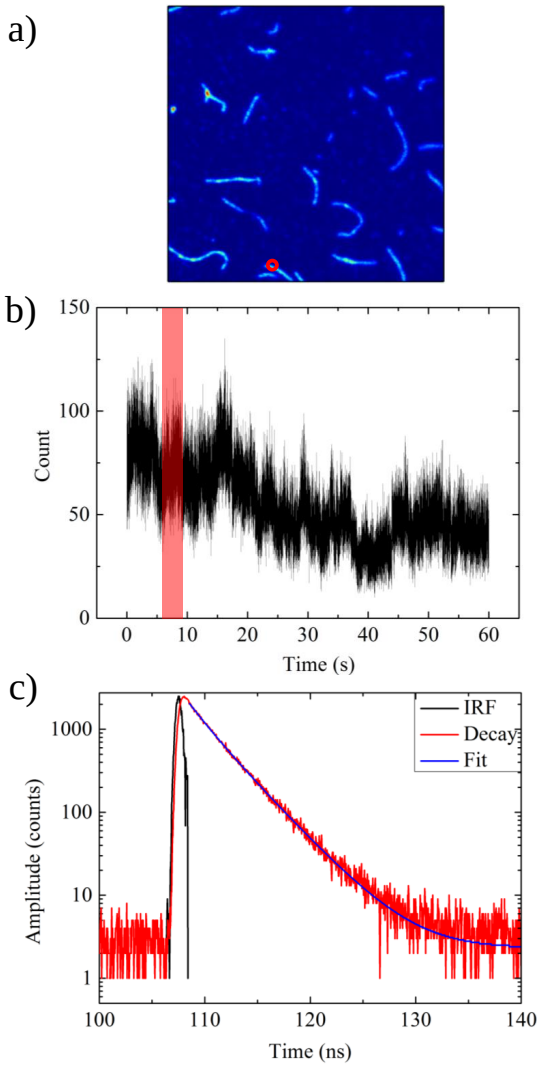


**Figure 5.9:** Fluorescent properties of the emitters on 100 % labeled tubes. a) Fluorescence image of the emitters stabilized on DNA tubes immobilized in PVA (imaged area: 40X40 $\mu$m). The fluorescence signal appears more uniform than in the case of 50 % labeled tubes. b) Timetrace of the emitters show multiple steps indicating numerous emitters in the excitation spot (red circle in a)). c) To estimate the average lifetime of the emitters in the interval from 6 to 9 s (red interval in b)), it is necessary to fit the double exponential curve (3.3 ns and 1.7 ns, the contribution of the longer component is 3 times larger).

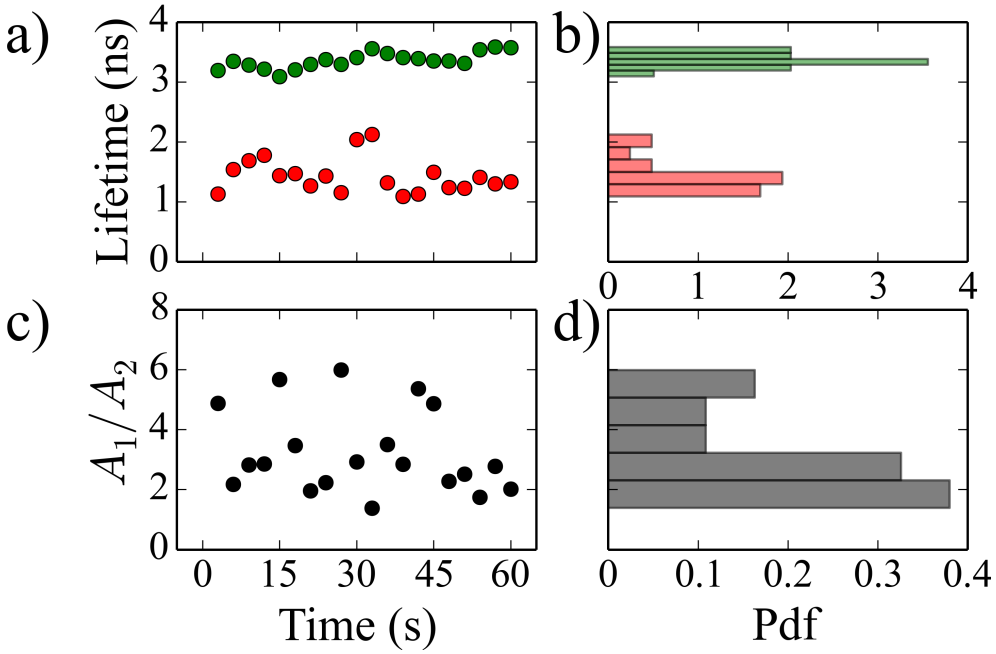


**Figure 5.10:** Lifetime of the emitters on 100 % labeled DNA tubes in PVA. a) The lifetime of the emitters averaged every 3 s show that the lifetime curves can be approximated with double exponential curves. b) The average value of for longer and lifetime components are 3.4 $\pm$ 0.1 ns and 1.4 $\pm$ 0.3 ns, respectively. c) The contribution of the longer and shorter lifetimes is given by the ratio of the amplitudes $A_1$ and $A_2$. d) From the histogram of the amplitude ratio, it seems that 75 % of time, the contribution of the shorter lifetime component is higher than 25 %. PDF represents probability density distribution of the ratio between the longer and shorter lifetime component.

process and the lifetime values are not related. As presented in Figure 5.8 d, it seems that half of the time, the shorter lifetime components are more than 20 % present. We note that Figure 5.8 c indicates that the shorter lifetime becomes more important after some initial period ($\sim$ 30 s). A possible explanation is that if single emitters bleach there is no optical signal left, but if one of the interacting emitters bleach there is still an optical signal remaining.

Finally, we performed similar measurements on the 100 % labeled tubes. In Figure 5.9 a one can see that the coverage of the tubes is much larger than in the case of 50 % labeled tubes. However, the intensity change is still visible

along the tubes. In Figure 5.9 b, one can see the typical time trace. As in the case of multiple emitters, the emitters blink and bleach during the excitation process as is visible by the intensity jumps. To estimate the average lifetimes during the collection time, we divide again the time trace into 20 equal intervals. The decay can be approximated with the double exponential curves presented in Figure 5.9c. The longer lifetime value is 3.3 ns and the shorter is 1.7 ns.

The lifetime values averaged over 3 s are presented in Figure 5.10 a. From the histogram presented in Figure 5.10 b, it follows that the average value of the longer lifetime is 3.4 $\pm$ 0.1 ns and that of the shorter is 1.4 $\pm$ 0.3 ns. The shorter lifetime component contributes more significantly (a factor of $\sim$ 2 more) to the intensity decay curve than in the case of the 50 % covered tubes as can be observed in Figure 5.10 c. From the PDF in Figure 5.10 d, it seems that the contribution of the shorter lifetime component in the fluorescent decay is higher than 25 % in three quarters of the exposure period.

## 5.7 Conclusion

In this research, we have shown that the single exponential decay functions can be used to fit the emission decay of single emitters. In order to make systems of interacting emitters, we investigate three different possibilities. The first way is to increase the concentration of Ag:DNAs which leads to the aggregation of several Ag:DNAs. In the other two cases we use self-assembled nanotubes to stabilize Ag:DNAs (tubes are covered with dockers (50 % or 100 %) which stabilize silver clusters. In all three cases several emitters are excited at the same time and the fluorescence decay can be approximated with a double exponential decay curve. The longer lifetime component corresponds to the lifetime of single emitters while the shorter lifetime is ascribed to the interaction between nearby Ag:DNAs. If we deal with the emitters attached to the 50 % labeled tubes, it seems that the appearance of two lifetimes is somewhat similar to the case of multiple emitters, except that the shorter lifetimes are typically shorter (1.2 $\pm$ 0.3 ns) than in the case of several emitters randomly distributed in the diffraction limited spot (2.1 $\pm$ 0.3 ns). For the 100 % labeled tubes, we see the reduction of the shorter lifetime component (1.4 $\pm$ 0.3 ns) compared to the case of multiple emitters. We also observe the increase of the contribution of a shorter lifetime component in the decay com-

pared to the 50 % labeled tubes (the amplitude ratio, $A_1 / A_2$, is larger for 100 % labeled tubes than for the 50 % labeled tubes). This is consistent with the fact that the average distance between the emitters on the tubes is smaller in the case of 100 % labeled tubes, which increases the interaction probability.

# CHAPTER 6

## Strings of colloidal particles glued by DNA tubes

We investigate the formation of strings of colloidal particles in a magnetic field and their stabilization by DNA tubes. Colloidal particles can form strings in an external magnetic field. However, as soon as the magnetic field is turned off, the strings fall apart due to the thermal motion of the particles. Here we show that DNA tubes can be used as a nano-contact glue which keeps colloidal particles functionalized with short DNA strands into stable strings. These strings remain flexible, which is a desirable characteristics for the examination of the colloids interaction or network formation.

## 6.1 Introduction

Self-assembly of colloidal particles into desired configurations is one of the most important goals in colloidal physics and material science [106–108]. Since their sizes are typically on the micrometer scale, these microscopic mechanisms can be directly observed and followed with optical microscope.

Over the years, different assembly schemes have been suggested, including the microwave-assisted self-organization of colloidal particles [109], a field-assisted assembly of oppositely charged particles [107], and using patching particles [110]. Also DNA linkers appear as a very good nanocontact glue between the colloids [106, 108].

Colloids aligned in a string represent one of the important configurations, whose realization is not very demanding. In principle, particles with dielectric or magnetic susceptibilities align in an electric or magnetic field, respectively, and form the strings of colloids [111]. However, the main issue is that after the field is switched off, strings fall apart due to the lack of interactions which would hold the colloidal particles together. There are several approaches how to keep the strings stable that include an annealing process [111], electrostatic interactions [107] or using the self-protected DNA strands [108].

In the previous years, it has been shown that the DNA scaffolds [23] can stabilize organic dyes [25, 26], plasmonic particles [26, 78, 97], and colloidal particles into desirable configurations. It has also been shown that the DNA origami structures can be driven by short DNA strands to change reversibly from one configuration to the other [28]. The particle size in these cases is typically much smaller than a micrometer.

Here we demonstrate a new approach to glue the colloidal particles together using DNA nanotubes. DNA nanotubes with programmable circumference have been developed in the group of John Reiff [34]. In this chapter, we use a slightly modified procedure [35, 36] for 6-helix tubes in order to allow the attachment of the DNA functionalized colloidal particles to the DNA tubes. The modified tubes have dockers which are single-stranded protrusions from the DNA tubes that can bind to the complementary DNA strands on the colloids.

| | Name | DNA sequence (5′-3′) |
|---|---|---|
| 1 | linker 1 | biotin-GTA-GAA-GTA-GG-organic dye |
| 2 | linker 2 | biotin-TTT-AAT-ATT-A-organic dye |
| 3 | U1mod | CCT-ACT-TCT-ACT-TGG-CGA-TTA-GGA-CGC-TAA-GCC-ACC-TTT-AGA-TCC-TGT-ATC-TGG-T |
| 4 | U2 | GGA-TCT-AAA-GGA-CCA-GAT-ACA-CCA-CTC-TTC-CTG-ACA-TCT-TGT |
| 5 | U3 | GGA-AGA-GTG-GAC-AAG-ATG-TCA-CCG-TGA-GAA-CCT-GCA-ATG-CGT |
| 6 | U4 | GGT-TCT-CAC-GGA-CGC-ATT-GCA-CCG-CAC-GAC-CTG-TTC-GAC-AGT |
| 7 | U5 | GGT-CGT-GCG-GAC-TGT-CGA-ACA-CCA-ACG-ATG-CCT-GAT-AGA-AGT |
| 8 | T6 | GGC-ATC-GTT-GGA-CTT-CTA-TCA-CCT-AAT-CGC-CTG-GCT-TAG-CGT |

**Table 6.1:** DNA sequences. DNA oligomers used for functionalization of colloids (1-2), creation of 6-helix DNA tubes (3-8). Strand 2 is complementary with the docker of strand 3, which enables the connection of the tubes and the functionalized colloidal particles. Strand U1mod is a modified strand U1 from the reference [34] (a docker and two thymines are added at the 5′ end of the strand).

## 6.2 Microscopy

To follow the formation of the strings of colloids, we used a Nikon eclipse Ti-E microscope system with a Nikon 100x/1.45 NA Oil immersion DIC H objective, Nikon FITC (Excitation: 465-495 nm, Dichoric mirror 505 nm, Emission: 515-555 nm) and TRITC (Excitation: 540/25 nm, Dichroic mirror 565 nm, Emission: 605/55 nm) filters and a Nikon Intensilight C-HGFIE lamp. For the detection, we used a Nikon Digital Sight DSQi1Mc camera in combination with Nikon NIS Elements 4 software. DNA strands used to functionalize the colloids are also appended with the organic dye molecules in order to improve the visualization process: 6-FAM (FITC filters) and Cy3 (TRITC filters).

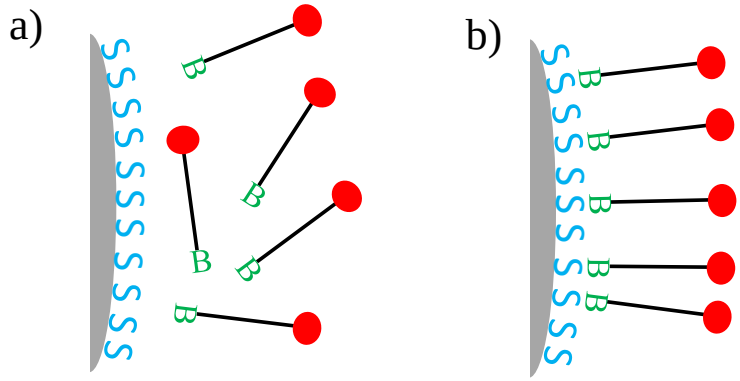


**Figure 6.1:** Functionalization of the colloidal particles with single-stranded DNA. a) The surface of the colloidal particle (gray) is covered with Streptavidin (S). Biotinylated (B) DNA strands with organic dye (red circle) at the 3′ are mixed with streptavidin-coated particles. The fluorescent dye is appended to the DNA in order to facilitate the visualization of colloids. b) The attachment of the biotin (B) and streptavidin (S ) enables functionalization of the particles with DNA strands.

## 6.3 Functionalization of colloidal particles

We purchased the streptavidin-coated superparamagnetic particles (Dynabeads MyOne Streptavidin C1) from Life Technologies. In order to functionalized them with single stranded DNA oligonucleotides (Integrated DNA Technologies), we followed the procedure published by Dreyfus et al. [112]. Biotinylated oligonucleotides attach to the streptavidin-coated colloids (Figure 6.1) by suspending 5 $\mu$L of 10 mg/mL Dynabeads and 5 $\mu$L of 6 $\mu$M DNA in 65 $\mu$L phosphate buffered saline (PBS; 10 mM phosphate, 47 mM NaCl, 0.5 % w/w Pluronic surfactant F127 and 3 mM $NaN_3$, pH 7.5) and placing this suspension in an oven for 30 minutes at 55°C. The excess and unbound DNA was washed out by centrifuging the particles for 45 seconds at 3000 rpm and pipetting out the liquid above the sedimented colloids. After adding 100 $\mu$L PBS, the washing procedure was repeated 3 times.

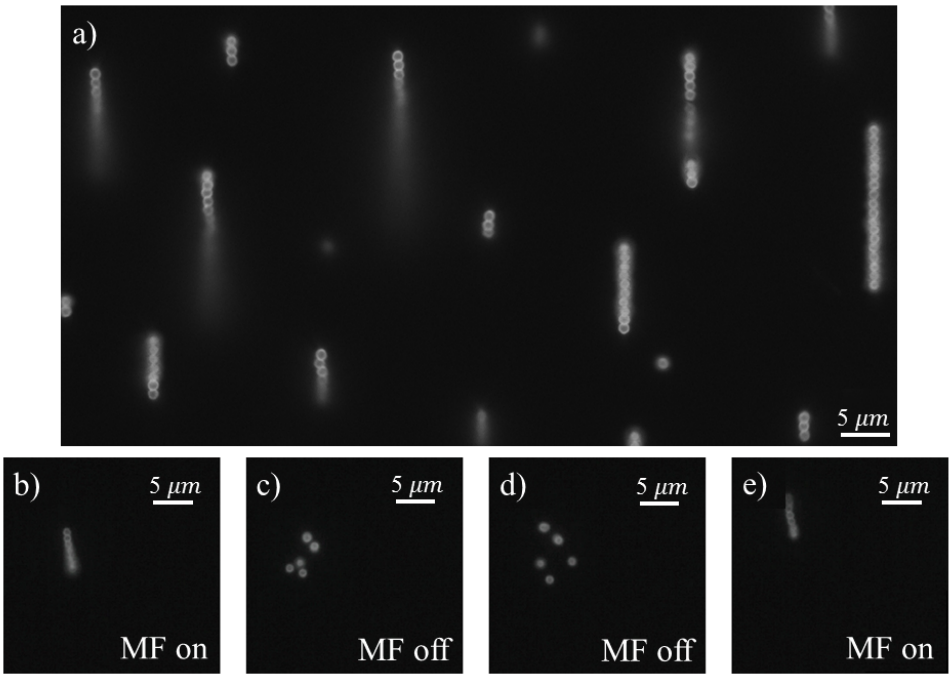


**Figure 6.2:** Strings of self-organized colloids in a magnetic field. a) Superparamagnetic colloids organize in the magnetic fields (MF) into strings. b) When the MF is on, a string is stable. c)-d) We follow the behavior of the string when the MF is turned off. The attraction between the particles stops and they diffuse apart due to thermal motion. As the time progresses, the particles are further apart due to the diffusion process. e) If we switch on again the MF, the particles reorganize into a string.

## 6.4 Tube synthesis

Following the procedure given by Yin et al. [34] and including modification suggested by Copp et al. [35], we mixed the DNA oligonucleotides with buffer at the final concentrations: 3 $\mu$M U1mod- U5 and T6 (Table 6.1) and 12.5 mM magnesium acetate and 20 mM ammonium acetate. This solution was then heated to 95°C and left to slowly cool down in a thermos flask for two days to let the DNA strands self-assemble into DNA tubes (Figure 6.3).

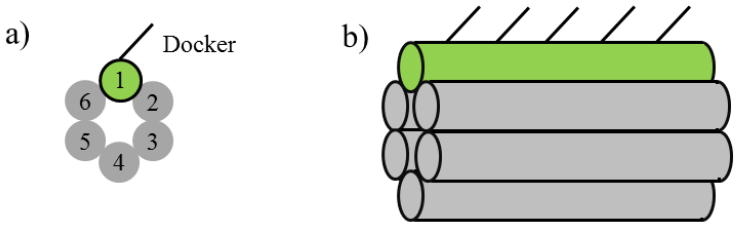


**Figure 6.3:** Formation of the DNA tubes. a) Strands: docker-TT-U1, U2-U5 and T6 self-assemble into the DNA tubes. b) Schematic representation of the DNA tube with the docker protruding out of the tube. The dockers are single strands of the DNA responsible for the attachment to the colloids functionalized with the complementary strands.

## 6.5 Results

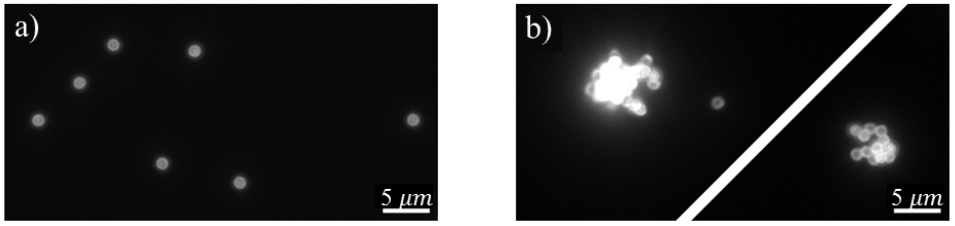


**Figure 6.4:** Colloids functionalized with non-complementary (a), and self-complementary (b) single stranded DNA. a) Colloids with non-complementary strands do not attach to each other. Even if the collision occurs, they diffuse away without permanent attachment. b) The self-complementary DNA strands tend to bunch together into clumps of particles without possibility to control the process. This is why the organization of the colloidal particles with complementary strands is not a good approach.

Colloidal particles functionalized with DNA do not attach to each other if the strands are not complementary (linker 1 in Table 6.1) as presented in Figure 6.4 a. If the strands are self-complementary (linker 2 in Table 6.1), they form clumps as presented in Figure 6.4 b. The colloids labeled with

complementary strands bunch together and cannot form the strings.

The superparamagnetic particles in MF form strings such that the free colloids are attracted by the growing magnetic field of the string, so they attach onto the ends of the string. In the Figure 6.2 a, one can see the strings of different lengths formed in the solution when the MF is on. These strings can exist only when the MF is on. One of these strings is shown in the Figure 6.2 b. Some of the colloids appear blurry, because they are out-of-focus. However, it the MF is off, the emitters start diffusing away (Figure 6.2 c, d). If we switch on the MF again, and if the colloids are sufficiently close together, they will form the strings again. But, as it can be seen, the strings deteriorate as soon as the MF is off.

In order to keep them together, some kind of 'glue' is necessary to form the stable structure. Our approach is to use DNA tubes and try to organize the colloidal particles. The schematic representation of the tubes is given in Figure 6.3. These tubes have dockers, strands complementary to the ones used for functionalization of the colloidal particles. The Watson-Crick pairing will enable the binding of the tubes and colloidal particles.

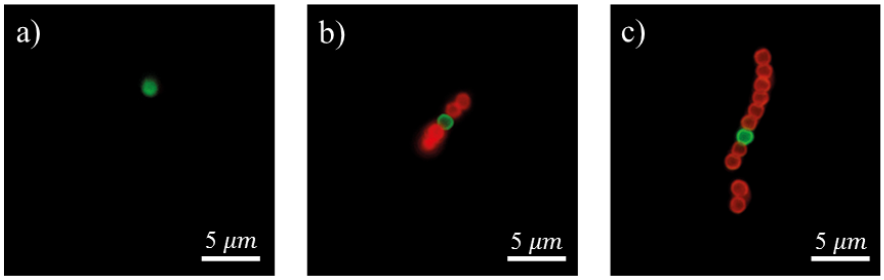


**Figure 6.5:** Formation of the strings of colloids connected with DNA tubes. a) Single colloidal particle attached to the DNA tubes (tubes are not visible). b) In the magnetic field, the colloids form string. c) The colloids stay in the string even after switching off the magnetic field. The DNA tubes are responsible for this stability, because they act as a 'glue' which holds the colloids together.

The most efficient procedure that we found for forming strings consists of several steps. First, we mix small concentration of the colloids with DNA tubes (labeled with FAM). Then we add this solution on the cover slip and image the colloid (Figure 6.5 a). In order to track the procedure, the colloids which we add subsequently are labeled with the different organic dye (Cy3).

If the MF is on, they will form a string (Figure 6.5 b). The longer the MF is on, the more colloids will attach to the string, which is now stable, due to the fact that the dockers on DNA tubes mediate between the string and the colloids which attach (Figure 6.5 c).

It is also possible to connect two or more strings together. The underlying mechanism is that the tubes in the magnetic field attract each other strongly. On the other hand, as we have already seen, only the magnetic field is not sufficient to keep the colloids together. The 'unused' dockers of the DNA tubes at the ending part of the strings must connect efficiently to the colloids of the adjacent string. In Figure 6.6 a, we see the two strings approaching each other. At the beginning, the collided strings in Figure 6.6 b are kept together due to the MF. The two strings stay together even if the MF is off ( 6.6 c); the DNA tubes glue the two strings together.

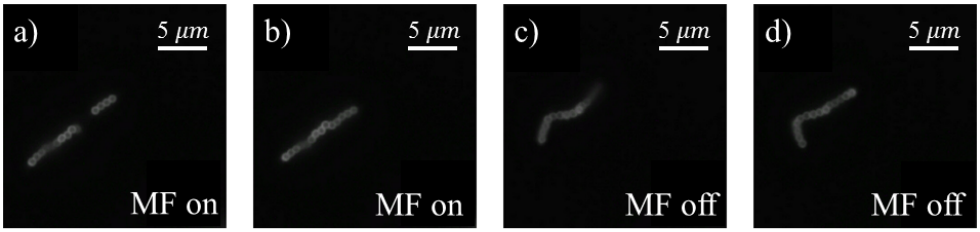


**Figure 6.6:** The attachment of two strings. a) If the MF is on two strings attract each other with their induced magnetic fields. b) These two strings collide and form a larger string. c) Even if we switch off the magnetic field, the strings stay together, due to the fact that free dockers on DNA tubes which are at the end points of the string connect to the colloids of the neighboring string making a strong bond. d) The string is not rigid and it changes its shape in time. DNA tubes enable somewhat flexible connections between the colloids.

This system is flexibile, as we can see that the shape of the string has changed in 6.6 d with respect to the shape of the string in Figure 6.6 c. This means that DNA tubes behave as the flexible bonds between the colloids. It is also important to mention that the solution with the strings still contains 'unused' DNA tubes which can be picked up by the moving strings of colloids. This is also one of the possible explanations why there are still some active dockers on the ending points of the strings. The lengths of the strings

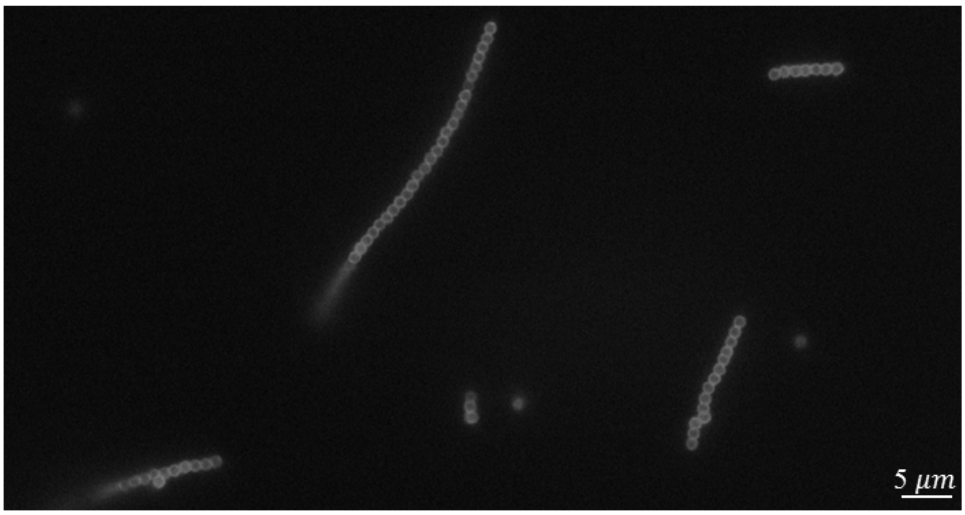


**Figure 6.7:** Strings of colloids formed in magnetic field and connected with DNA tubes. The length of the strings is arbitrary and is related to the length of the interval when the magnetic field was switched on.

can have arbitrary lengths. In principle, the longer the MF is on, the longer strings can be formed. In Figure 6.7, one can observe that the string length ranges from a few to few dozens of colloids. Typically the smaller strings append to each other and form 'superstrings'.

## 6.6 Conclusion

We have shown that DNA is a promising material for organization of the colloidal particles. When the particles were functionalized with complementary DNA strands, they simply bunched together and formed irregular shapes. However, DNA tubes with dockers represent an excellent nano-contact glue between the DNA functionalized colloids aligned in magnetic field. In the approach we took, stable strings of arbitrary lengths were formed. The DNA tubes form a type of 'glue' that allows flexibility of the strings of colloids which is an important property for the formation of larger self-assembled structures.

# Summary

The field of nanotechnology has completely changed since the moment DNA has been programmed to execute various functions different from those in living cells. From that moment, DNA was more than a molecule responsible for the transfer of genetic information from one generation of organisms to the next. It became a building block of the elaborate programmable structures, a drug carrier, a breadboard for accurate distance measurements, a dynamic system, which changes shape and function on demand. The complementary binding between DNA bases, the possible chemical modifications on the DNA strands, and the attachment of organic dyes and proteins are only some of the characteristics that make DNA nanotechnology such a vibrant field of science.

The focus of this thesis is on small silver clusters (typically 10-20 atoms) stabilized by short DNA strands. DNA-hosted silver clusters (Ag:DNAs) bridge the gap between the individual silver atoms and large plasmonic silver particles. The DNA base sequence that stabilizes silver clusters determines their size and shape. Moreover, the absorption and emission properties of the clusters are determined by the base sequence. This makes their emission wavelength tunable in the range from 400-900 nm. Encapsulated by DNA, these fluorescent nanoparticles are widely used for detection of heavy ions and single-base mutations in DNA, but also as biomarkers for cell imaging.

Since the moment of their discovery, Ag:DNAs have been intensively studied, making the field of research and application very broad. Here we focus on the fundamental questions related to their structure and shape, their optical properties, as well as their temperature stability. To address these questions we apply different experimental techniques, such as UV-visible spectrophotometry, fluorimetry, cryogenic spectroscopic and polar-

ization measurements, and room-temperature time-resolved measurements. Generally speaking, from the measurements performed on an ensemble of emitters, one can extract values averaged over a large number of emitters. In many cases, this is sufficient, but for many fundamental and practical questions it is essential to examine individual emitters well separated from their neighbors. In this case the information, otherwise lost in the ensemble averaging, is accessible.

Immobilized in poly(vinyl alcohol) (PVA), the emitters are cooled to cryogenic temperatures (1.7 K). First, we observe that a significant increase of the emission intensity with the temperature decrease. Second, their excitation and emission spectra appear very broad despite the fact that a environmental vibrational degrees of freedom are suppressed. Based on our experimental results and following the theoretical predictions, we conclude that Ag:DNAs behave as plasmonic particles despite the small number of electrons that participate in the optical processes. Furthermore, we performed polarization measurements on the immobilized emitters. The results clearly show that the emission is highly linearly polarized, whereas the excitation does not strongly depend on the polarization of the excitation light. Our polarization microscopy studies prove that Ag:DNAs differ in distinctive ways from the characteristic behaviors of both the molecular and metal nanoparticle regimes. Purified and unpurified samples of Ag:DNAs have shown similar results.

The complementarity of DNA strands can be utilized through binding of carefully programmed DNA oligonucleotide sequences. Namely, short strands bind to each other forming micrometer-long structures with a programmed periodicity and functionality.

The fact that five different DNA strands can form larger structures is employed to construct DNA tiles and nanotubes with DNA loops (DX tubes), which can stabilize silver clusters. We examine the optical properties and thermal stability of emitters formed on the tiles and tubes and compare them with free emitters in solution. Free emitters in solution start breaking at elevated temperatures, whereas the emitters that are formed on the tiles and tubes are more temperature-resistant. They even show a fluorescence increase with the temperature increase, which we ascribe to the reorganization of the silver cluster within the hairpin structures. The change of the absorption spectra upon heating suggests the formation of new emitters of the same

type.

DNA tubes enable the precise positioning of Ag:DNAs at the predetermined sites. Ten different carefully programmed oligonucleotides form HX tubes with single-stranded protrusions (dockers). In this case, the minimal distance between the dockers is 7.1 nm. Purified Ag:DNAs with linkers (a part of the oligonucleotide, which does not participate in the cluster formation) bind complementary to the dockers and decorate DNA tubes. Our idea is that the emitters in close proximity will interact and the interaction can be detected through the change of the fluorescence lifetime. Individual Ag;DNAs immobilized in PVA are used as a reference and they exhibit single-exponential fluorescence decay. The lifetime changes slightly during the exposure period. Fluorescence decay of emitters spin-casted at very high density and the emitters on the DNA tubes can be approximated with double-exponential decay curves. Longer lifetimes are similar to the case of individual emitters and the shorter lifetimes are ascribed to the interaction between the emitters.

Not only do they stabilize Ag:DNAs, but the HX tubes are excellent scaffolds for organization of colloidal particles whose diameter is two orders of magnitude larger than the diameter of the tubes. Superparamagnetic colloidal particles form strings in a magnetic field. These strings are unstable and thermal motion breaks them apart. However, colloidal particles functionalized with short DNA strands complementary to the dockers on the HX tubes can form stable strings in a magnetic field. They act as a nano-contact glue, making the system stable even without magnetic field. These structures are flexible, which will open a new way to applications.

In this study, we present the first detailed analysis of spectral and polarization properties of individual Ag:DNAs. Our results also prove that DNA meets the requirements of modern science and technology for a multi-scale fabrication of DNA constructs with a nanometer-precision control.

# Samenvatting

Het onderzoeksgebied nanotechnologie kreeg een enorme impuls op het moment dat ontdekt werd dat DNA kon worden geprogrammeerd voor taken verschillend van de functies die in levende cellen plaatsvinden. Vanaf dat moment was DNA meer dan slechts een molecuul dat verantwoordelijk is voor de overdracht van genetische informatie van de ene generatie van organismen naar de volgende. Het werd een bouwsteen voor uitgebreide programmeerbare structuren, een drager van medicijnen, een mechanisme voor accurate afstandsbepalingen, en een dynamisch systeem dat op afroep van vorm en functie kan veranderen. De complementaire binding tussen DNA baseparen, de mogelijke chemische aanpassingen van de DNA-strengen, en het bevestigen van organische kleurstoffen en eiwitten zijn slechts enkele voorbeelden van de eigenschappen die er voor zorgen dat DNA nanotechnologie een zeer dynamische wetenschapstak is.

Dit proefschrift richt zich op kleine zilverclusters (typisch bestaand uit 10-20 atomen) die gestabiliseerd worden door korte DNA-strengen. Deze door DNA gebonden zilverclusters (Ag:DNAs) zitten in het overgangsgebied tussen individuele zilveratomen en grote zilverdeeltjes met plasmonische eigenschappen. De volgorde van de DNA baseparen, die de zilverclusters stabiliseren, bepalen ook hun grootte en vorm. Hierdoor worden ook de absorptie- en emissie-eigenschappen van de clusters bepaald door de basenvolgorde. De emissiegolflengte kan aangepast worden over een bereik van 400-900 nm. Omvat door DNA, worden deze fluorescerende nanodeeltjes veel gebruikt voor de detectie van zware ionen en mutaties van enkele basen in DNA, maar ook als bio-markers voor het afbeelden van cellen.

Sinds hun ontdekking zijn Ag:DNAs intensief onderzocht, en zijn het onderzoeksgebied en de toepassingsmogelijkheden zeer uitgebreid. In dit proefschrift leggen wij de nadruk op fundamentele vraagstukken gerelateerd

aan hun structuur en vorm, de optische eigenschappen, en de temperatuurbestendigheid. Om dit te onderzoeken maken wij gebruik van verscheidene experimentele technieken, zoals UV-spectrografie, fluorescentiespectroscopie, cryogene spectroscopie- en polarisatiemetingen, en tijds-opgeloste metingen bij kamertemperatuur.

In het algemeen kunnen metingen van een verzameling van emitters iets leren over de gemiddelde eigenschappen van de verzameling. In veel gevallen is dit voldoende, maar voor veel fundamentele en praktische vraagstukken is het essentieel om individuele emitters te onderzoeken. In dat geval kan extra informatie achterhaald worden die tijdens het middelen over de verzameling verloren gaat.

Gedemobiliseerd in polyvinyalcohol (PVA) worden de emitters gekoeld tot cryogene temperaturen (1.7 K). Ten eerste observeren wij dat de emissie-intensiteit toeneemt als de temperatuur afneemt. Ten tweede, hun excitatie- en emissiespectra blijken erg breed te zijn ondanks het feit dat de vibrationele vrijheidsgraden van de omgeving onderdrukt worden. Gebaseerd op de experimentele resultaten en daaropvolgende theoretische voorspellingen, concluderen wij dat Ag:DNAs zich gedragen als plasmonische deeltjes ondanks het bescheiden aantal elektronen dat deelneemt in de optische processen.

Verder hebben wij polarisatiemetingen verricht op de gedemobiliseerde emitters. Deze resultaten laten zien dat de emissie sterk lineair gepolariseerd is, terwijl de excitatie niet sterk afhankelijk is van de polarisatie van het excitatielicht. Onze polarisatiemicroscopiestudie bewijst dat Ag:DNAs zich anders gedragen dan het karakteristieke gedrag van moleculaire of metaalachtige nano-deeltjes. Gezuiverde en ongezuiverde monsters van Ag:DNAs hebben vergelijkbare resultaten laten zien.

De complementariteit van DNA-strengen zorgt ervoor dat vooraf geprogrammeerde DNA oligonucleotidestrengen op gecontroleerde wijze aan elkaar binden. Hierdoor vormen korte strengen micrometerlange structuren met een geprogrammeerde periodiciteit en functionaliteit.

Het feit dat vijf verschillende soorten DNA strengen grotere structuren kunnen vormen is gebruikt om DNA tegels en nano-buisjes met DNA lussen (DX tubes) te vormen, welke zilverclusters kunnen stabiliseren. Wij onderzoeken de optische eigenschappen en de thermische stabiliteit van de emitters die op de tegels en buisjes binden, en vergelijken deze met vrije emitters in een oplossing. Vrije emitters in een oplossing vallen uit elkaar bij ver-

hoogde temperaturen, terwijl de emitters die gevormd worden op de tegels en buisjes beter temperatuurbestendig zijn. Deze laten zelfs een toename van de fluorescentie zien bij hogere temperaturen welke wij toeschrijven aan een reorganisatie van de zilverclusters in de haarspeldstructuren. De verandering van de absorptiespectra na het opwarmen suggereert dat nieuwe emitters van eenzelfde soort gevormd zijn.

DNA buisjes maken het mogelijk om heel precies Ag:DNAs op vooraf bepaalde posities te positioneren. Tien verschillende zorgvuldig geprogrammeerde oligonucleotides vormen HX buisjes met enkel-strengs uitsteeksels, welke als 'bindplaats' voor zilverdeeltjes fungeren. In dit geval is de minimale afstand tussen de bindingsplaatsen 7.1 nm. Gezuiverde Ag:DNAs met linkers (een onderdeel van de oligonucleotide dat niet deelneemt aan de clusterformatie) binden complementair aan de bindingsplaatsen en larderen zo de DNA buisjes. Ons idee is dat nabijgelegen emitters met elkaar een interactie zullen hebben die gedetecteerd kan worden door middel van een verandering van de fluorescentielevensduur. Individuele Ag:DNAs gedemobiliseerd in PVA worden gebruikt als referentie en laten een enkelvoudig exponentieel verval zien. De levensduur verandert slechts lichtjes tijdens de blootstellingsperiode. Fluorescentieverval van emitters die met een hoge dichtheid gedeponeerd zijn en de emitters op de DNA buisjes laten echter bij benadering een dubbel exponentieel verval zien. De waarde van de lange levensduur is vergelijkbaar met het geval van individuele emitters, terwijl de kortere levensduur wordt toegeschreven aan de interactie tussen de emitters.

Niet alleen kunnen zij Ag:DNAs stabiliseren, maar de HX buisjes zijn ook een uitstekend raamwerk voor de organisatie van colloïdale deeltjes wiens diameter twee ordegroottes groter is dan de diameter van de buisjes. Superparamagnetische colloïdale deeltjes vormen strengen in een magneetveld. Deze strengen zijn instabiel en thermische beweging breekt hen. Echter, colloïdale deeltjes waaraan korte DNA strengen zijn toegevoegd die complementair zijn aan de bindingsplaatsen op de HX buisjes, kunnen stabiele strengen vormen in een magneetveld. Deze werken als het ware als nanolijm en maken het systeem stabiel zelfs in afwezigheid van een magnetisch veld. De structuren zijn erg flexibel en maken daardoor de weg vrij voor toepassingen.

Samenvattend, in dit proefschrift presenteren wij de eerste gedetailleerde analyse van de spectrale en polarisatie eigenschappen van individuele

Ag:DNAs. Ons werk laat zien dat DNA aan de eisen voldoet van de moderne wetenschap en technologie om DNA structuren op grote schaal en met nanometer precisie te fabriceren.

# Bibliography


[1] M. B. Mohamed, V. Volkov, S. Link, and M. A. El-Sayed, *The 'lightning' gold nanorods: fluorescence enhancement of over a million compared to the gold metal*, Chem. Phys. Lett. **317**, 517 (2000).

[2] A. Gaiduk, M. Yorulmaz, and M. Oritt, *Correlated absorption and photoluminescence of single gold nanoparticles*, ChemPhysChem **12**, 1536 (2011).

[3] M. Yorulmaz, S. Khatua, P. Zijlstra, A. Gaiduk, and M. Orrit, *Luminescence quantum yield of single gold nanorods*, Nano Lett. **12**, 4385 (2012).

[4] J. Walter, M.and Akola, O. Lopez-Acevedo, P. D. Jadzinsky, G. Calero, C. J. Ackerson, R. L. Whetten, H. Grönbeck, and H. Häkkinen, *A unified view of ligand-protected gold clusters as superatom complexes*, PNAS **105**, 9157 (2008).

[5] S. Raut, R. Chib, R. Rich, D. Shumilov, Z. Gryczynski, and I. Gryczynski, *Polarization properties of fluorescent BSA protected $Au_{25}$ nanoclusters*, Nanoscale **5**, 3441 (2013).

[6] J. Zheng and R. M. Dickson, *Individual water-soluble dendrimer-encapsulated silver nanodot fluorescence*, J. Am. Chem. Soc. **124**, 13982 (2002).

[7] H. Xu and K. S. Suslick, *Sonochemical synthesis of highly fluorescent Ag nanoclusters*, ACS Nano **4**, 3209 (2010).

[8] J. Yu, S. Patel, and R. Dickson, *Invitro and intracellular production of peptide-encapsulated fluorescent silver nanoclusters*, Angew. Chem. **46**, 2028 (2007).

[9] D. Schultz and E. Gwinn, *Stabilization of fluorescent silver clusters by RNA homopolymers and their DNA analogs: C,G versus A,T(U) dichotomy*, Chem. Commun **47**, 4715 (2011).

[10] J. T. Petty, J. Zheng, N. V. Hud, and R. M. Dickson, *DNA-templated Ag nanocluster formation*, J. Am. Chem. Soc. **126**, 5207 (2004).

[11] L. Berti and G. A. Burley, *Nucleic acid and nucleotide-mediated synthesis of inorganic nanoparticles*, Nature Nanotechnology **3**, 81 (2008).

[12] S. M. Swasey, L. E. Leal, O. Lopez-Acevedo, J. Pavlovich, and E. G. Gwinn, *Silver (I) as DNA glue: $Ag^{+}$-mediated guanine pairing revealed by removing Watson-Crick constraints*, Scientific Reports **5**, 1 (2015).

[13] E. G. Gwinn, P. O'Neill, A. J. Guerrero, D. Bouwmeester, and D. Fygenson, *Sequence-dependent fluorescence of DNA-hosted silver nanoclusters*, Adv. Mater. **20**, 279 (2008).

[14] W. Guo, J. Yuan, Q. Dong, and E. Wang, *Highly sequence-dependent formation of fluorescent silver nanoclusters in hybridized DNA duplexes for single nucleotide mutation identification*, J. Am. Chem. Soc. **132**, 932 (2010).

[15] J. M. Obliosca, C. Liu, and H.-C. Yeh, *Fluorescent silver nanoclusters as DNA probes*, Nanoscale **5**, 8443 (2013).

[16] W. Guo, J. Yuan, and E. Wang, *Oligonucleotide-stabilized Ag nanoclusters as novel fluorescence probes for the highly selective and sensitive detection of the $Hg^{2+}$*, Chem. Commun. **23**, 3395 (2009).

[17] J. Yu, S. Choi, C. Richards, Y. Antoku, and R. Dickson, *Live cell surface labeling with fluorescent Ag nanocluster conjugates*, Photochem. Photobiol. **84**, 1435 (2008).

[18] Y. Tao, E. Li, Z. Ju, J. Ren, and X. Qu, *One-step DNA-programmed growth of CpG conjugated silver nanoclusters: a potential platform for simultaneous enhanced immune response and cell imaging*, Chem. Commun. **49**, 6918 (2013).

[19] D. Schultz, K. Gardner, S. S. R. Oemrawsingh, N. Markešević, K. Olsson, M. Debord, D. Bouwmeester, and E. Gwinn, *Evidence for rod-shaped DNA-stabilized silver nanocluster emitters*, Adv. Mater. **25**, 2797 (2013).

[20] S. S. R. Oemrawsingh, N. Markešević, E. G. Gwinn, E. R. Eliel, and D. Bouwmeester, *Spectral properties of individual DNA-hosted silver nanoclusters at low temperatures*, J. Phys. Chem. C **116**, 25568 (2012).

[21] S. M. Copp, D. Schultz, S. Swasey, J. Pavlovich, M. Debord, A. Chiu, K. Olsson, and E. Gwinn, *Magic numbers in DNA-stabilized fluorescent silver clusters lead to magic colors*, J. Phys. Chem. Lett. **5**, 959 (2014).

[22] E. B. Guidez and C. M. Aikens, *Theoretical analysis of the optical excitation spectra of silver and gold nanowires*, Nanoscale **4**, 4190 (2012).

[23] P. W. K. Rothemund, *Folding DNA to create nanoscale shapes and patterns*, Nature **440**, 297 (2006).

[24] D. Han, S. Pal, J. Nangreave, Z. Deng, Y. Liu, and H. Yan, *DNA origami with complex curvatures in three-dimensional space*, Science **332**, 342 (2011).

[25] I. H. Stein, V. Schüller, P. Böhm, P. Tinnefeld, and T. Liedl, *Single-molecule FRET*

*ruler based on rigid DNA origami blocks*, ChemPhysChem **12**, 689 (2011).

[26] R. Schreiber, J. Do, E.-M. Roller, T. Zhang, V. J. Schüller, P. C. Nickels, J. Feldmann, and T. Liedl, *Hierarchical assembly of metal nanoparticles, quantum dots and organic dyes using DNA origami scaffolds*, Nature Nanotechnology **9**, 74 (2014).

[27] X. Shen, A. Asenjo-Garcia, Q. Liu, Q. Jiang, F. J. G. de Abajo, N. Liu, and B. Ding, *Three-dimensional plasmonic chiral tetramers assembled by DNA origami*, Nano Lett. **13**, 2128 (2013).

[28] A. Kuzyk, R. Schreiber, H. Zhang, A. O. Govorov, T. Liedl, and N. Liu, *Reconfigurable 3D plasmonic metamolecules*, Nature Materials **13**, 862 (2014).

[29] C. Zhou, X. Duan, and N. Liu, *A plasmonic nanorod that walks on DNA origami*, Nature Communications **9**, 1 (2015).

[30] Q. Zhang, Q. Jiang, N. Li, L. Dai, Q. Liu, L. Song, J. Wang, Y. Li, J. Tian, B. Ding, and Y. Du, *DNA origami as an in vivo drug delivery vehicle for cancer therapy*, ACS Nano **8**, 6633 (2014).

[31] S. Sellner, S. Kocabey, K. Nekolla, F. Krombach, T. Liedl, and M. Rehberg, *DNA nanotubes as intracellular delivery vehicles in vivo*, Biomaterials **53**, 453 (2015).

[32] P. O'Neill, P. W. K. Rothemund, A. Kumar, and D. K. Fygenson, *Sturdier DNA nanotubes via ligation*, Nano lett. **6**, 1379 (2006).

[33] P. R. O'Neill, K. Young, D. Schiffels, and D. K. Fygenson, *Few-atom fluorescent silver clusters assemble at programmed sites on DNA nanotubes*, Nano Lett. **12**, 5464 (2012).

[34] P. Yin, R. F. Hariadi, S. Sahu, H. T. M. Choi, S. H. Park, T. H. LaBean, and J. H. Reif, *Programming DNA tube circumferences*, Science **321**, 824 (2008).

[35] S. M. Copp, D. E. Schultz, S. Swasey, and E. G. Gwinn, *Atomically precise arrays of fluorescent silver clusters: A modular approach for metal cluster photonics on DNA nanostructures*, ACS Nano **9**, 2303 (2015).

[36] D. Schiffels, T. Liedl, and D. K. Fygenson, *Nanoscale structure and microscale stiffness of DNA nanotubes*, ACS Nano **7**, 6700 (2013).

[37] J. Zheng, P. R. Nicovich, and R. M. Dickson, *Highly Fluorescent Noble Metal Quantum Dots*, Annu. Rev. Phys. Chem. **58**, 409431 (2007).

[38] W. Harbich, S. Fedrigo, F. Meyer, D. Lindsay, J. Lignieres, J. Rivoal, and D. Kreisle, *Deposition of mass selected silver clusters in rare gas matrices*, J. Chem. Phys **93**, 8535 (1990).

[39] J. Tiggesbäumker, L. L. Köller, H. O. Lutz, and K. H. Meiwes-Broer, *Giant resonances in silver-cluster photofragmentation*, Chem. Phys. Lett. **190**, 42 (1992).

[40] C. Félix, C. Sieber, W. Harbich, J. Buttet, I. Rabin, W. Schulze, and G. Ertl, *Fluorescence and excitation spectra of $Ag_4$ in an argon matrix*, Chem. Phys. Lett. **313**, 105 (1999).

[41] C. Sieber, W. Buttet, J.and Harbich, C. Félix, R. Mitrić, and V. Bonačić-Koutecký, *Isomer-specific spectroscopy of metal clusters trapped in a matrix: $Ag_9$*, Phys. Rev. A **70**, 041201 (2004).

[42] R. L. Whetten, J. T. Khoury, M. M. Alvarez, S. Murthy, I. Vezmar, Z. L. Wang, P. W. Stephens, C. L. Cleveland, W. D. Luedtke, and U. Landman, *Nanocrystal gold molecules*, Adv. Mater. **8**, 428 (1996).

[43] A. C. Templeton, W. P. Wuelfing, and R. W. Murray, *Monolayer-protected cluster molecules*, Acc. Chem. Res. **33**, 27 (2000).

[44] T.-H. Lee and R. M. Dickson, *Single-molecule LEDs from nanoscale electroluminescent junctions*, J. Phys. Chem. B **107**, 7387 (2003).

[45] X. Yang, M. Shi, R. Zhou, X. Chen, and H. Chen, *Blending of $HAuCl_4$ and histidine in aqueous solution: a simple approach to the $Au_{10}$ cluster*, Nanoscale **3**, 2596 (2011).

[46] S. Choi, R. Dickson, J. Lee, and J. Yu, *Generation of luminescent noble metal nanodots in cell matrices*, Photochem. Photobiol. Sci. **11**, 274 (2012).

[47] Z. Wu and R. Jin, *On the ligands role in the fluorescence of gold nanoclusters*, Nano Lett. **10**, 2568 (2010).

[48] M. S. Devadas, S. Bairu, H. Qian, E. Sinn, R. Jin, and G. Ramakrishna, *Temperature-dependent optical absorption properties of monolayer-protected $Au_{25}$ and $Au_{38}$ clusters*, J. Phys. Chem. Lett. **2**, 2752 (2011).

[49] C. I. Richards, S. Choi, J.-C. Hsiang, Y. Antoku, T. Vosch, A. Bongiorno, Y.-L. Tzeng, and R. M. Dickson, *Oligonucleotide-stabilized Ag nanocluster fluorophores*, J. Am. Chem. Soc. **130**, 5038 (2008).

[50] B. Sengupta, K. Springer, J. G. Buckman, S. P. Story, O. H. Abe, Z. W. Hasan, Z. D. Prudowsky, S. E. Rudisill, N. N. Degtyareva, and J. T. Petty, *DNA templates for fluorescent silver clusters and i-motif folding*, J. Phys. Chem. C **113**, 19518 (2009).

[51] P. R. O'Neill, L. R. Velazquez, D. G. Dunn, E. G. Gwinn, and D. Fygenson, *Hairpins with poly-C loops stabilize four types of fluorescent $Ag_n$: DNA*, J. Phys. Chem. C **113**, 4229 (2009).

[52] J. Sharma, H. Yeh, H. Yoo, J. Werner, and J. Martinez, *A complementary palette of fluorescent silver nanoclusters*, Chem. Commun. **46**, 3280 (2010).

[53] D. Schultz and E. G. Gwinn, *Silver atom and strand numbers in fluorescent and*

*dark Ag:DNAs*, Chem. Commun. **48**, 5748 (2012).

[54] K. Ma, Y. Shao, Q. Cui, F. Wu, S. Xu, and G. Liu, *Base-stacking-determined fluorescence emission of DNA abasic site-templated silver nanoclusters*, Langumir **28**, 15313 (2012).

[55] T. Li, L. Zhang, J. Ai, S. Dong, and E. Wang, *Ion-tuned DNA/Ag fluorescent nanoclusters as versatile logic device*, ACS Nano **5**, 6334 (2011).

[56] S. W. Yang and T. Vosch, *Rapid detection of microRNA by a silver nanocluster DNA probe*, Anal. Chem. **83**, 6935 (2011).

[57] S. A. Patel, M. Cozzuol, J. M. Hales, C. I. Richards, M. Sartin, J.-C. Hsiang, T. Vosch, J. W. Perry, and R. M. Dickson, *Electron transfer-induced blinking in Ag nanodot fluorescence*, J. Phys. Chem. C **113**, 20264 (2009).

[58] K. Baishya, J. C. Idrobo, S. Öğüt, M. Yang, K. Jackson, and J. Jellinek, *Optical absorption spectra of intermediate-size silver clusters from first principles*, Phys. Rev. B **78**, 075439 (2008).

[59] J. Pacheco, R. Broglia, and B. Mottelson, *The intrinsic line width of the plasmon resonances in metal microclusters at very low temperatures: quantal surface fluctuations*, Z. Phys. D **21**, 289 (1991).

[60] G. Weick, R. A. Molina, D. Weinmann, and R. A. Jalabert, *Lifetime of the first and second collective excitations in metallic nanoparticles*, Phys. Rev. B **72**, 115410 (2005).

[61] G. Weick, G.-L. Ingold, R. A. Jalabert, and D. Weinmann, *Surface plasmon in metallic nanoparticles: Renormalization effects due to electron-hole excitations*, Phys. Rev. B **74**, 165421 (2006).

[62] J. Lermé, *Size evolution of the surface plasmon resonance damping in silver nanoparticles: confinement and dielectric effects*, J. Phys. Chem. C **115**, 14098 (2011).

[63] R. Fournier, *Theoretical study of the structure of silver clusters*, J. Chem. Phys. **115**, 2165 (2001).

[64] P. Yu, X. Wen, Y.-R. Toh, and J. Tang, *Temperature-dependent fluorescence in $Au_{10}$ nanoclusters*, J. Phys. Chem. C **116**, 6567 (2012).

[65] V. Soto-Verdugo, H. Metiu, and E. G. Gwinn, *The properties of small Ag clusters bound to DNA bases*, J. Chem. Phys. **132**, 195102 (2010).

[66] S. Krause, P. F. Aramendia, D. Tauber, and C. von Borczyskowski, *Freezing single molecule dynamics on interfaces and in polymers*, Phys. Chem. Chem. Phys. **13**, 1754 (2011).

[67] M. Hussels and M. Brecht, *Effect of glycerol and PVA on the conformation of photo-*

*system I*, Biochemistry **50**, 3628 (2011).

[68] Y. Zhang, S. Hartmann, and F. Moshary, *Fluorescence-line-narrowing spectroscopy of nile blue in glass and polymer at 5 K: Determination of a single-site line shape function*, J. Chem. Phys. **104**, 4371 (1996).

[69] N. Verdal and A. M. Kelley, *Temperature dependence of phonon sidebands in line-narrowed fluorescence spectra of chromophores in glasses*, J. Chem. Phys. **118**, 7985 (2003).

[70] R. Hildner, L. Winterling, U. Lemmer, U. Scherf, and J. Köhler, *Single-molecule spectroscopy on a ladder-type conjugated polymer: electron-phonon coupling and spectral diffusion*, ChemPhysChem **10**, 2524 (2009).

[71] P. Gruene, D. M. Rayner, B. Redlich, A. F. G. van der Meer, J. T. Lyon, G. Meijer, and A. Fielicke, *Structures of neutral $Au_7$, $Au_{19}$, and $Au_{20}$ clusters in the gas phase*, Science **321**, 674 (2008).

[72] S. Kümmel, K. Andrae, and P. G. Reinhard, *Collectivity in the optical response of small metal clusters*, Appl. Phys. B **73**, 293 (2001).

[73] E. J. Heilweil and R. M. Hochstrasser, *Nonlinear spectroscopy and picosecond transient grating study of colloidal gold*, J. Chem. Phys. **82**, 4762 (1985).

[74] S. Fedrigo, W. Harbich, and J. Buttet, *Optical response of $Ag_2$, $Ag_3$, $Au_2$, and $Au_3$ in argon matrices*, J. Chem. Phys. **99**, 5712 (1993).

[75] W. Harbich, S. Fedrigo, and J. Buttet, *The optical absorption spectra of small silver clusters (n=5-11) embedded in argon matrices*, J. Chem. Phys. Lett. **195**, 613 (1992).

[76] J. T. Petty, C. Fan, S. S. Story, B. Sengupta, A. S. J. Iyer, Z. Prudowsky, and R. M. Dickson, *DNA encapsulation of ten silver atoms produces a bright, modulatable, near infrared-emitting cluster*, J. Phys. Chem. Lett. **1**, 2524 (2010).

[77] J. P. Wilcoxon, J. E. Martin, F. Parsapour, B. Wiedenman, and D. F. Kalley, *Photoluminescence from nanosize gold clusters*, J. Chem. Phys. **108**, 9137 (1998).

[78] A. Kuzyk, R. Schreiber, Z. Fan, G. Pardatscher, E. M. Roller, A. Högele, F. C. Simmel, A. O. Govorov, and T. Liedl, *DNA-based self-assembly of chiral plasmonic nanostructures with tailored optical response*, Nature **483**, 311 (2012).

[79] I. Chakraborty, S. Bag, U. Landman, and T. Pradeep, *Atomically precise silver clusters as new SERS substrates*, J. Phys. Chem. Lett. **4**, 2769 (2013).

[80] D. Schultz, S. M. Copp, N. Markešević, K. Gardner, S. S. R. Oemrawsingh, D. Bouwmeester, and E. Gwinn, *Dual-color nanoscale assemblies of structurally stable, few-atom silver clusters, as reported by fluorescence resonance energy transfer*, ACS Nano **7**, 9798 (2013).

[81] J. Yan and S. Gao, *Plasmon resonances in linear atomic chains: Free-electron behavior and anisotropic screening of d electrons*, Phys. Rev. B **78**, 235413 (2008).

[82] A. Ojanperä, M. J. Puska, and O. Lopez-Acevedo, *First-principles study of excited state evolution in a protected gold complex*, J. Phys. Chem. C **117**, 11837 (2013).

[83] M. Zhou, S. Vdović, S. Long, M. Zhu, L. Yan, Y. Wang, Y. Niu, X. Wang, Q. Guo, R. Jin, and A. Xia, *Intramolecular charge transfer and solvation dynamics of thiolate-protected $Au_{20}(SR)_{16}$ clusters studied by ultrafast measurement*, J. Phys. Chem. A **117**, 10294 (2013).

[84] F. Güttler, J. Sepiol, T. Plakhotnik, A. Mitterdorferr, A. Renn, and U. P. Wild, *Single molecule spectroscopy - fluorescennce excitation spectra with polarized light*, J. Lumin. **56**, 29 (1993).

[85] F. Güttler, M. Croci, A. Renn, and U. P. Wild, *Single molecule polarization spectroscopy: pentacene in p-terphenyl*, Chem. Phys. **211**, 421 (1996).

[86] T. Ha, T. Enderle, D. S. Chemla, P. R. Selvin, and S. Weiss, *Single molecule dynamics studied by polarization modulation*, Phys. Rev. Let. **77**, 3979 (1996).

[87] S. A. Empedocles, R. Neuhauser, K. Shimizu, and M. G. Bawendi, *Photoluminescence from single semiconductor nanostructures*, Adv. Mater. **11**, 1243 (1999).

[88] T. Ha, T. A. Laurence, D. S. Chemla, and S. Weiss, *Polarization spectroscopy of single fluorescent molecules*, J. Phys. Chem. B **103**, 6839 (1999).

[89] A. Tcherniak, S. Dominguez-Medina, W.-S. Chang, P. Swanglap, L. S. Slaughter, C. F. Landes, and S. Link, *One-photon plasmon luminescence and its application to correlation spectroscopy as a probe for rotational and translational dynamics of gold nanorods*, J. Phys. Chem. C **115**, 15938 (2011).

[90] W.-S. Chang, J. W. Ha, L. S. Slaughter, and S. Link, *Plasmonic nanorod absorbers as orientation sensors*, PNAS **107**, 2781 (2010).

[91] C. Sönnichsen, T. Franzl, T. Wilk, G. von Plessen, J. Feldmann, O. Wilson, and P. Mulvaney, *Drastic reduction of plasmon damping in gold nanorods*, Phys. Rev. Lett. **88**, 077402 (2002).

[92] O. L. Muskens, G. Bachelier, N. D. Fatti, F. Valle, A. Brioude, X. Jiang, and M.-P. Pileni, *Quantitative absorption spectroscopy of a single gold nanorod*, J. Phys. Chem. C **112**, 8917 (2008).

[93] K. Becker, E. Da Como, J. Feldmann, F. Scheliga, E. Thorn Csányi, S. Tretiak, and J. M. Lupton, *How chromophore shape determines the spectroscopy of phenylene-vinylenes: origin of spectral broadening in the absence of aggregation*, J. Phys. Chem. B **112**, 4859 (2008).

[94] J. M. Lupton, *Chromophores in conjugated polymers - all straight?*, ChemPhys-

Chem **13**, 901 (2012).

[95] O. Schubert, J. Becker, L. Carbone, Y. Khalavka, T. Provalska, I. Zins, and C. Sönnichsen, *Mapping the polarization pattern of plasmon modes reveals nanoparticle symmetry*, Nano Lett. **8**, 2345 (2008).

[96] M. P. Busson, B. Rolly, B. Stout, N. Bonod, and S. Bidault, *Accelerated single photon emission from dye molecule-driven nanoantennas assembled on DNA*, Nature Communications **3**, 1 (2012).

[97] M. P. Busson, B. Rolly, B. Stout, N. Bonod, E. Larquet, A. Polman, and S. Bidault, *Optical and topological characterization of gold nanoparticle dimers linked by a single DNA double strand*.

[98] H.-C. Yeh and I.-M. V. D. M. J. W. J. Sharma, J.and Shih, *A fluorescence light-up Ag nanocluster probe that discriminates single-nucleotide variants by emission color*, J. Am. Chem. Soc. **134**, 11550 (2012).

[99] N. Markešević, S. S. R. Oemrawsingh, D. Schultz, E. G. Gwinn, and D. Bouwmeester, *Polarization Resolved Measurements of Individual DNA-Stabilized Silver Clusters*, Adv. Optical Mater. **2**, 765 (2014).

[100] Z. Yuan, Y.-C. Chen, H.-W. Li, and H.-T. Chang, *Fluorescent silver nanoclusters stabilized by DNA scaffolds*, Chem. Commun. **50**, 9800 (2014).

[101] E. Gwinn, D. Schultz, S. M. Copp, and S. Swasey, *DNA-protected silver clusters for nanophotonics*, Nanomaterials **5**, 180 (2015).

[102] T. Driehorst, P. O'Neill, P. M. Goodwin, S. Pennathur, and D. K. Fygenson, *Distinct conformations of DNA-stabilized fluorescent silver nanoclusters revealed by electrophoretic mobility and diffusivity measurements*, Langmuir **27**, 8923 (2011).

[103] T. L. Jennings, M. P. Singh, and G. F. Strouse, *Fluorescent lifetime quenching near d = 1.5 nm gold nanoparticles: probing NSET validity*, J. Am. Chem. Soc. **128**, 5462 (2006).

[104] M. P. Busson and S. Bidault, *Selective excitation of single molecules coupled to the bright mode of a plasmonic cavity*, Nano Lett. **14**, 284 (2014).

[105] E. N. Hooley, V. Paolucci, Z. Liao, M. R. Carro Temboury, and T. Vosch, *Single-molecule characterization of near-infrared-emitting silver nanoclusters*, Adv. Optical Mater. **3**, 1109 (2015).

[106] C. A. Mirkin, R. L. Letsinger, R. C. Mucic, and J. J. Storhoff, *A DNA-based method for rationally assembling nanoparticles into macroscopic materials*, Nature **382**, 607 (1996).

[107] B. Bharti, G. H. Findenegg, and O. D. Velev, *Analysis of the field-assisted permanent assembly of oppositely charged particles*, Langmuir **30**, 6577 (2014).

[108] M. E. Leunissen, R. Dreyfus, F. C. Cheong, D. G. Grier, R. Sha, N. C. Seeman, and P. M. Chaikin, *Switchable self-protected attractions in DNA-functionalized colloids*, Nature Mat. **8**, 590 (2009).

[109] S. Y. Kim, S.-H.and Lee, G.-R. Yi, D. J. Pine, and S.-M. Yang, *Microwave-assisted self-organization of colloidal particles in confining aqueous droplets*, J. Am. Chem. Soc. **128**, 10897 (2006).

[110] A. B. Pawar and I. Kretzschmar, *Fabrication, assembly, and application of patchy particles*, Macromol. Rapid Commun. **31**, 150 (2010).

[111] F. Smallenburg, H. R. Vutukuri, A. Imhof, A. van Blaaderen, and M. Dijkstra, *Self-assembly of colloidal particles into strings in a homogeneous external electric or magnetic field*, J. Phys.: Condens. Matter **24**, 464113 (2012).

[112] R. Dreyfus, M. E. Leunissen, R. Sha, A. V. Tkachenko, N. C. Seeman, D. J. Pine, and P. M. Chaikin, *Simple quantitative model for the reversible association of DNA coated colloids*, Phys. Rev. Lett. **102**, 048301 (2009).

# Curriculum Vitae

**Nemanja Markešević**

| | |
|---|---|
| 16 May 1985 | Born in Čačak, Serbia |
| 1992-2004 | Primary and secondary education, Čačak, Serbia |
| 2000-2004 | Research activities at the Republic Center for Talented Students (focus on amorphous alloys), Serbia |
| 2004-2010 | Faculty of Physics, department of Theoretical and Experimental Physics, Belgrade, Serbia |
| | Diploma Thesis: *Morphologies of thin TPD films* (Thesis supervisor: dr. Vojislav Srdanov) |
| 2010-2011 | Researcher at the Institute of Physics (focus on organic materials for light emitting devices) |
| 2011-2015 | Ph.D. researcher at Leiden University, department of Quantum Matter and Optics, the Netherlands |
| | Thesis: *Optical properties of DNA-hosted silver clusters* (Thesis supervisor: prof. dr. Dirk Bouwmeester) |
| | My research has been presented at Dutch and international conferences and workshops |
| | Teaching assistant for Signal and Noise Processing, and for Physics Research Laboratory |
| | Research and thesis supervisor of four bachelor students and one master student |
| 2016- | Postdoctoral researcher at the Langevin Institute, department of Optical Antennas, Paris, France (Supervisor: dr. Sébastien Bidault) |

# List of publications

- **N. Markešević**, S. M. Copp, D. de Bruin, S. S. R. Oemrawsingh, E. G. Gwinn and D. Bouwmeester, *Optical properties of the DNA-hosted silver clusters on DNA tiles and tubes*, in preparation. (Chapter 4 of this thesis)

- **N. Markešević**, S. S. R. Oemrawsingh, D. Schultz, E. Gwinn, D. Bouwmeester, *Polarization resolved measurements of individual DNA-stabilized silver clusters*, Adv. Optical Mater., **2**, 765-770 (2014). (Chapter 3 of this thesis)

- Z. Tomović, **N. Markešević**, M. Scarpellini, S. Bovio, E. Luccenti, P. Milani, R. Zikic, V. P. Jovanović, V. I. Srdanov, *Stabilization of N,N-bis(3-methylphenyl)-N,N-bis (phenyl) benzidine thin film morphology with UV light*, Thin solid films, **562**, 99-103 (2014).

- D. Schultz, S. M. Copp, **N. Markešević**, K. Gardner, S. S. R. Oemrawsingh, D. Bouwmeester, E. Gwinn, *Dual-color nanoscale assemblies of structurally stable, few-atom silver clusters, as reported by fluorescence resonance energy transfer*, ACS Nano, **7**, 9798-9807 (2013) .

- D. Schultz, K. Gartner, S. S. R. Oemrawsingh, **N. Markešević**, K. Olsson, M. Debord, D. Bouwmeester and E. G. Gwinn, *Evidence for rod-shaped DNA-stabilized nanocluster emitters*, Adv. Mater., **25**, 2797-2803 (2013).

- S. S. R. Oemrawsingh, **N. Markešević**, E. G. Gwinn, E. R. Eliel and D. Bouwmeester, *Spectral properties of individual DNA-hosted silver nanoclusters at low temperatures*, J. Phys. Chem. C, **116**, 25568-25575 (2012). (Chapter 2 of this thesis)

# Acknowledgement

This thesis is a product of interaction with many people. Some of them are directly connected to the work presented in this thesis. They were involved in the experiments, discussed the results, carefully read manuscripts, etc. Others, equally important to me, had almost no scientific input, but had a great influence on my personal life and well-being. If it is possible to sum up my impressions in one sentence, I would say that all these people changed my perception of life and improved my professional and human qualities.

Firstly, I would like to express my gratitude to Professor Dirk Bouwmeester for his patient supervision and encouragement to strive for new discoveries. Also, I am thankful for the scientific freedom I got to conduct my research projects. Secondly, I would like to thank a postdoctoral researcher, Dr. Sumant Oemrawsingh, for his careful guidance and daily supervision in the first half of my PhD project.

I am thankful to our collaborator, Professor Elisabeth Gwinn for her insightful thoughts on the Ag:DNA project and discussions we had during my PhD. The discussions with Beth's PhD students Stacy M. Copp, Danielle Schultz and Steven Swasey led to the interesting research projects we worked on together. Some of them would have been impossible without the purified DNA material we received from UCSB.

Collaboration with Doctor Daniella Kraft brought new insight into the interaction between colloidal particles and DNA. I am thankful to Professor Thijs Aartsma for allowing me to use the setup for time-resolved measurements and for discussions on the experimental results.

I would like to thank my bachelor students Irina Komen, Steffie Ypma, Donny de Bruin and Marnix van de Stolpe for their dedication and perseverance in conducting scientific research.

I am grateful to Henriette van Leeuwen for the secretary work.

Also, people from the Fine Mechanical Department and the Electronics Department took care that some technical parts of the experiments went smoothly.

I would like to thank Morten Bakker for the Dutch translation of my summary. My dear friends and paranymphs, Marija Mučibabić and Saša Vrbica, were (and still are) important both for the scientific discussions, and personal support when things were not going smoothly.

I would like to thank the people from the Biophysics group and Cell Observatory for scientific discussions.

I would like to thank my colleagues in the Quantum Optics group for making a friendly and fruitful scientific environment for work and living.

Also, I am grateful to my Serbian friends for keeping me connected to the roots and giving me an orientation in life.

Finally, I express gratitude to my family for their love, patience and support during all these years.